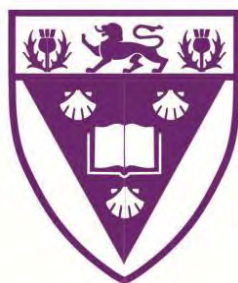


**THE DEVELOPMENT OF PLATINUM AND PALLADIUM-SELECTIVE  
POLYMERIC MATERIALS**

**A THESIS SUBMITTED IN FULFILMENT OF THE  
REQUIREMENTS FOR THE DEGREE OF  
MASTER OF SCIENCE  
IN THE FACULTY OF SCIENCE  
OF  
RHODES UNIVERSITY**



**by**

**OMOLOLA ESTHER FAYEMI**

**DECEMBER 2012**

# ABSTRACT

The adsorption and separation of platinum(IV) and palladium(II) chlorido species ( $\text{PtCl}_6^{2-}$  and  $\text{PdCl}_4^{2-}$ ) on polystyrene-based beads and nanofibers as well as silica microparticles functionalized with polyamine centres derived from ethylenediamine (EDA), diethylenetriamine (DETA), triethylenetriamine (TETA) and *tris*-(2-aminoethyl)amine (TAEA) is described. The functionalized sorbent materials were characterized by using microanalysis, SEM, XPS, BET and FTIR. The nanofiber sorbent material functionalized with ethylenediamine (F-EDA) had the highest loading capacity which was attributed to its high nitrogen content (10.83%) and larger surface area ( $241.3 \text{ m}^2/\text{g}$ ).

The adsorption and loading capacities of the sorption materials were investigated using both the batch and column studies in 1 M HCl. The adsorption studies for both  $\text{PtCl}_6^{2-}$  and  $\text{PdCl}_4^{2-}$  on the polystyrene-based sorbent materials fit the Langmuir isotherm while the silica-based sorbents fitted the Freundlich isotherm with  $R^2$  values  $> 0.99$ . In the column experiment the highest loading capacity of Pt and Pd were 7.4 mg/g and 4.3 mg/g respectively on the nanofiber sorbent material based on ethylenediamine (EDA). The polystyrene and silica-based resins with triethylenetetramine (TETA) functionality (M-TETA and S-TETA) showed selectivity for platinum and palladium, respectively.

Metal chlorido complexes loaded on the sorbent materials were recovered by using 3% m/v thiourea solution as the eluting agent with quantitative desorption efficiency under the selected experimental conditions. The separation of platinum from palladium was partially achieved by selective stripping of  $\text{PtCl}_6^{2-}$  with 0.5 M of  $\text{NaClO}_4$  in 1.0 M HCl

while  $\text{PdCl}_4^{2-}$  was eluted with 0.5 M thiourea in 1.0 M HCl. The selectivity of the M-TETA and S-TETA sorbent materials was proved by column separation of platinum(IV) and palladium(II), respectively, from synthetic solutions containing iridium(IV) and rhodium(III). The loading capacity for platinum on M-TETA was 0.09 mg/g while it was 0.27 mg/g for palladium on S-TETA.

**Keywords:** Platinum, palladium, microparticles, nanofibers, amine functionalization, adsorption, column separation.

# ACKNOWLEDGEMENTS

I will first give special thanks to the Almighty God for His grace, guidance and provision over the duration of this study.

My next appreciation goes to my supervisor, Prof. Z.R. Tshentu indeed. He has mentored and groomed me for a better future. He is always available and willing to see that all is well with me.

Prof Nelson Torto is acknowledged for open door access to the electrospinning equipment.

DST/Mintek NIC (Prof. Nyokong and Dr Antunes) is acknowledged for access to XPS and BET.

Dr Pierre Kempgens is also acknowledged for the  $^{195}\text{Pt}$  NMR experiments and Mr Sunday Ogunlaja for the BET experiments.

I would also like to thank Prof G. Watkins for his contribution, and the entire Department of Chemistry.

Rhodes University is acknowledged for giving me the opportunity to study towards a Master of Science degree in Chemistry.

My sincere thanks goes to all the support staff of the Chemistry Department including; A. Adriaan, V. Dondashe, J. Fourie and F. Chindeka, for all their help with the ICP and other instruments. Thanks to Labs F2, F3, F5, F12, and S22 group members.

Special thanks go to my husband, lovely girls and members of the body of Christ. I will not fail to mention members of Deeper Life Campus fellowship, UFH, Alice, DLCF LUTH, Lagos Nigeria, Bro. Adebayo, Paulina Sakarai, Ogbodu Racheal. I am also thankful to friends and labmates like Awokoya Kehinde, Oluwakemi Moronkola, Avela Majavu, Pastor Okewole, and never to forget Phumelele Kleyi.

Finally, I would like to thank NRF South Africa for financial support.

# TABLE OF CONTENTS

<b>ABSTRACT</b>	<b>ii</b>
<b>ACKNOWLEDGEMENTS</b>	<b>iv</b>
<b>TABLE OF CONTENTS</b>	<b>vi</b>
<b>LIST OF FIGURES</b>	<b>xi</b>
<b>LIST OF SCHEMES</b>	<b>xvi</b>
<b>LIST OF TABLES</b>	<b>xvii</b>
<b>CHAPTER 1</b>	<b>1</b>
INTRODUCTION	1
1.1    Platinum group metals (PGMs)	1
1.1.1    Applications of PGMs	2
1.1.2    Recovery of PGMs	3
1.2    Methods of separation	5
1.2.1    Precipitation	5
1.2.2    Solvent extraction	6
1.2.3    Ion-exchange	7
1.3    Chemistry of PGMs	9

1.3.1	Chlorido chemistry of PGMs	9
1.3.2	Redox chemistry of PGMs	14
1.4	Fabrication of ion exchange materials	16
1.4.1	N-containing ion-exchange materials	16
1.5	Fabrication of nanofiber materials	19
1.5.1	Self-assembly	20
1.5.2	Dry spinning	20
1.5.3	Drawing method	21
1.5.4	Phase separation	21
1.5.5	Wet spinning	22
1.5.6	Electrospinning	22
1.6	Scope of the study	28
<b>CHAPTER 2</b>		<b>29</b>
MATERIALS, EXPERIMENTAL TECHNIQUES AND METHODS		29
2.1	Materials	29
2.2	Spectroscopic techniques	31
2.2.1	NMR Spectrometry	31
2.2.2	Infrared Spectroscopy	31
2.3	Analytical methods	32
2.3.1	Elemental analysis	32

2.3.2	Inductively coupled plasma (ICP) spectrometry	32
2.4	Surface characterization techniques	35
2.4.1	Scanning electron microscopy	35
2.4.2	X-ray photoelectron spectroscopy	36
2.5	Adsorption experiments	37
2.5.1	Brunauer, Emmett, Teller (BET) surface area analysis	38
2.5.2	Langmuir isotherm	40
2.5.3	Freundlich isotherm	41
2.6	Column experiment	41
<b>CHAPTER 3</b>		<b>42</b>
	ADSORPTION AND SEPARATION OF PLATINUM GROUP METALS USING POLYAMINE-FUNCTIONALIZED POLYSTYRENE-BASED BEADS AND NANOFIBERS	42
3.1	Introduction	42
3.2	Experimental	43
3.2.1	Synthesis of poly(vinylbenzylchloride) (PVBC)	43
3.2.2	Fabrication of PVBC nanofibers	44
3.2.3	Functionalization of PVBC nanofibers	45
3.2.4	Functionalization of styrene-based beads	46
3.2.5	Preparation of metal solutions	46
3.2.6	Batch adsorption studies	48

3.2.7	Adsorption isotherms	49
3.2.8	Column (dynamic) studies	48
3.3	Results and Discussion	50
3.3.1	Characterization of the sorbent materials	50
3.3.2	$^{195}\text{Pt}$ NMR	50
3.3.3	Batch adsorption studies	60
3.3.4	Column (dynamic) studies	65
3.4	Conclusions	73
<b>CHAPTER 4</b>		<b>75</b>
ADSORPTION AND SEPARATION OF PLATINUM GROUP METALS USING POLYAMINE-FUNCTIONALIZED SILICA MATERIAL		75
4.1	Introduction	75
4.2	Experimental	77
4.2.1	Functionalization of silica-based microparticle	77
4.2.2	Batch adsorption studies	79
4.2.3	Separation of chlorido complexes of Pt(IV) and Pd(II)	78
4.2.4	Separation of chlorido complexes of Pd from Pt, Ir and Rh	78
4.3	Results and Discussion	80
4.3.1	Characterization of the sorbent materials	80
4.3.2	Batch adsorption studies	84

4.3.3	Column (dynamic) studies	87
4.4	Conclusions	93
<b>CHAPTER 5</b>		<b>95</b>
	CONCLUSIONS AND FUTURE WORK	95
5.1	Conclusions	95
5.2	Future work	96
<b>References</b>		<b>99</b>

# LIST OF FIGURES

<b>Figure 1.1</b>	The global distribution of palladium and platinum .....	2
<b>Figure 1.2</b>	PGM refining flowsheet [11] .....	4
<b>Figure 1.3</b>	Structure on imidazole-bearing resin [19].....	8
<b>Figure 1.4</b>	The species distribution curves for platinum(II) as a function of the log of the chloride ion concentration [26] .....	10
<b>Figure 1.5</b>	The species distribution curves for palladium(II) as a function of the log of the chloride ion concentration [29] .....	11
<b>Figure 1.6</b>	The species distribution curves for rhodium(III) as a function of the log of the chloride ion concentration [29] .....	13
<b>Figure 1.7</b>	Structures of Amberlite IRA 35 [47].....	17
<b>Figure 1.8</b>	Structures of silica-based (poly)amine anion exchanges with (a) monoamine (b) ethylenediamine and (c) diethylenetriamine functionalities [63] .....	18
<b>Figure 1.9</b>	The chemical structures of amines used for functionalization; (A) EDA, (B) DETA, (C) TETA and (D) TAEA.....	19
<b>Figure 1.10</b>	The picture of the electrospinning set-up used in this study.....	24
<b>Figure 1.11</b>	Schematic diagram of an electrospinning set-up [67].....	24
<b>Figure 3.1</b>	Structures of (a) polystyrene and (b) Merrifield resin [132]. .....	43

<b>Figure 3.2</b>	SEM images of unfunctionalized (a) nanofibers and (b) beads .....	51
<b>Figure 3.3</b>	SEM images of nanofibers functionalized with (a) EDA, (b) DETA, (c) TETA and (d) TAEA .....	53
<b>Figure 3.4</b>	SEM images of beads functionalized with (a) EDA, (b) DETA, (c) TETA and (d) TAEA .....	53
<b>Figure 3.5</b>	The XPS spectra of the nanofibers; (a) unfunctionalized, (b) EDA, (c) DETA, (d) TETA, and (e) TAEA-functionalized nanofibers.....	56
<b>Figure 3.6</b>	The XPS spectra of Merrifield beads; (a) unfunctionalized and (b) EDA, (C) DETA, (d) TETA, and (e) TAEA-functionalized beads.....	56
<b>Figure 3.7</b>	FT-IR spectra of (a) unfunctionalized Merrified beads and functionalized beads (b) M-EDA, (c) M-DETA, (d) M-TETA and (e) M-TAEA .....	57
<b>Figure 3.8</b>	FT-IR spectra of (a) unfunctionalized and functionalized styrene-based nanofibers (b) F-EDA, (c) F-DETA, (d) F-TETA and (e) F-TAEA .....	58
<b>Figure 3.9</b>	<sup>195</sup> Pt NMR (recorded at 20 <sup>0</sup> C) spectra of (a) 0.01 M PdCl <sub>4</sub> <sup>2-</sup> (b) PtCl <sub>6</sub> <sup>2-</sup> prepared by oxidizing PtCl <sub>4</sub> <sup>2-</sup> in 1 M HCl followed by 20 mL of H <sub>2</sub> O <sub>2</sub> and heated at 50°C for 30 minutes. ....	60
<b>Figure 3.10</b>	The effect of contact time on the percentage adsorption (A %) using 3 mL of 0.01 M PtCl <sub>6</sub> <sup>2-</sup> and PdCl <sub>4</sub> <sup>2-</sup> on 0.15 g of F-EDA at room temperature ...	61

**Figure 3.11** Plots of the (a) Langmuir and (b) Freundlich isotherm at room temperature using 3 mL of 0.01 M  $\text{PtCl}_6^{2-}$  and  $\text{PdCl}_4^{2-}$  adsorption on 0.15 g EDA-functionalized nanofibers ..... 62

**Figure 3.12** Adsorption/elution profiles using 5 mL of 0.01 M  $\text{PtCl}_6^{2-}$  and  $\text{PdCl}_4^{2-}$  on 0.3 g amine-functionalized beads: F-EDA, F-DETA, F-TETA and F-TAEA were respectively washed with 1 M HCl and eluted with 3% w/v thiourea at room temperature..... 66

**Figure 3.13** Adsorption/elution profiles using 5 mL of 0.01 M  $\text{PtCl}_6^{2-}$  and  $\text{PdCl}_4^{2-}$  on 0.3 g amine-functionalized beads: M-EDA, M-DETA, M-TETA and M-TAEA were respectively washed with 1 M HCl and eluted with 3% w/v thiourea at room temperature.....67

**Figure 3.14** Breakthrough curves using 5 mL of 0.01 M  $\text{PtCl}_6^{2-}$  and  $\text{PdCl}_4^{2-}$  on 0.3 g of M-TETA sorbent at room temperature in 1 M HCl..... 69

**Figure 3.15** The separation profile using 5 mL of 0.01 M mixture of  $\text{PtCl}_6^{2-}$  and  $\text{PdCl}_4^{2-}$  on 0.3 g M-EDA, F-EDA, F-TETA and F-TAEA by selective stripping of Pt and Pd with  $\text{NaClO}_4$  and thiourea respectively at room temperature ..... 71

**Figure 3.16** The adsorption/elution profile of Pt from the mixture of Pt, Ir and Rh on 0.3 g M-TETA by washing, stripping and eluting with 1 M HCl, 0.5 M  $\text{HClO}_4$  and 3% w/v thiourea respectively at room temperature..... 72

**Figure 4.1** Structure of silica gel functionalized with 4-amino-2-mercaptopyrimidine [151]..... 76

<b>Figure 4.2</b>	SEM images of silica-based sorbents; (a) unfunctionalized, silica and (b-e) silica functionalized with amines EDA, DETA, TETA and TAEA respectively (before sieving).....	79
<b>Figure 4.3</b>	Micrographs of silica-based sorbents; (a) unfunctionalized silica, and (b-e) silica functionalized with amines EDA, DETA, TETA and TAEA respectively .....	80
<b>Figure 4.4</b>	The XPS spectra of (a) EDA, (b) DETA, (c) TETA and (d) TAEA functionalized material .....	82
<b>Figure 4.5</b>	FT-IR spectra of (a) 3-chloropropyltrimethoxysilane (b) S-EDA (c) S-DETA (d) S-TETA (e) S-TAEA and (f) unfunctionalized silica.....	83
<b>Figure 4.6</b>	Effect of contact time on adsorption percentage (A %) using 3 mL of 0.01 M platinum and palladium chlorido species on 0.15 g of S-DETA at room temperature.....	84
<b>Figure 4.7</b>	Plots of Freundlich isotherm model using 3 mL of 0.01 M ■Pt and ▲Pd on 0.15 g of S-DETA at room temperature.....	85
<b>Figure 4.8</b>	Adsorption/elution profiles using 5 mL of 0.01 M $\text{PtCl}_6^{2-}$ and $\text{PdCl}_4^{2-}$ on 0.3 g of amine-functionalized silica-based sorbents: S-EDA, S-DETA, S-TETA and S-TAEA respectively by eluting with 3% w/v thiourea at room temperature.....	88
<b>Figure 4.9</b>	Breakthrough curves using 5 mL of 0.01 M $\text{PtCl}_6^{2-}$ and $\text{PdCl}_4^{2-}$ on 0.3 g of S-TETA sorbent at room temperature in 1 M HCl .....	90

<b>Figure 4.10</b>	The curves of separation using 5 mL of 0.01 M Pt and Pd by selective stripping of Pt with NaClO <sub>4</sub> and Pd with thiourea using 0.3 g of S-EDA sorbent at room temperature.....	91
<b>Figure 4.11</b>	The adsorption/elution profile of Pd from the mixture of Pt, Ir and Rh on 0.3 g S-TETA by eluting with 3% w/v thiourea at room temperature .....	92
<b>Figure 5.1</b>	The possible chemical structures of the proposed S-TETA resin.....	97
<b>Figure 5.2</b>	The possible chemical structures of the proposed M-TETA resins .....	98

# LIST OF SCHEMES

<b>Scheme 3.1</b> Synthesis of PVBC.....	44
<b>Scheme 3.2</b> Functionalization of nanofibers with ethylenediamine (F-EDA) .....	45
<b>Scheme 3.3</b> Synthesis of ethylenediaminefunctionalized Merrifield beads (M-EDA) ...	46
<b>Scheme 4.1</b> Functionalization of silica-based sorbent with ethylenediamine (S-EDA).	77

# LIST OF TABLES

<b>Table 1.1</b>	Dominant iridium(III)/(IV) species as a function of HCl.....	14
<b>Table 1.2</b>	Polymer solvent systems for electrospinning .....	29
<b>Table 2.1</b>	List of chemicals and reagents used .....	29
<b>Table 2.2</b>	ICP-OES method and operating parameters .....	34
<b>Table 3.1</b>	The single point surface area measurements for the unfunctionalized, EDA, DETA, TETA and TAEA-functionalized sorbent materials.....	53
<b>Table 3.2</b>	Langmuir and Freundlich parameters for adsorption of $\text{PtCl}_6^{2-}$ and $\text{PdCl}_4^{2-}$ on functionalized nanofibers .....	63
<b>Table 3.3</b>	Langmuir and Freundlich parameters for adsorption of $\text{PtCl}_6^{2-}$ and $\text{PdCl}_4^{2-}$ on functionalized beads .....	64
<b>Table 3.4</b>	The column experimental loading capacities (mg/g) of 0.3 g functionalized sorbent materials for Pt and Pd.....	70
<b>Table 4.1</b>	The single point surface area measurements for the unfunctionalized, EDA, DETA, TETA and TAEA-functionalized sorbent materials.....	81
<b>Table 4.2</b>	Langmuir and Freundlich parameter for adsorption of $\text{PtCl}_6^{2-}$ and $\text{PdCl}_4^{2-}$ on functionalized silica-based microparticles .....	86
<b>Table 4.3</b>	Loading capacities of sorbents for Pt and Pd (mg/g) at room temperature .....	89

# LIST OF ABBREVIATIONS

AIBN	Azobisisobutyronitrile
BET	Brunauer, Emmett and Teller (BET)
CTMEOS	3-chloropropyltrimethoxysilane
DETA	Diethylenetriamine
DMF	<i>N,N</i> -dimethylformamide
EDA	Ethylenediamine
F	Fiber
F-EDA	PVBC nanofibers functionalized with ethylenediamine
F-DETA	PVBC nanofibers functionalized with diethylenetriamine
F-TAEA	PVBC nanofibers functionalized with <i>tris</i> -(2-aminoethyl)amine
F-TETA	PVBC nanofibers functionalized with triethylenetetramine
HCl	Hydrochloric acid
ICP-OES	Inductively coupled plasma-optical emission spectrometer
M	Merrified resin
M-EDA	Merrified beads functionalized with ethylenediamine
M-DETA	Merrified beads functionalized with diethylenetriamine

M-TAEA	Merrified beads functionalized with <i>tris</i> -(2-aminoethyl)amine
M-TETA	Merrified beads functionalized with triethylenetetramine
NMR	Nuclear magnetic resonance
PGMs	Platinum group metals
PVBC	Polyvinylbenzylchloride
S-EDA	Silica microparticles functionalized with ethylenediamine
S-DETA	Silica microparticles functionalized with diethylenetriamine
S-TAEA	Silica microparticles functionalized with <i>tris</i> -2-(aminoethyl)amine
S-TETA	Silica microparticles functionalized with triethylenetetramine
TAEA	<i>Tris</i> -(2-aminoethyl)amine
TETA	Triethylenetetramine
THF	Tetrahydrofuran
VBC	Vinylbenzylchloride

# CHAPTER 1

## INTRODUCTION

### 1.1 Platinum group metals (PGMs)

Platinum group metals (PGMs) are platinum (Pt), palladium (Pd), osmium (Os), ruthenium (Ru), rhodium (Rh) and iridium (Ir) and are referred to as rare elements. Platinum is the most common having abundance of  $10^{-6}$  % while others are  $10^{-7}$  % of the earth's crust [1]. PGMs together with gold and silver form the family of precious metals [1]. They are included in group VIII B of the periodic table, and possess different chemical behaviour compared with other elements of the group such as Fe, Co, and Ni. Their metallic properties suggest the classification in pairs as Ru/Os, Rh/Ir and Pd/Pt. They are subdivided into two groups where the platinum and palladium make up the primary group and the other elements form the secondary PGMs. The classification is based on the fact that with conventional hydrometallurgical methods of treatment of the concentrates of precious metals is achieved by means of lixiviation with aqua regia. This yields the first separation as soluble part and the second as the insoluble residue [2, 3]. The soluble metals are the gold and primary platinum group while the insoluble metals are silver and the secondary PGMs. The global distribution of the PGMs it is apparent that these metals are predominantly found only in two countries namely, South Africa and Russia. In South Africa the main PGM mine houses are Anglo American, Lonmin, Northam and Impala Platinum. The mining of the platinum group metals forms a major part of the South African economy.

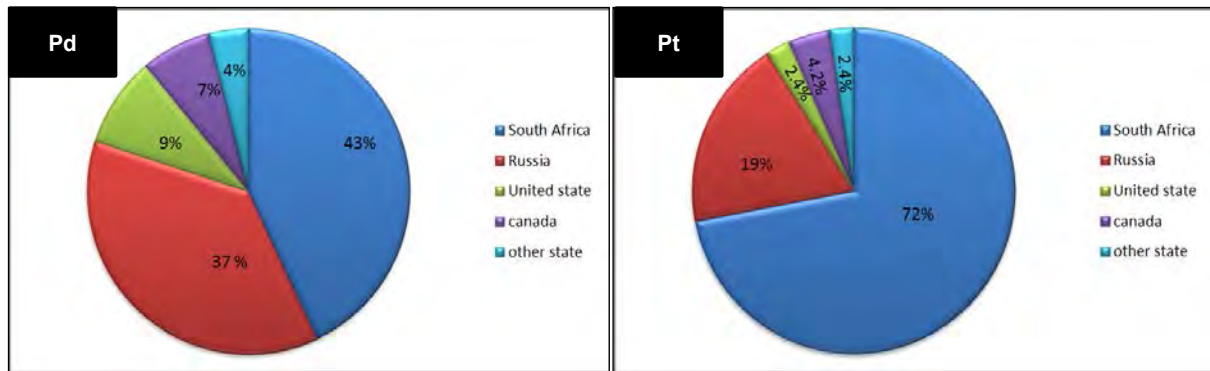


**Figure 1.1** The global distribution of palladium and platinum

### 1.1.1 Applications of PGMs

One of the main uses of platinum is in the automotive industry as auto-emission control catalyst for diesel engines to remove undesirable exhaust emissions. It is also used in the chemical industry in process catalysis. In the electrical industry, platinum is used to enhance the magnetic qualities of the cobalt alloy which coats the hard-disk surface where the data is stored on personal computers [4, 5]. An increasing need of high data-storage capacity, and high quality graphics and sound have led to a rapid increase in the use of platinum in the manufacture of hard disks. The demand of palladium is ever increasing especially in the electronics industry. It is used in the production of multi-layer ceramic capacitors (MLCC) which are used in mobile phones and automotive electronics. Palladium is also used in surge-resistor networks that protect telecommunications equipment from damage by large voltage. It is also being used as an alloying component and as a whitening agent in jewelry.

The catalytic properties of the PGMs are presently exerting a positive impact on the environment through the development of automotive emission control catalysts. The combined catalytic properties of Pt, Pd and Rh are very important in automotive emission control catalysts, and in the year 2000 approximately 60% of the annual world production of the PGM was used in automotive exhaust catalysts [6-8]. Platinum-based catalysts are also suitable for eliminating volatile organic compounds which are emitted from many industrial processes. Fuel cells which use platinum composite electrodes are also being developed for the production of zero emissions vehicles and efficient power generators [9]. Thus the precious metals have become, in one way or the other, essential parts of our everyday life. Hence their judicious use is necessary in order to tackle the ever increasing demand.

### **1.1.2 Recovery of PGMs**

The recovery of platinum group metals (PGMs) which are present in low concentration in the earth's crust is of great challenge to the industry due to the increase in the demand for these metals. Precious metals refining processes have changed considerably in recent years. Improved separation and refining procedures have been developed, and have incorporated both solvent extraction and ion exchange techniques. These improved processes have delivered increased PGM recoveries, lower refining costs and shorter processing times. The separation and purification of the PGMs is largely carried out by exploring differences in the chemistry of their anionic chlorido complexes which include; ligand substitution kinetics, ammonium salt solubility, ion-

exchange reactions and redox potentials [10]. The actual processes are proprietary; however a typical flowsheet which highlights the intricate and complex nature of PGM refining is shown in Figure 1.2.

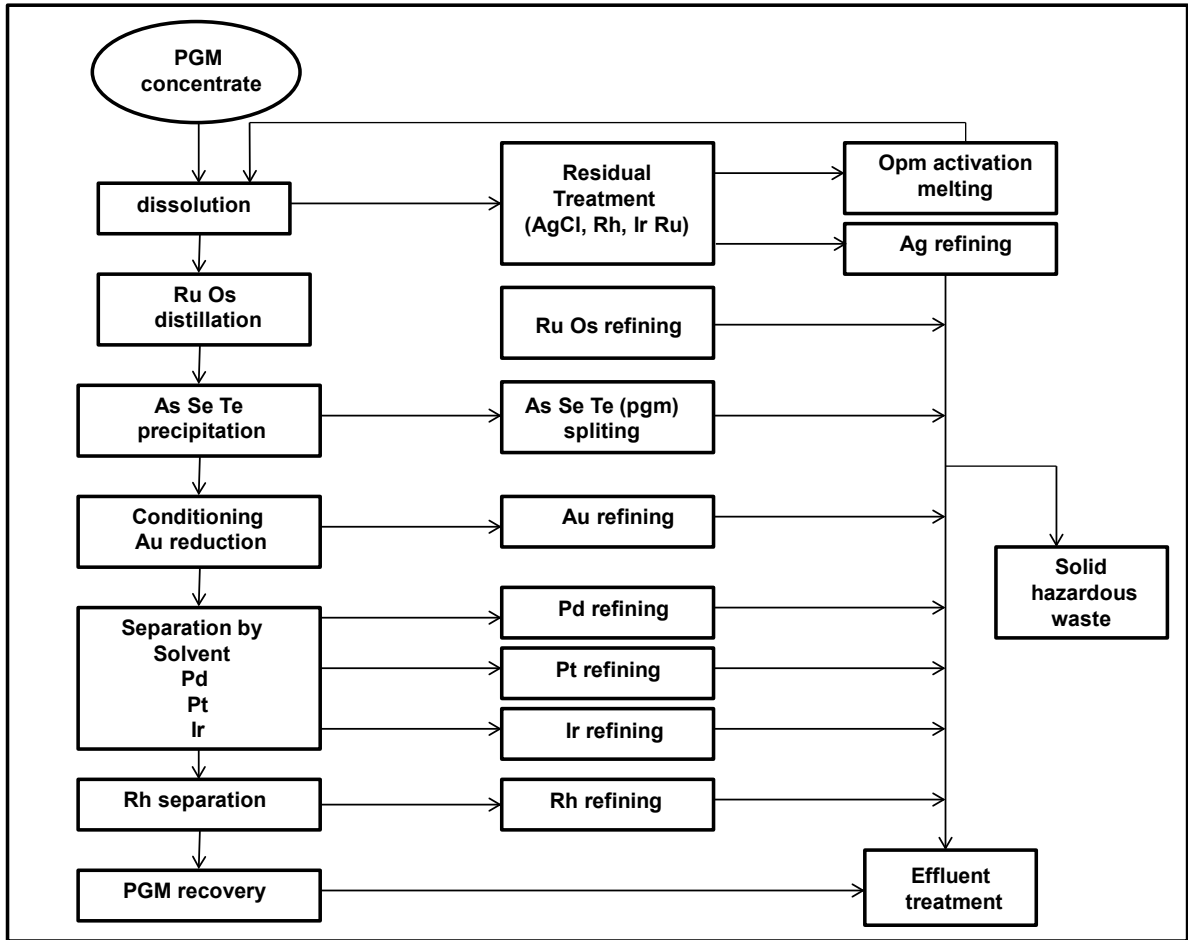


Figure 1.2 PGM refining flowsheet [11]

## 1.2 Methods of separation

The current separation processes make use of various combinations of precipitation, ion-exchange, distillation and solvent extraction. Many of these techniques still have current industrial applications [12].

### 1.2.1 Precipitation

Precipitation is the basic process that has been used for the separation of the largest quantities of platinum group metals since the beginning of separation technology to form a precipitate of ammonium hexachloroplatinate(IV) complex  $[(\text{NH}_4)_2\text{PtCl}_6]$ . The precipitation process can be optimized in many ways by influencing solubilities (e.g., by valence changes, addition of a common ion, or changing the temperature and the rate of precipitation) [13]. The first step in the separation of platinum group metals is usually to precipitate platinum as  $(\text{NH}_4)_2\text{PtCl}_6$ . If the dissolved platinum is present as Pt(II), it must first be oxidized to Pt(IV) which can be achieved by using chlorine. Excess dissolved chlorine is driven off by boiling. The palladium that had been oxidized to Pd(IV) is reduced to Pd(II) using iron(II) salts or ascorbic acid. The ammonium hexachloroplatinate(IV) is precipitated preferably by slow addition of concentrated ammonium chloride solution at room temperature with stirring. The hydrochloric acid concentration should be 1 M and the platinum content should be 50-200g/L [14].

### 1.2.2 Solvent extraction

Solvent extraction also known as liquid-liquid extraction involves the distribution of the components between two immiscible phases which are usually the aqueous and organic phase. The organic phase is a solution containing a lipophilic extractant which forms complexes with the metal ion (or ion pairs with an anionic complex) existing in the aqueous solutions which are transferred to the organic phase. The process must be reversible to cause the transfer of metal from the organic phase to the aqueous phase when chemical conditions are changed [14]. The variety of chemical species that can be treated by solvent extraction methods is greater than those treated by other methods like precipitation or ion exchange. The recovery and separation of Pt(IV) from Pd(II) has been accomplished through the supported liquid membrane (SLM) impregnated with 15% (v/v) LIX 26 and 10% (v/v) 1-octanol in kerosene. The Pt(IV) in the 1 M H<sub>2</sub>SO<sub>4</sub> or HNO<sub>3</sub> feed solution will then be separated into a weakly acidic product solution. Pt(IV) is transported into the product solution while the Pd(II) is built up in the LIX 26 - SLM [15]. The solvent extraction and separation performances of Pd(II) and Pt(IV) from hydrochloric acid solutions were investigated using dibutyl sulfoxide (DBSO) diluted in kerosene. Pd(II) was strongly extracted by a lower concentration DBSO in a lower concentration hydrochloric acid solution while the reverse was obtained for Pt(IV) extraction [16].

The use of solvent extraction technology to replace traditional processes has been of high interest in research and development efforts since the 1970s. This technique has been in use commercially since 1995 in at least three of the principal refineries [14]. Upon the identification of suitable extractants and using a multistage process, solvent

extraction can be used to extract individual metals from a mixture. Solvent extraction is a relatively high cost process, owing to the special organic extractants required, the expenses of recovery and storage of organic solvents.

### **1.2.3 Ion-exchange**

An ion exchange is the reversible exchange of ions between a liquid and a solid phase. There are three general types of ion exchange resins which are defined based on those that exchange positive ions called the cation resins and those that exchange negative ions called anion resins as well as amphoteric resin. The ion exchange groups are usually hosted on polymeric materials. Ion-exchange resins are particularly suitable stationary phases because of versatility and stability. Ion-exchange has been employed for the separation of mixtures of either cationic or anionic species of PGMs [17]. Separation is based on the variation in distribution coefficient of the PGM species on anion or cation exchangers.

The anion exchangers appear to be preferred to the cationic exchange resins because they require smaller column size and smaller volumes of eluates. The selectivity of anion exchange resins is much higher towards chlorido-complexes rather than the hydroxy-complexes [18]. PGMs, like the other transition metals, form a range of complexes with a variety of different ligands. The PGM-chlorido complexes are well studied complexes since the aqueous chloride solution is the only cost-effective medium in which all the PGMs can be brought into solution and concentrated.

Platinum and palladium were efficiently recovered from HCl solutions using a vinylbenzyl chloride-divinylbenzene resin reacted with the sodium salt of diethylmalonate followed by reaction with 3-aminopropyl imidazole (Figure 1.3). The metal complexes loaded on the resin were recovered using 0.1M thiourea solution as the eluent, with desorption efficiency exceeding 95% under the selected experimental conditions [19]. It must be borne in mind that the nitrogen groups become protonated in high HCl medium, and provide cationic sites for the ion-pairing of the anionic chlorido complexes of the PGMs.

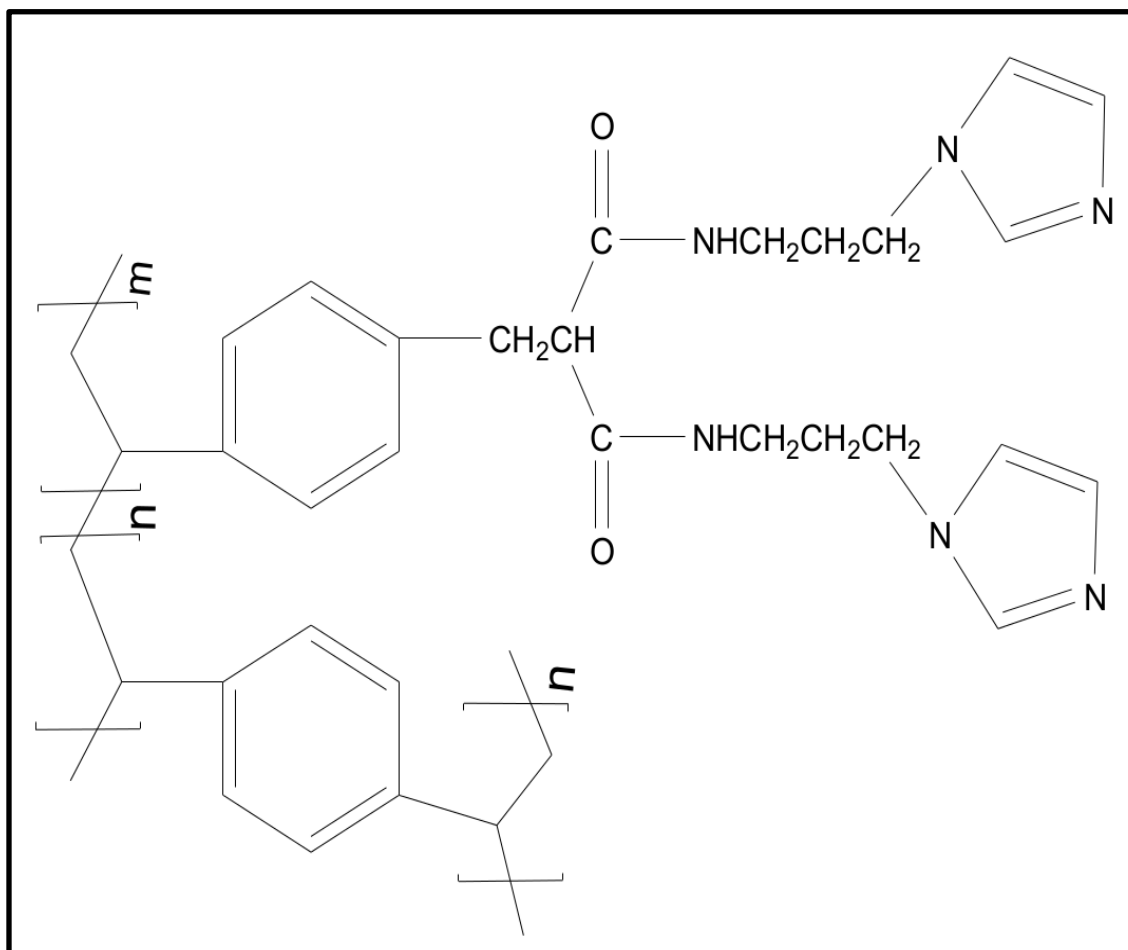


**Figure 1.3** Structure on imidazole-bearing resin [19]

## 1.3 Chemistry of PGMs

### 1.3.1 Chlorido chemistry of PGMs

The PGMs exist in a variety of oxidation states that can be stabilized by chloride ligands [20-22]. For example, Pt(IV) forms the hexachloridoplatinate(IV) complex in excess chloride medium [23]. The separation and recovery methods of the PGMs on a large scale essentially depend on the selective distribution of the stable, kinetically inert chlorido complex of these elements between acidic, chloride-rich aqueous phases and suitable non-aqueous (organic) receptor phases [24,25].

#### (a) Platinum chlorido species

The chemistry of platinum can conveniently be compared with that of its 4d analogue palladium, bearing in mind the difference between a 4d and 5d transition metal. The first thing to consider will be the much slower kinetics of substitution for  $\text{PtCl}_6^{2-}$  in comparison to  $\text{PdCl}_4^{2-}$  and the greater relative stability of Pt(IV) compared to Pd(IV) [26].

The species distribution curves for the chlorido complexes of platinum(II) are given in Figure 1.4 [26], while the complete constants for the formation of  $\text{PtCl}_6^{2-}$  are not found in literature. Platinum(IV) will, in a 1 M chloride ion concentration, be virtually completely present as  $\text{PtCl}_6^{2-}$ , provided that the chloride to platinum mole ratio is larger than six [26]. A simple instance is that where the chloride concentration is 1 M then the platinum concentration should be significantly less than 0.16 M. This criterion is important in practice, since if a solution contains 60 g of platinum per litre (i.e. 0.308 M platinum),

then 1 M chloride will not be sufficient to ensure complete formation of  $\text{PtCl}_6^{2-}$  from a thermodynamic perspective, since kinetics will certainly play a role as well [27].

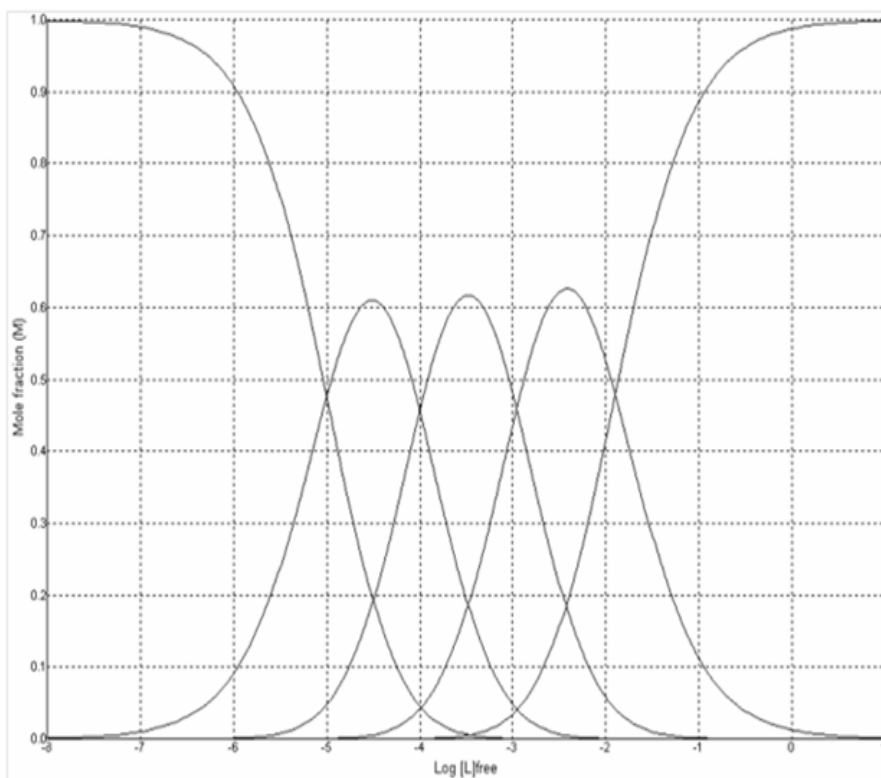
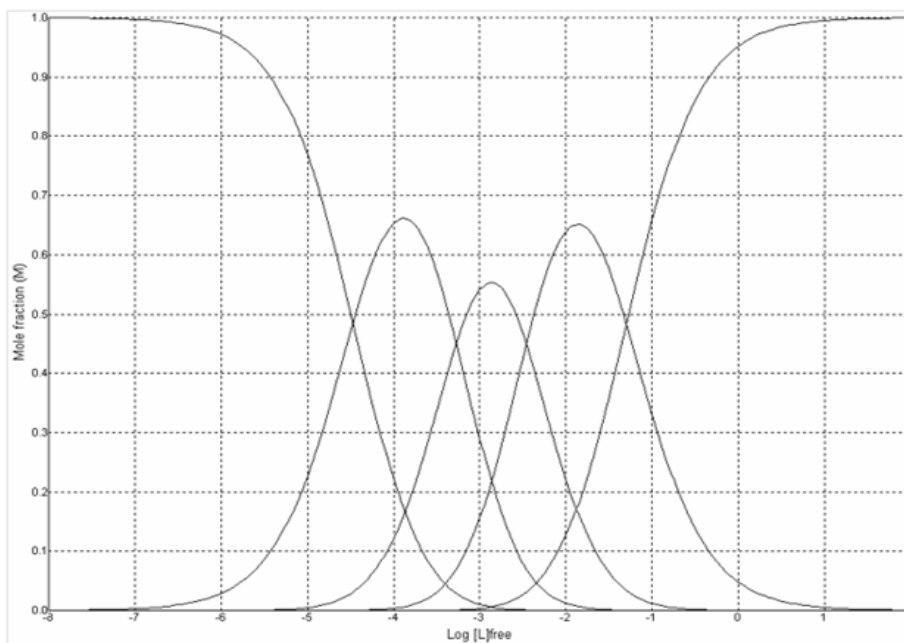


**Figure 1.4** The species distribution curves for platinum(II) as a function of the log of the chloride ion concentration [26]

### (b) Palladium chlorido species

The common square planar species found for palladium in chloride medium is  $\text{PdCl}_4^{2-}$ , although a dimeric species, namely  $\text{Pd}_2\text{Cl}_6^{2-}$  [28] is also found. The species distribution curves [29] for the chlorido complexes of palladium(II) are given in Figure 1.5. In dilute hydrochloric acid medium hydrolysis of the chlorido species can readily occur, for example, in 0.1 M chloride 33% of the palladium(II) is already in the form of  $\text{PdCl}_3(\text{H}_2\text{O})^-$

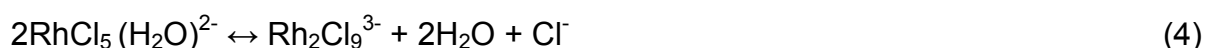
at equilibrium. This gives some indication of how complexation with sulfur-donor ligands, which will be thermodynamically driven, will rapidly exchange with aquated or even chloro palladium species thus facilitating its selective removal in the absence of gold. These substitution reactions are particularly possible for  $[\text{PdCl}_3(\text{H}_2\text{O})]^-$  and  $\text{PdCl}_4^{2-}$  due to the lability of the Pd-Cl bond compared with the Pt-Cl bond in  $\text{PtCl}_6^{2-}$  [30,31]. In 1 M chloride solutions Pd(II) exists as  $\text{PdCl}_4^{2-}$  and since the dominant Pt(IV) chloride complex under these conditions is  $\text{PtCl}_6^{2-}$ , it therefore follows that our species of interest in separations being investigated are  $\text{PdCl}_4^{2-}$  and  $\text{PtCl}_6^{2-}$ .



**Figure 1.5** The species distribution curves for palladium(II) as a function of the log of the chloride ion concentration [29]

### (c) Rhodium chlorido species

There is a comparison between rhodium and palladium in that both are 4d transition metals. Ligand exchange for rhodium(III) species is again much faster than their group analogue iridium(III). Rhodium(III) forms stepwise various chlorido complexes. However, in hydrochloric acid medium the most important ones would be  $[\text{RhCl}_3(\text{H}_2\text{O})_3]$ ,  $[\text{RhCl}_4(\text{H}_2\text{O})_2]^-$ ,  $[\text{RhCl}_5(\text{H}_2\text{O})]^{2-}$  and  $\text{RhCl}_6^{3-}$  [32,33]. The formation constants of the chlorido species of rhodium have been determined by a number of authors [34-37]. The distribution curves presented in Figure 1.6 show that the  $[\text{RhCl}_5(\text{H}_2\text{O})]^{2-}$  species is an important species in a wide range of chloride ion concentrations. This is important in the separation chemistry since the  $\text{Rh}_2\text{Cl}_9^{3-}$  species readily forms from this species by the reaction given below:



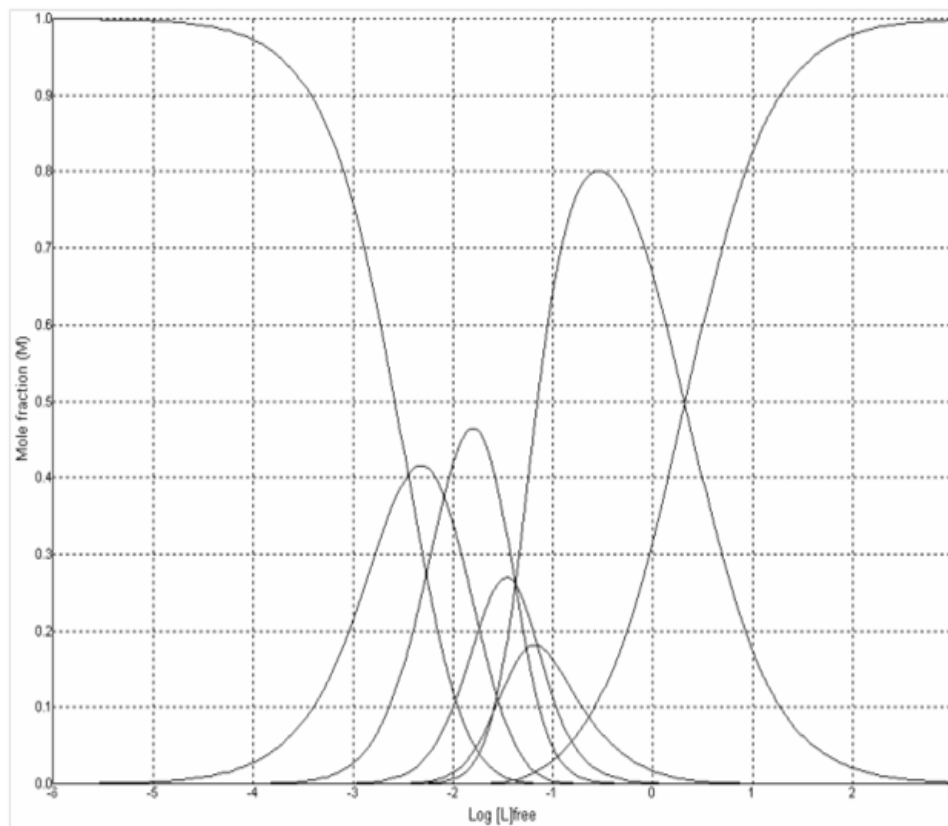


**Figure 1.6** The species distribution curves for rhodium(III) as a function of the log of the chloride ion concentration [29]

**(d) Iridium chlorido species**

The chemistry of rhodium and iridium is similar. The normal differences between a 4d and 5d metal is that 5d metal are very much slower in ligand exchange than the 4d metal and secondly the greater readiness to which the 5d is oxidized to the higher oxidation state. The two oxidation states of iridium hexachlorido species, namely (III) and (IV), can occur in practical separation chemistry apart from the various aquated forms of each of the two [38]. A further important aspect to consider in a two-phase separation system is the fact that the relative concentration of the iridium(IV)/iridium(III)

species can greatly be altered by the presence of cationic species which prefers the one over the other as compared to the homogeneous system (single phase). A great similarity in the behaviour of  $\text{IrCl}_6^{2-}$  and  $\text{PtCl}_6^{2-}$  is a major problem in their separation chemistry. The formation constants for iridium are not available, however the species distribution curves [39,40] of iridium(III) can be expected to be similar to those of rhodium(III) while that of iridium(IV) similar to platinum(IV).

**Table 1.1** Dominant chlorido iridium(III)/(IV) species as a function of HCl [40]

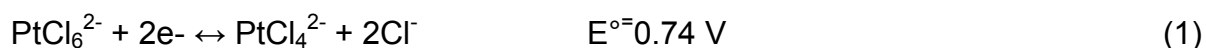
[HCl]	Dominant species for iridium(III)	Dominant species for iridium(IV)
0.1 M	$\text{IrCl}_3(\text{H}_2\text{O})_3$	
1.4 M	$\text{IrCl}_3(\text{H}_2\text{O})_3$	
4 M	$\text{IrCl}_4(\text{H}_2\text{O})^{2-}$	
6 M	$\text{IrCl}_4(\text{H}_2\text{O})_2^-$	$\text{IrCl}_5(\text{H}_2\text{O})^-$ , $\text{IrCl}_6^{2-}$
8 M	$\text{IrCl}_5(\text{H}_2\text{O})^{2-}$	

### 1.3.2 Redox chemistry of PGMs

The equilibrium redox behavior of PGMs in chloride medium depicts that it is harder to achieve the higher oxidation states as one moves across the period, and an increase in stability of the higher oxidation states in moving from top to the bottom of the group [22]. Kinetic and thermodynamic factors are involved in redox reactions, therefore the oxidation states of PGM can be "tuned" by selective oxidation or reduction such that a

variety of combinations are possible. It is very possible to achieve separation by the successive manipulation of the oxidation states of the metals.

The first thing to consider will be the much slower kinetics of substitution for both  $\text{PtCl}_4^{2-}$  and  $\text{PtCl}_6^{2-}$  and the greater relative stability of Pt(IV) as compared to Pd(IV):



In the case of palladium the redox potential to obtain  $\text{PdCl}_6^{2-}$  is so high (equation 2) that it is readily decomposed and rarely plays a significant role in separation chemistry. The  $E^\circ$  value of the



Secondly, a further important parameter is the kinetics of substitution which is faster by an approximate factor of  $1 \times 10^5$  than the analogous platinum kinetics. This factor is quite important since this enables the separation of palladium(II) from platinum(IV) [26].

The Rh(III)/Rh(IV) redox potentials is similar to that palladium [29].



Equation 3 implies that Rh(IV) is not significant in its separation chemistry.

The difference in their  $E^\circ$  value allows for the exploitation of their redox properties as the oxidation of iridium(III) to iridium(IV) in chloride medium is 0.96 V (equation 5).



## **1.4 Fabrication of ion exchange materials**

A wide range of sorbent materials with different functionalities have been used to study the adsorption and separation of metal ions by solid phase extraction using materials such as silica gel, activated carbon and polymer resins [41-44]. The most adequate classification for these sorbents materials will be based on the kind of functional group responsible for their performances (selectivity and capacity). The nitrogen, sulfur, oxygen and phosphorus-functionalized polymer materials as well as activated carbon-based sorbents have been employed [45].

### **1.4.1 N-containing ion-exchange materials**

Polystyrene-based matrix functionalized with mono-, di-, aliphatic and polyamines have been used as ion exchange materials and recoveries of over 95% were achieved for noble metals [46,124-131]. Amberlite IRA 35 (Figure 1.7) sorbent has proved efficient and selective for enrichment of chlorido complexes of Au(III), Pd(II), and Pt(IV) from complex solution containing other metal ions and salts in acidic solutions [47]. Dowex 1-X8 resin has been utilized for enrichment of noble metals from geological samples [48-51], for Pd from copper ores and concentrates [52], and also Pd and Pt from environmental samples [53-55].

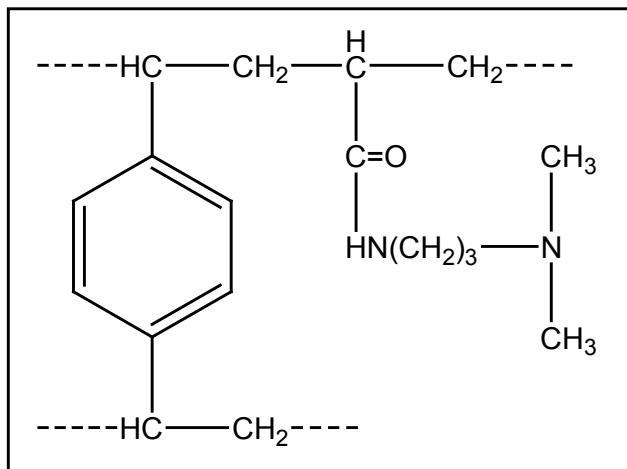


**Figure 1.7** Structures of Amberlite IRA 35 [47]

Application of modified silica gel with functional groups has been employed in several solid phase supported systems such as in catalysis [56,57], ion-exchange [56,58], chromatography [59,60], solid phase extraction and metal ion pre-concentration [61,62]. The attraction was due to its good mechanical strength, swelling stability and fast metal exchange kinetics required for its use in different types of chromatographic systems. Silica-based polyamine anion-exchangers containing monoamine, ethylenediamine, and diethylenetriamine functionalities (Figure 1.5 a-c) have shown high selectivity towards Pd and Pt and are successfully applied for their recovery from precious metals refinery effluents [63, 144-150].

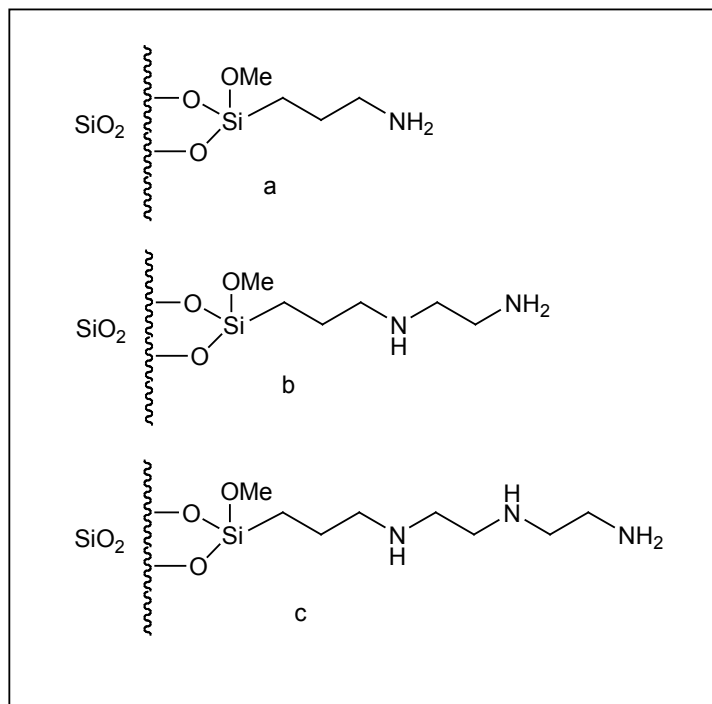


**Figure 1.8** Structures of silica-based polyamine anion exchanges with (a) monoamine, (b) ethylenediamine, and (c) diethylenetriamine functionalities [63]

An interesting aspect of this investigation is the use of polystyrene-based sorbents containing ammonium functionalities at a nanoscale (in a form of nanofibers). The high surface area and porosity offered by nanofibers may lead to high loading capacities and the porosity may result in materials that are good for use under flow conditions. The surface functionalization (which is possible through post-electrospinning functionalization) may also improve the kinetics of metal uptake. The polystyrene-based nanofibers were functionalized with ammonium centres derived from ethylenediamine (EDA), diethylenetriamine (DETA), triethylenetriamine (TETA) and *tris*-(2-aminoethyl)amine (TAEA). The performance of the polystyrene-based nanofibers was

compared with the microspherical beads for similar functionalities. The selective separation of  $\text{PtCl}_6^{2-}$  from  $\text{PdCl}_4^{2-}$  was investigated as well as the separation of  $\text{PtCl}_6^{2-}$  from chlorido species of rhodium(III) and iridium(IV) under 1 M HCl conditions.

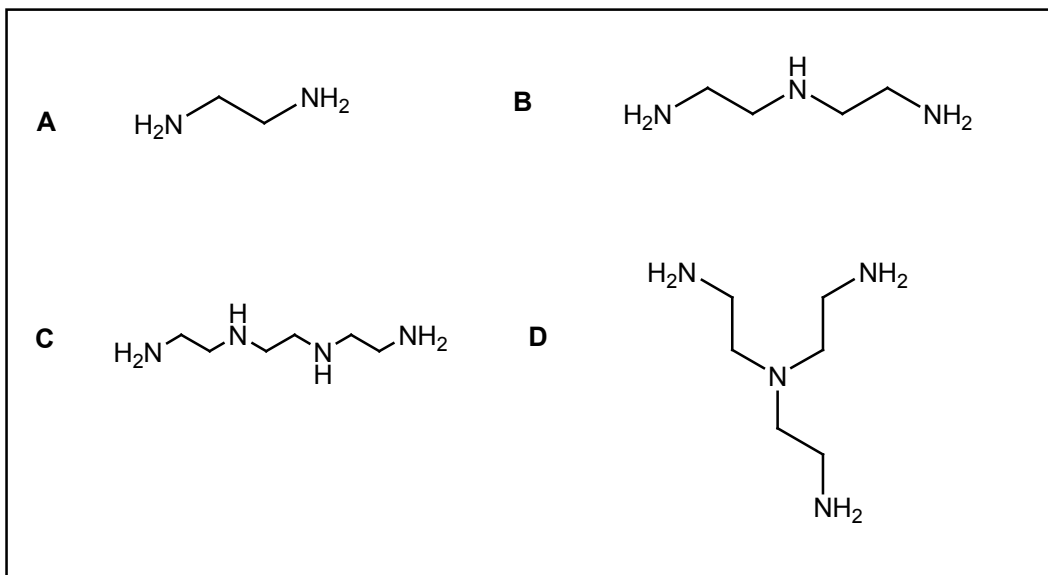


**Figure 1.9** The chemical structures of amines used for functionalization; (A) EDA, (B) DETA, (C) TETA and (D) TAEA

### 1.5 Fabrication of nanofiber materials

Nanofibers are an exciting new class of materials used for several value added applications such as medical, filtration, barrier, wipes, personal care, composite, garments, insulation, energy storage [64,65], sample clean-up [66,67] and catalysis [68], to mention but a few. Nanofibers with a diameter range of 10 to 2000 nm can be achieved by choosing suitable electrospinning parameters [69]. Electrospinning is an

effective method for producing nanofibers under the influence of electrical charges [70-73]. An advantage of nanofibers is the ease of surface chemistry modification in order to accommodate various functionalities. Nanofibers also possess unique characteristics such as high surface area per unit mass, high porosity, excellent structural mechanical properties and high axial strength combined with extreme flexibility. A number of techniques have been employed in the production of fibrous scaffolds. These are self-assembly, drawing, template synthesis, phase separation, wet spinning, electrospinning and combinations of these [74, 75].

### **1.5.1 Self-assembly**

This method involves the arrangement of atoms and molecules via weak non-covalent interactions (H-bonding, hydrophobic forces, electrostatic interactions) producing stable structures [76]. It produces fibers of smaller diameters. Its major disadvantage is that it is a complex, long, and extremely elaborate technique with low productivity [76].

### **1.5.2 Dry spinning**

This is a method used to form polymeric fibers from solution. It involves the dissolution of polymer in a volatile solvent and the solution is pumped through a spinneret composed of numerous holes. Stretching of the fibers provides for orientation of the polymer chains along the fiber axis. This technique is used only for polymers that cannot be melt spun [77].

### **1.5.3 Drawing method**

Drawing method is similar to dry spinning and single nanofibers can be produced. It requires a minimum amount of equipment, and is a discontinuous process. A micropipette is dipped into a droplet near the solution solid surface contact line *via* a micromanipulator. Then the micropipette is withdrawn from the liquid at a certain speed, yielding a nanofiber. These steps are repeated many times on each droplet. The solution viscosity, however, increases with solvent evaporation and some fiber breaking occurs due to instabilities that occur during the process [78]. Drawing process is disadvantageous since it requires solutions of only viscoelastic materials, which can undergo strong deformations that are cohesive enough to withstand the stresses developed during pulling. The fiber size is dependent on the orifice size of the extrusion mould and it is difficult to obtain fiber diameters less than 100 nm.

### **1.5.4 Phase separation**

This process has five steps, namely polymer dissolution, gelation, solvent extraction, freezing, and freeze-drying. The polymer is first dissolved in an appropriate solvent at the desired concentration and stirred at a required temperature for a period of time until a homogeneous solution is obtained. The solution is then transferred into a refrigerator for gelation. The resultant gel is immersed in water several times to allow solvent exchange. Finally, the gel is removed from water, transferred to a freezer (-70°C), and then the frozen gel is lyophilized [79]. Phase separation occurs due to physical incompatibility and yields nanofibers. The disadvantage of this method is that no long

continuous fibers are produced and only the polymers that have gelation capability can be used to produce the nanofibrous structure.

### **1.5.5 Wet spinning**

This method is based on precipitation, which starts by dissolving the polymer in a suitable organic solvent or in a weak inorganic solvent in order to prepare the spinning dope. The polymer solution is then transferred to a reservoir of a (glass) spinneret whose free end is positioned in a bath containing a polymer. The solution is then allowed to flow under gravity through the spinneret into the non-solvent and precipitation or coagulation occurs. This results in fibers with a diameter range varying from 10 to 100  $\mu\text{m}$  [80].

### **1.5.6 Electrospinning**

The most preferred method for fabrication of fibers in nano and low micro-scale is electrospinning. Since the 1980s and especially in the last 10 years there has been an increase in the attention paid by researchers to this method due to an increased interest in nanotechnology.

Electrospinning is a novel and efficient fabrication process that can be utilized to assemble fibrous polymer mats composed of fiber diameters ranging from several microns down to 100 nm [81-84]. The schematic of the electrospinning set-up are shown in Figures 1.10 and 1.11. The electrospinning apparatus consists of three

components, namely; the syringe connected to a spinneret (needle), a high voltage power supply and a grounded metal sheet collector. An electric field is subjected to the end of a capillary tube that contains the polymer fluid held by its surface tension. The high voltage electric field induces a charge on the surface of the liquid and the mutual charge repulsion causes a force directly opposite to the surface tension [85]. As the intensity of the electric field is increased, the hemispherical surface of the fluid at the tip of the capillary tube elongates to form a conical shape known as the Taylor cone (the base region). With increasing field, a critical value is attained when the repulsive electrostatic force overcomes the surface tension and a charged jet of fluid is ejected from the tip of the Taylor cone. The discharged polymer solution jet undergoes a whipping process wherein the solvent evaporates, leaving behind a charged polymer fiber, which is highly stretched and reduced in diameter as it travels before it lays itself randomly on a grounded collecting metal screen (the jet region).

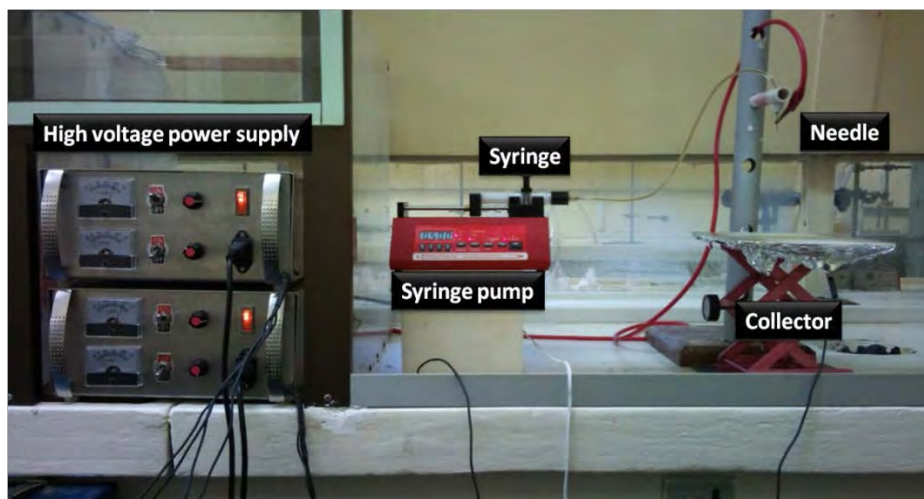


**Figure 1.10** The picture of the electrospinning set-up used in this study

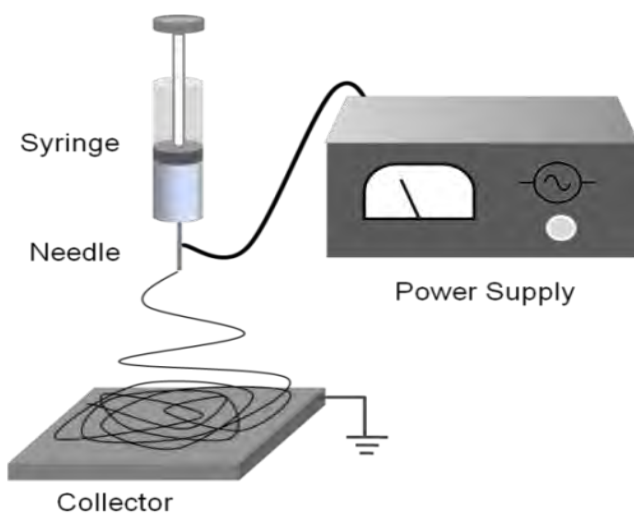


**Figure 1.11** Schematic diagram of an electrospinning set-up [67]

### **(a) Factors that affect electrospinning and fibers morphology**

Electrospinning and fibers morphology can be influenced by the following factors; polymer properties (e.g. polymer structure, molecular weight, solubility), solvent (e.g. boiling point, dielectric properties), solution properties (e.g. viscosity, concentration, conductivity, surface tension), operation parameters (e.g. applied voltage, collecting distance, flow rate), and ambient environment (e.g. temperature, gas environment, humidity).

**Process parameter:** This current study also proved that higher potentials give rise to fibers with thinner diameters. Pore size also has been reported to decrease with potential increase because the drawing rate and fiber crossings increase [86]. The hydrostatic pressure in the capillary tube of the needle can also affect the results. The polymer solution is forced out of the needle orifice by the applied electric field [87], gravity [88], or a pump [89]. Flow rate and needle size has also been found to influence electrospinning process. Fiber diameter can be affected by the size of the needle, smaller needle orifices have been reported to contribute to thinner fiber formation [90]. Another parameter is the distance between needle and collector. A decrease in distance, regardless of the concentration of the polymer solution, results in the formation of wet fibers and beaded structures [90, 91].

**Ambient Parameters:** The following are the three major environment-related parameters that should be taken into consideration; solution temperature, medium

humidity, and air velocity in the electrospinning chamber. An increase in solution temperature results in solution chain formation, decrease in solution viscosity and increase in solvent evaporation. All these factors influence fiber morphology. An increase in humidity leads to an increase in diameter, number, shape and distribution of pores. A relative humidity higher than 30% led to micro- and nano-structured pores on the surface of fibers [92].

**Polymer and Solvent-Related Parameters:** The structure of a polymer has a great impact on its solubility. Polymer with higher molecular weight is less soluble and takes longer time to dissolve than polymer with lower molecular weight using the same solvent. This is because the intermolecular forces between longer chain molecules are stronger and the solvent molecule takes longer time to diffuse into the bulk. The architecture of the polymer also affects processing; for instance, branched polymers seem to need a higher concentration than linear polymers in order to form defect-free nanofibers [93].

The properties of the solution such as surface tension, conductivity and viscosity determines its stretching potential. The rate of evaporation will influence the viscosity of the solution. Viscosity appears to be very important factor in this configuration. It is related to the extent of polymer molecule chains entanglement within the solution. At lower viscosity polymer chain entanglements are lower and this leads to formation of beaded fibers and this can also result into electrospaying. Electrospaying occurs, when entanglement of polymer chains does not occur but still undergoes a bending

instability that causes a whip-like motion between the capillary tip and the grounded target. Very high viscosities, on the other hand, prevent ejection of the solution from the syringe tip due to a high surface tension and this is called suppression [94-97]. An appropriate solution viscosity is important for an efficient electrospinning process.

To achieve nanofibers in the range of 100 to 2000 nm diameter appropriate polymer solvent system must be chosen [98]. Table 1.2 gives list of some of polymer solvent systems used in electrospinning.

**Table 1.2** Polymer solvent systems for electrospinning [98]

<b>POLYMER</b>	<b>SOLVENTS</b>
Nylon 6 and nylon 66	Formic Acid
Polyacrylonitrile	Dimethyl formaldehyde
PET	Trifluoroacetic acid/Dimethyl chloride
PVA	Water
Polystyrene	DMF/Toluene
Nylon-6-co-polyamide	Formic acid
Polybenzimidazole	Dimethyl acetamide
Polyamide	Sulfuric acid
Polyimides	Phenol

## **(b) Functionalization of nanofibers**

An exciting feature about nanofibers is the ease of surface modification in order to accommodate various functionalities [99,100]. Functionalization can be achieved before electrospinning process which is termed pre-electrospinning functionalization. This involves the introduction of functional groups into the polymer solution before spinning. The other is post-electrospinning functionalization. In this case the nanofibers are functionalized after electrospinning. This study has employed the latter to introduce amine functional groups onto the polymeric materials.

### **1.6 Scope of the study**

The aim of this study entails the functionalization of ion exchange materials for the separation of PGMs through the functionalization of polystyrene-based microparticles and nanofibers as well as silica microparticles with amines. It is also desirable to investigate factors that influence the performance of these materials such as level of functionalization, surface area and particle sizes. The objectives are as follows:

- (a) Functionalization of silica and polystyrene-based microparticles with amines
- (b) Fabrication of polystyrene-based nanofibers and their functionalization with amines
- (c) The evaluation of the sorption capacity and the selectivity of these ion-exchange materials towards  $\text{PtCl}_6^{2-}$  and  $\text{PdCl}_4^{2-}$ .

# CHAPTER 2

## MATERIALS, EXPERIMENTAL TECHNIQUES AND METHODS

### 2.1 Materials

**Table 2.1** List of chemicals and reagents used

<b>Chemicals</b>	<b>Purity/Concentration/ Particle size</b>	<b>Supplier</b>
Hydrochloric acid(HCl)	0.0364 g/ml	Merck Chemicals
Azobisisobutyronitrile(AIBN)	98%	Sigma-Aldrich
Vinylbenzylchloride(VBC)	90%	Sigma-Aldrich
Thiourea	99%	Sigma-Aldrich
Ethylenediamine(EDA)	75-80%	Sigma-Aldrich
Diethylenetriamine(DETA)		Sigma-Aldrich
Triethylenetetramine(TETA)	97%	Sigma-Aldrich
<i>Tris</i> -(2-aminoethyl)amine (TAEA)	96%	Sigma-Aldrich
3-chloropropyltrimethoxysilane (CTMEOS)	97%	Sigma-Aldrich
Silica	230 – 400 mesh	Merck Chemicals
Merrifield resin	1% crosslinked, [Cl]: 1.2mmol/g, 40-60 mesh	Sigma-Aldrich

**Table 2.1** Continued

Sodium iodide (NaI)	99%	Saarchem
Potassium tetrachloropalladate(II) (K <sub>2</sub> PdCl <sub>4</sub> )	98%	Merck Chemicals
Potassium tetrachloroplatinate(II) (K <sub>2</sub> PtCl <sub>4</sub> )	98%	Merck Chemicals
Hydrogenperoxide (H <sub>2</sub> O <sub>2</sub> )	30%	Merck Chemicals
Iridium(III)chloride hydrate (IrCl <sub>3</sub> ·xH <sub>2</sub> O)	99.9%	Sigma-Aldrich
Rhodium(III)chloride (RhCl <sub>3</sub> )	98%	Sigma-Aldrich
Hydrochloric acid (HCl)	32%	Merck Chemicals
Toluene	99%	Merck chemicals
Tetrahydrofuran (THF)	99.5%	Merck Chemicals
Methanol (CH <sub>3</sub> OH)	99.9%	Sigma-Aldrich
Ethanol (EtOH)	99%	Sigma-Aldrich
Diethyl ether	99%	Merck Chemicals
<i>N,N</i> -Dimethylformamide (DMF)	99%	Merck Chemicals

## 2.2 Spectroscopic techniques

### 2.2.1 NMR Spectrometry

The identity of  $\text{PtCl}_6^{2-}$  was determined by  $^{195}\text{Pt}$  NMR spectroscopy. The isotopes of platinum in decreasing order of their relative abundance are; 196 (18), 195 (9), 194 (7) and 192 (1) [101]. Relevant properties are that the  $^{195}\text{Pt}$  nucleus is 34% abundant with a spin of 1/2 and is homonuclear. It is therefore free of quadrupolar effects and a Ruderman–Kittel indirect exchange coupling between nuclear spins produces narrowing of the dipolar line width [101, 102]. Platinum nuclear spins have a short spin-lattice relaxation time. There is a great advantage in performing NMR experiments at low temperatures.

The use of high-resolution  $^{195}\text{Pt}$  NMR spectroscopy as a tool to examine the distribution and speciation of Pt(II/IV) complexes in chloride-rich aqueous solutions has been studied showing the utility of  $^{195}\text{Pt}$  “chemical-shift-trend” analysis as a means of rapid assignment of, for example, the entire series of  $[\text{PtCl}_{6-n}(\text{H}_2\text{O})_n]^{2-}$  ( $n = 0-6$ ) and  $[\text{PtCl}_{6-m-n}\text{Br}_m(\text{H}_2\text{O})_n]^{2-}$  ( $m, n = 0-6$ ) complexes in synthetic solutions intended to mimic process solutions [103]. Therefore  $^{195}\text{Pt}$  NMR spectroscopic “fingerprint” was used for identification of Pt(IV) chlorido complex used in this study.

### 2.2.2 Infrared Spectroscopy

The sorbent materials were characterised by using infrared spectroscopy and recorded on either a Perkin Elmer 400 FTIR spectrometer in the mid-IR range ( $4000 - 400 \text{ cm}^{-1}$ )

as KBr pellets or as neat compounds with a Perkin Elmer 100 FTIR-ATR (4000 – 650  $\text{cm}^{-1}$ ) spectrometer.

## **2.3 Analytical methods**

### **2.3.1 Elemental analysis**

Elemental analysis was carried out with a Vario Elementary ELIII Micro-cube CHNOS elemental analyser [104]. The basic principle of quantitative CHNOS analysis is high temperature combustion of organic and many inorganic solid or liquid samples [105]. The gaseous combustion products are purified, separated into their various components and analyzed with a suitable detector such as thermal conductivity detector (TCD), optional infrared detector (IR) for sulfur, etc. The calibration of the instrument was done using standards.

Standard 1: Sulfanamide; C, 41.81; H, 4.65; N, 16.25 and S; 18.62%

Standard 2: Acetanilide; C, 71.09; H, 0.67; N, 10.36 and O; 12.0%

### **2.3.2 Inductively coupled plasma (ICP) spectrometry**

Metal ion analyses were carried out with a Thermo Electron (iCAP 6000 Series) inductively coupled plasma (ICP) spectrometer equipped with an OES detector. The ICP/AAS metal standards, dissolved in 1 M HCl, were used to prepare standard solutions for the construction of calibration curves using distilled, deionized, milliQ water

for the dilutions. The elements were analysed at the following US-EPA [106] specified wavelengths (nm) for minimal interferences; 214.4 Pt(IV), 342.1 Pd(II), 343.4 Rh(III) and 224.2 Ir(IV). The calibration ranges were 0.5-4 ppm for Pt(IV) and Pd(II), and 1-5 ppm for Ir(IV) and Rh(III).

The Thermo Electron iCAP 6000 Series-optical emission spectrometer was operated with the parameters in Table 2.2. The elements (atoms) are excited and when they return to low energy status, emission rays are released and the emission rays that correspond to the photon wavelength are measured [107]. The element type is determined based on the element emission line at specific wavelength, and the content of each element is further determined based on the rays' intensity.

To generate plasma, first, argon gas is supplied to the torch coil, and high frequency electric current is applied to the work coil at the tip of the torch tube. Using the electromagnetic field created in the torch tube by the high frequency current, argon gas is ionized and plasma is generated. This plasma has high electron density and temperature (10000 K), and this energy is used in the excitation-emission of the sample. Solution samples are introduced into the plasma in an atomized state through the narrow tube in the centre of the torch tube.

**Table 2.2** ICP-OES method and operating parameters

<b>Parameter</b>	<b>Setting</b>
Applied radio frequency (RF) power	1150 W
Plasma (Ar) gas Flow rate	5.0 L/min
Auxiliary gas flow rate	0.5 L/min
Nebulizer Ar gas flow rate	1.5 L/min
Sampling depth	8.5 mm
Sample pump rate	50 rpm
Time scan acquisition	50 ms/point
Cooled spraying chamber temperature	4°C
The camera temperature	46.63°C
Generator temperature	24°C
Optics temperature	36.9°C
Total integration time	30 s per analyte
Sample flush time	30 s
Number of replicates	3

## **2.4 Surface characterization techniques**

### **2.4.1 Scanning electron microscopy**

Samples were prepared for scanning electron microscopy (SEM) by mounting on the SEM stubs using double-sided graphite tape and then sputter coated with gold using a Balzers' union sputtering device [108]. The samples were viewed using a TESCAN Vega TS 5136LM typically at 20 kV at a working distance of 20 mm.

A scanning electron microscope (SEM) is a form of electron microscope used for producing images of a sample by scanning it with a beam of electrons in form of raster scan patterns. The electrons are made to interact with the atoms of the samples thereby producing signals that contain information about the sample's surface topography as well as its composition [109].

Electron beam which possess energy ranging from 0.2 k eV to 40 k eV, is focused by one or two condenser lenses to a spot about 0.4 nm to 5 nm in diameter. As the beam of electron passes through pairs of scanning coils or pairs of deflector plates in the electron column in the final lens, the beam is deflected so that it scans in a rectangular fashion over an area of the sample surface. As the primary beam interacts with the sample, the electrons lose energy by repeated random scattering and absorption within a teardrop-shaped volume of the specimen known as the interaction volume, which extends from less than 100 nm to around 5  $\mu\text{m}$  into the surface [110]. The electron's landing energy, the atomic number of the specimen and the specimen's density are all determining factors of the size of the interaction volume [111]. The high-energy electrons is as a result of the reflection energy exchange between the electron beam

and the sample and this can be detected by specialized detectors. The specimen absorbs the beam current which can be detected and used to create images. SEM micrograph is known to have magnification of a range of up to six orders of magnitude from about 10 to 500,000 times [112].

#### **2.4.2 X-ray photoelectron spectroscopy**

X-ray photoelectron spectroscopy (XPS) is a quantitative spectroscopic technique that measures the elemental composition, empirical formula, chemical state and the electronic state of the elements that exist on a surface of a material [113]. X-ray photoelectron spectroscopy (XPS) measurements were performed with a Kratos Axis Ultra X-ray Photoelectron Spectrometer equipped with a monochromatic Al  $K_{\alpha}$  source (1486.6 eV). The base pressure of the system was below  $3 \times 10^{-7}$  Pa. XPS experiments were recorded with 75 W power source using hybrid-slot spectral acquisition mode and an angular acceptance angle of  $\pm 20^{\circ}$ . The analyzer axis made an angle of  $90^{\circ}$  with the specimen surface, with the specimen surface making an angle of  $45^{\circ}$  with the X-ray angle. Charge neutraliser was used due to the insulating surface used to prepare the sample. The elemental analysis and element core level were recorded with a step of 1eV and pass energy of 160 eV. XPS data analysis was performed with Kratos version 2 programs.

The XPS spectra are produced from the irradiation of a material with a beam of X-rays while simultaneously measuring the kinetic energy and number of electrons that escape from the top to 1 to 10 nm of the materials that is being analyzed [114]. The basic

principle of this technique is based on the irradiation of the sample surface with monochromatic X-rays. This radiation hits the core electrons of the atoms. The core electrons are targeted because being closer to the nucleus their binding energies are characteristics of their particular elements [115]. By targeting these electrons information on the elements of the particular sample can be obtained.

The kinetic energies of the ejected electrons differ depending on the orbitals from which they originate, these energies are then related to the orbital ionization potential of the molecule or sample atom [116]. Since core level electrons in solid state atoms are quantized, the resulting energy spectra exhibit resonance peaks characteristic of the electronic structure for the atom at the sample surface. For each and every element, there will be a characteristic binding energy associated with each core atomic orbital, i.e. each element will give rise to a characteristic set of peaks in the photoelectron spectrum at kinetic energies determined by the photon energy and the respective binding energies. Furthermore, because the binding energies differ not only from chemical species to species, but also vary with the bonding conditions in which the element is found, this technique also provides information on the actual compounds present on the surface. The XPS technique is highly surface specific due to the short range of the photoelectrons that are excited from the solid. The energy of the photoelectrons leaving the sample is determined using a Concentric Hemispherical Analyser (CHA), and this gives a spectrum with a series of photoelectron peaks [117].

## **2.5 Adsorption experiments**

Adsorption is a process that occurs when a gas or liquid solute accumulates on the surface of a solid or liquid (adsorbent), forming a molecular or atomic film (the

adsorbate). It is operative in most natural physical, biological, and chemical systems, and is widely used in industrial applications such as activated charcoal, synthetic resins for water purification [118].

Adsorption is usually described through isotherms, that is, functions which connect the amount of adsorbate on the adsorbent, with its pressure (if gas) or concentration (if liquid). There are several models describing process of adsorption, namely Freundlich isotherm, Langmuir isotherm, BET isotherm, etc [119-122]. The Freundlich and Langmuir isotherms have been used extensively to describe adsorption of analytes onto solid phases from aqueous solutions, despite the fact that the initial development of these models was intended for application in gas adsorption.

### **2.5.1 Brunauer, Emmett, Teller (BET) surface area analysis**

Carbon dioxide adsorption/desorption isotherms were measured at 77K using a Micromeritics ASAP 2020 Surface Area and Porosity Analyzer. Nitrogen was not used as an adsorbate because carbondioxide used as the adsorbate has a greater degree of penetration and is more energetic even at an appreciable higher temperature [123]. Prior to each measurement, samples were degassed for a minimum of one week to ensure complete removal of adsorbed impurities. Degassing was performed at 70°C for the linear polymers and at 150°C for cross-linked polymers, unless mentioned otherwise. Approximately 0.2 g of sample was used and an equilibration interval of 20 seconds was allowed during the run. The surface area (BET), were calculated from these isotherms.

The theory of BET which explains the physical adsorption of gas molecules on a solid surface provides the basis for the measurement of the specific surface area of a material [121]. The basis of the theory is an extension of the Langmuir theory which is summarized by equation (6). Langmuir theory deals with monolayer molecular adsorption and multilayer adsorption built on the hypothesis that gas molecules are adsorbed on solid layers infinitely and that there is no interaction between each adsorption layer.

$$\frac{1}{V[(P_0/P-1)]} = \frac{C^{-1}}{V_m C} \left( \frac{P}{P_0} \right) + \frac{1}{V_m C} \quad (6)$$

where  $P$  and  $P_0$  are the equilibrium and the saturation pressure of adsorbate at the temperature of adsorption,  $V$  is the adsorbed gas quantity (e.g., in volume units),  $V_m$  is the monolayer adsorbed gas quantity.  $C$  is the BET constant, which is expressed by equation (7);

$$C = \exp\left(\frac{E_1 - E_L}{RT}\right) \quad (7)$$

A plot known as BET plot can be generated by plotting the adsorption isotherm in equation 1 with  $V[(P_0 / P-1)]$  on the y-axis and  $\phi = P / P_0$  on the x-axis according to experimental results.

The BET method is widely used in surface science for the calculation of surface areas of solids by physical adsorption of gas molecules. A total surface area  $S_{total}$  and a specific surface area  $S$  are evaluated by the following equations 8 and 9

$$S_{BET,total} = \frac{(V_m N_s)}{V} \quad (8)$$

where  $v_m$  is in units of volume which are also the units of the molar volume of the adsorbate gas.

$$S_{\text{BET}} = \frac{S_{\text{total}}}{a} \quad (9)$$

where  $N$  is Avogadro's number,  $s$  is adsorption cross section of the adsorbing species,  $V$  is molar volume of adsorbate gas, and  $a$  is mass of adsorbent (g).

### 2.5.2 Langmuir isotherm

This isotherm explains that the adsorption mechanism on the surface of adsorbents is of monolayer coverage. This is expressed by the equation (10)

$$\frac{C_e}{Q_e} = \frac{1}{Q_m} + \frac{C_e}{bQ_m} \quad (10)$$

where  $C_e$  is the concentration of the metal ions at equilibrium in the solution (mg/l),  $Q_e$  is the amount of metal ions adsorbed per unit mass of the adsorbent (mg/g); the constant  $Q_m$  is the theoretical saturation adsorption capacity of the monolayer (mg/g) and  $b$  is related to the energy of adsorption (L/mg).

In order to predict the adsorption efficiency of the adsorption process, the dimensionless equilibrium parameter ( $R_L$ ) is used which was defined as  $R_L = 1 / 1 + b C_o$ , where  $b$  is the Langmuir constant and  $C_o$  is the initial concentrations of metal ions [118,120].  $R_L$  values within the range  $0 < R_L < 1$ , indicate favourable adsorption.

### 2.5.3 Freundlich isotherm

This isotherm describes the heterolayer adsorption on the surface of the adsorbents. It can as well be expressed by equation (11)

$$\text{Log } Q_e = \text{log } K_f + \frac{1}{n} \text{log } C_e \quad (11)$$

where  $C_e$  is the equilibrium concentration (mg/L);  $Q_e$  is the amount of metal ions adsorbed per gram of sorbent, and  $K_f$  and  $n$  (dimensionless) is the heterogeneity factor. The values of  $1/n$  less than 1 represent a favourable adsorption [121].

### 2.6 Column experiment

The fixed bed column experiments were conducted for metal solutions using glass columns of length 10 cm, inner and tip diameters of 3.5 and 1 mm respectively. The column was packed with adsorbent between two supporting layers of glass wool. The adsorbent was added from the top of the column and allowed to settle by gravity force. The column adsorption and separation protocol was carried out by conditioning the column with water and 1 M of hydrochloric acid for 24h. The column was loaded with the metal ions solutions, and equilibrated overnight. Washing and stripping of unloaded metal ions was carried out with HCl, HClO<sub>4</sub>, and NaClO<sub>4</sub>. Loaded metal ions were eluted with thiourea. The concentrations of metal ions in each fraction collected (0.5 mL) were determined by ICP-OES.

# CHAPTER 3

## ADSORPTION AND SEPARATION OF PLATINUM GROUP METALS USING POLYAMINE-FUNCTIONALIZED POLYSTYRENE-BASED BEADS AND NANOFIBERS

### 3.1 Introduction

There has been blossoming research activity centred on PGMs adsorption studies using a wide range of sorbent materials [44,124-126]. Anion exchange sorbents are effective and economical for PGMs separations compared to other methods such as precipitation and solvent extraction. Previous research works have been reported on adsorption of precious metals with the use of anion-exchange resins such as Amberlite resins (IRA-93, IRA-68 and IRA-400) [127], Amberyst A29 and A2 [128], TEVA resin [129], and Purolite A500 [130]. In all these studies, the chlorido anionic metal species interact *via* electrostatic interaction with the protonated or quaternized nitrogen of the amine functional groups. About 90% of all ion-exchange resins are based on a polystyrenic matrix.

The performance of polystyrene-based (Figure 3.1) systems can be improved by: (1) using heterogeneous cross-linked polystyrene and preparing the polymer in such a way that the functional groups are concentrated towards the surface of the resin, (2) using a cross-linker to heterogenize polystyrene in order to modulate the physical and chemical properties of the resin, (3) adding functional groups that provide desired properties (to

the polystyrene backbone), and (4) grafting styrene onto a heterogeneous support and the use of the graft as the point of substrate/reagent/catalyst attachment [131].

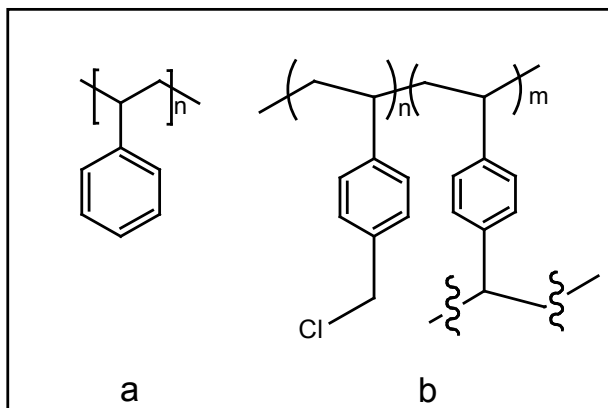
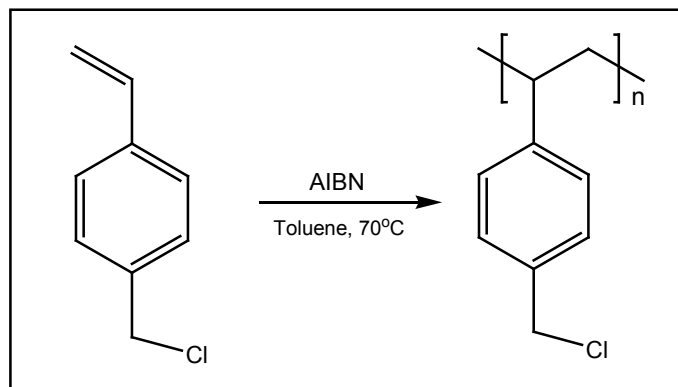


**Figure 3.1** Structures of (a) polystyrene and (b) Merrifield resin [132].

## 3.2 Experimental

### 3.2.1 Synthesis of poly(vinylbenzylchloride) (PVBC)

10 mL of 4-vinylbenzylchloride (VBC), 0.05 g of AIBN and 2 mL of toluene were stirred in a 20 mL vial. The mixture was polymerized under argon at 70°C for 9 h (Scheme 3.1). The product was dissolved in THF and the polymer was precipitated out with methanol, filtered and washed with methanol. The PVBC was allowed to dry in air. *Anal.* Found (%): C, 69.92; H, 6.82. Calculated (%): C, 70.83; H, 5.94; Cl, 23.23.



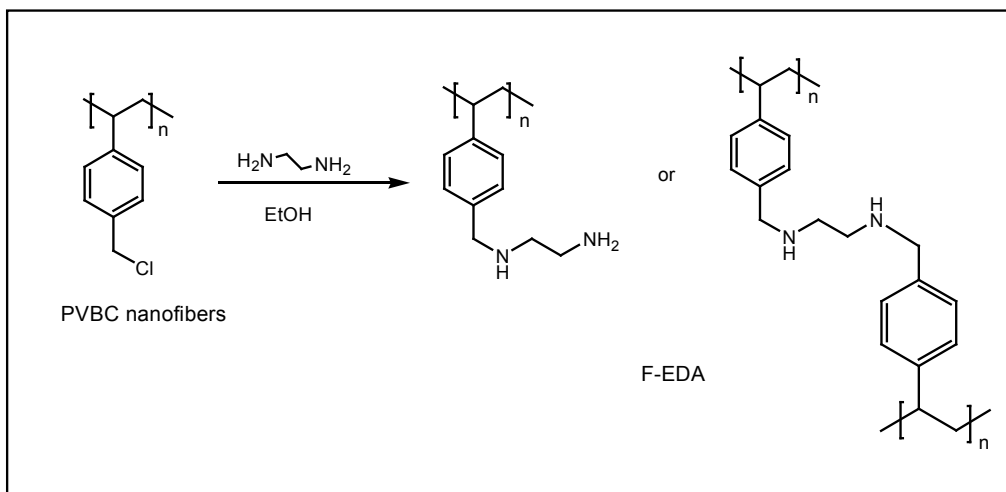
**Scheme 3.1** Synthesis of PVBC

### 3.2.2 Fabrication of PVBC nanofibers

25, 30, 35, 40 and 45wt% solutions of PVBC were prepared by weighing 1.25, 1.50, 1.75, 2.00, and 2.25 g respectively of the polymer and placing each in a 1:1 (v/v) ratio of DMF:THF solvent mixture. The mixtures were stirred at room temperature overnight until a homogeneous solution was formed. It was then transferred into a syringe. The syringe which was connected to an electrospinning set-up consisting of a high voltage supply and an aluminum collecting plate (Figure 1.7). The flow rate of the polymer solution was controlled using a programmable syringe pump. The solution was electrospun at a positive voltage of 20 kV, the tip-to-collector distance was 15 cm and the flow rate was 0.2 mL/h. All procedures were carried out at room temperature.

### 3.2.3 Functionalization of PVBC nanofibers

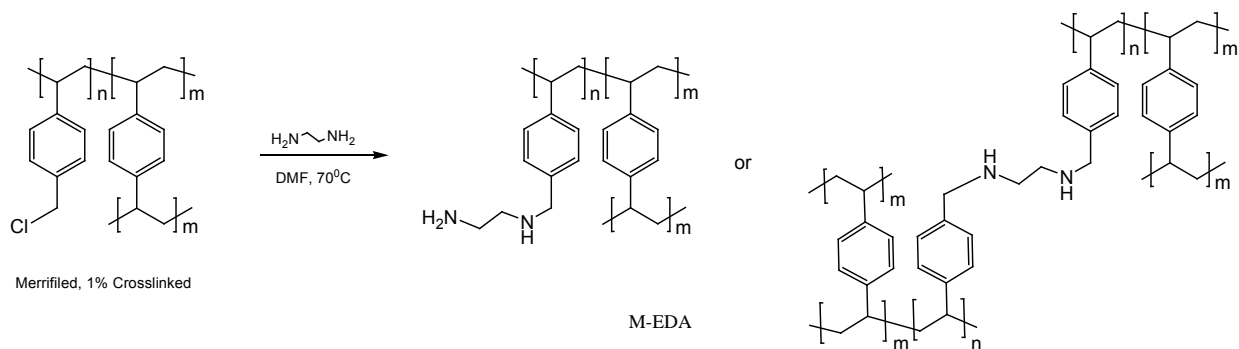
0.15 g of PVBC nanofiber (F) was soaked in 6.0 g of ethylenediamine (EDA) in 10 mL of ethanol and shaken on a mechanical shaker for five days (Scheme 3.2). The fibers were then removed, washed with methanol, Soxhlet extracted with methanol, and then dried in air. The same procedure was employed (for functionalization with other amines) except that 10.3 g of diethylenetriamine (DETA), 14.6 g of triethylenetriamine (TETA), and 14.6 g of tris-(2-aminoethyl) amine (TAEA) was used. *Anal.* Found (CHN, %): **F-EDA** (60.03, 8.82, and 10.83), **F-DETA** (69.25, 7.26, and 7.25), **F-TETA** (68.05, 7.19, and 2.05) and **F-TAEA** (31.88, 3.83, and 1.70).



**Scheme 3.2** Functionalization of nanofibers with ethylenediamine (F-EDA)

### 3.2.4 Functionalization of styrene-based beads

3 g of chloromethylated polystyrene beads (Merrified beads) were suspended in 30 mL of DMF and 18 g of ethylenediamine was added into the reaction mixture which was stirred for 15 h at 70°C (Scheme 3.3). The resin was then washed thoroughly with methanol and diethyl ether, and then Soxhlet extraction was carried out using methanol. The functionalized beads were collected and dried overnight in an oven at 40°C. The same procedure was employed for the (functionalization with) other amines. *Anal. Found* (CHN, %): **M-EDA** (85.15, 9.16, 5.61), **M-DETA** (73.53, 7.54, 7.87), **M-TETA** (83.08, 8.83, 5.45) and **M-TAEA** (75.38, 8.11, 7.72).



**Scheme 3.3** Synthesis of ethylenediamine functionalized Merrifield beads (M-EDA)

### 3.2.5 Preparation of metal solutions

An aqueous solution of 0.01 M  $\text{PdCl}_4^{2-}$  was prepared by dissolving 0.3 g of  $\text{K}_2\text{PdCl}_4$  in 1 M HCl and heated at 50°C for 30 minutes. A 0.01 M  $\text{PtCl}_6^{2-}$  solution was prepared by dissolving 0.2 g of  $\text{K}_2\text{PtCl}_4$  in 1 M HCl followed by 20 mL of  $\text{H}_2\text{O}_2$  and heated at 50°C for 30 minutes. Platinum, rhodium and iridium mixture was prepared by dissolving 0.2 g, 0.02 g and 0.01 g of  $\text{K}_2\text{PtCl}_4$ ,  $\text{RhCl}_3$  and  $\text{IrCl}_3 \cdot x\text{H}_2\text{O}$  respectively in 20 mL  $\text{H}_2\text{O}_2$  in 1 M

HCl, followed by heating at 50°C for 30 minutes. The platinum species were confirmed by using  $^{195}\text{Pt}$  NMR spectroscopy [101,103].

### 3.2.6 Batch adsorption studies

The batch adsorption studies were carried out by weighing 0.15 g of sorbents into a vial and then 3 mL of 0.01 M Pt(IV) and Pd(II) solutions in 1 M HCl medium were added. The mixture was shaken in a mechanical shaker for 1-30 min at room temperature. The solution was then filtered to remove the sorbent material and the concentrations of metal ions before and after adsorption were measured by ICP-OES.

The percentage adsorption (A %) of each metal ion was determined using equation 12:

$$A\% = \frac{C_o - C_e}{C_o} \times 100 \quad (12)$$

where  $C_e$  and  $C_o$  are the concentrations of the metal ions in the aqueous solutions after and before adsorption respectively.

The quantity of metal ions adsorbed onto the sorbents at equilibrium ( $Q_e$ , mg/g) was calculated using the mass balance equation:

$$Q_e = \frac{V(C_o - C_e)}{W} \quad (13)$$

where  $C_o$ ,  $C_e$ ,  $W$  and  $V$  are the initial metal concentration, equilibrium metal concentration, dry weight of adsorbent and solution volume respectively.

### 3.2.7 Adsorption isotherms

The adsorption mode of metal ions on sorbent materials is an important factor to investigate. Pt(IV) and Pd(II) metal ions solutions in the range 0.013 – 0.024 M were used to explain the adsorption model using the Langmuir and Freundlich isotherms, described by equations 10 and 11 (Chapter 2) respectively. The solutions were shaken for 30 minutes.

### 3.2.8 Column (dynamic) studies

A glass column was plugged with glass wool and packed with 0.3 g of the respective sorbent materials. The column was conditioned with 5 mL of water and 5 mL of 1 M HCl. 5 mL of 0.01 M metal ion solutions were loaded onto the column as single elements. The column was then washed with 5 mL of 1 M HCl. The adsorbed metal ions on the sorbent materials were eluted with 3% w/v of thiourea in 1 M HNO<sub>3</sub> medium. The concentration of metal ions in each fraction collected (0.5 mL) were determined by ICP-OES. The separation factor of each the metal ions was calculated as given by equation 14.

$$S = \frac{[A]_r}{[A]_s} \times \frac{[B]_s}{[B]_r} \quad (14)$$

where  $[A]_r$  and  $[A]_s$  are concentrations of metal ions A on the resin and in the solution at equilibrium respectively [133].

### **(a) Resin regeneration**

Regeneration of the resin for further usage was examined by loading the columns containing 0.3 g of the resin with 0.01 M solution of chlorido complexes of platinum(IV) and palladium(II). After reaching the maximum uptake, the resin was washed carefully with 1 M of HCl. The adsorbed metal ions were stripped and eluted with 3 % w/v of thiourea. After the elution, the resin was thoroughly washed with distilled water to make it ready for re-use for the second run of loading with a solution of the metal ions [133]. The elution efficiency was calculated by dividing the total uptake of the metal ion in the second run by that of the first run as given by equation [15].

$$\% \text{Regeneration efficiency} = \frac{\text{Uptake of } M^{n+} \text{ in the second run by the resin}}{\text{Uptake of } M^{n+} \text{ in the first run by the resin}} \times 100 \quad [15]$$

### **(b) Separation of $PtCl_6^{2-}$ and $PdCl_4^{2-}$**

The quantitative separation of mixture of hexachloroplatinate(IV) and tetrachloropalladate(II) complexes was studied by a dynamic column method. 0.3 g of resin was packed into the column, and conditioned with water and 1 M HCl. The column was loaded with a mixture of both metal ion solutions. The column was washed with 1 M HCl and then the adsorbed Pt(IV) ion was selectively stripped with 0.5 M  $NaClO_4$  in 1 M HCl, and 0.5 M thiourea in 1 M HCl was used for the elution of Pd(II). The concentrations of metal ions in each fraction collected (0.5 mL) were determined by ICP-OES.

### **(c) Separation of Pt from Ir and Rh**

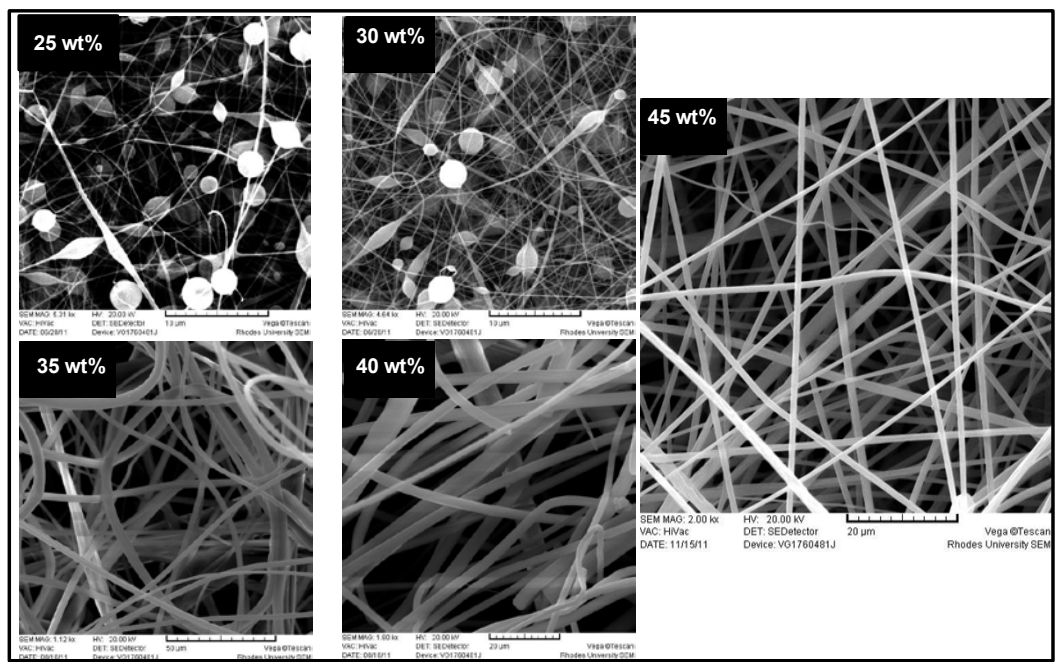
The glass column was packed with 0.3 g of the M-TETA sorbent. It was then conditioned with water and 1 M HCl. 5 mL of the mixture of the metal ions solutions was loaded onto the column. The column was washed with 1 M HCl, followed by stripping with 0.5 M HClO<sub>4</sub> and elution of the adsorbed hexachloroplatinate(IV) with 3% w/v of thiourea in 1 M HNO<sub>3</sub>. The concentrations of metal ions in each fraction collected (0.5 mL) were determined by ICP-OES.

## **3.3 Results and Discussion**

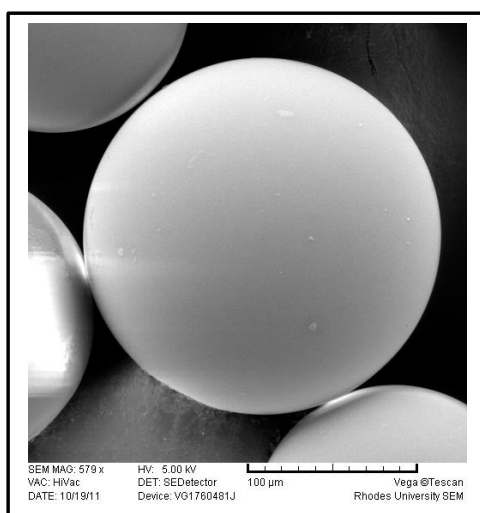
### **3.3.1 Characterization of the sorbent materials**

#### **(a) Scanning Electron Microscopy (SEM)**

The SEM images (Figures 3.2a) of the unfunctionalized styrene-based PVBC nanofibers revealed that the low viscosity of the solutions prepared (25 and 30 wt% solutions) produced beaded fibers, while 35 w% and 40wt% solutions produced fragile nanofibers with uneven diameters. The best morphology and diameter was observed with the 45 wt% solutions, with diameters ranging from 650–680 nm. The morphology and diameter of the unfunctionalized styrene-based beads were also observed using a scanning electron microscope (SEM). The images are shown in Figure 3.3. The diameters of the unfunctionalized beads were in the range 167–212 μm.



(a)



(b)

**Figure 3.2** SEM images of unfunctionalized (a) nanofibers, and (b) beads

The morphology of the functionalized styrene-based nanofibers is shown by the SEM images presented in Figure 3.3. The functionalized nanofiber materials containing the ion-exchange groups had the following range of diameters; 656–787 nm, showing a slight increase in fiber diameters after the introduction of the ion exchange groups. There was no change in morphology during the functionalization nor was there any change in shape since the fibers were not damaged.

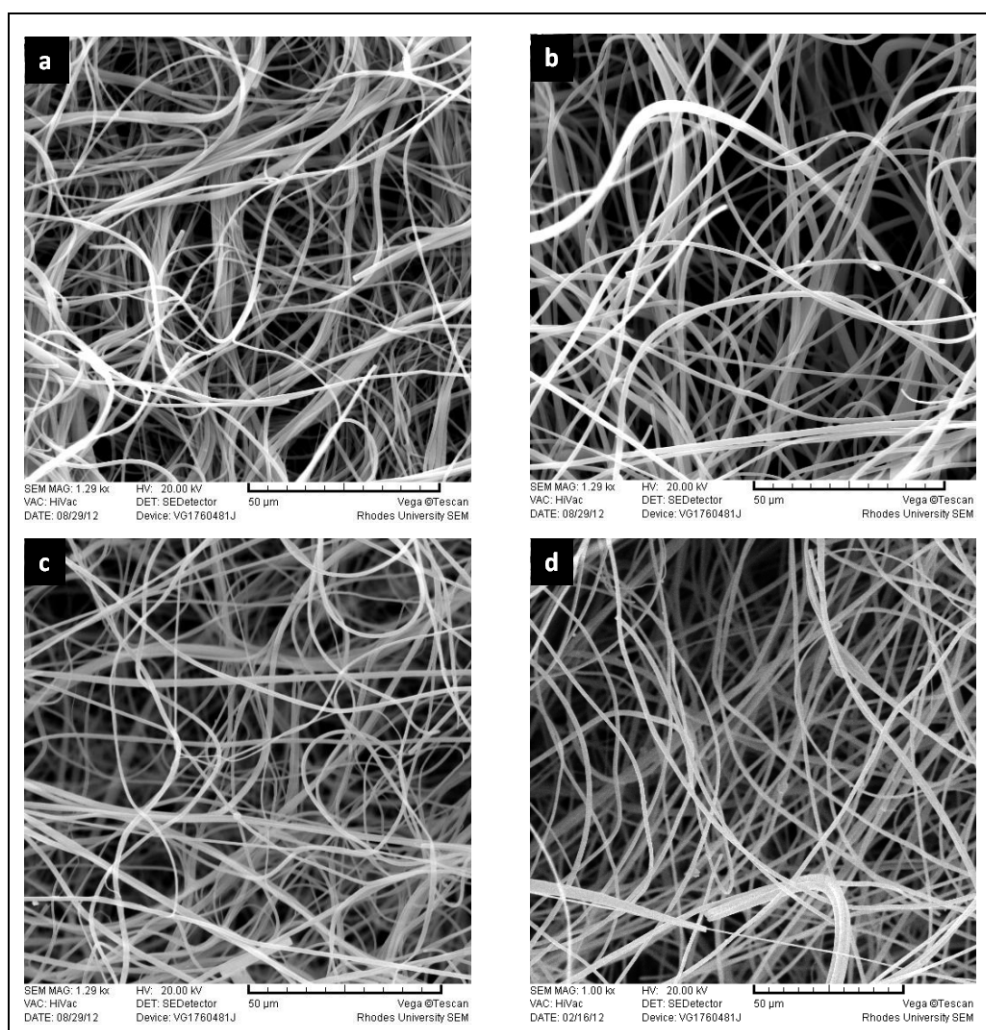


**Figure 3.3** SEM images of nanofibers functionalized with (a) EDA, (b) DETA, (c) TETA and (d) TAEA

The images of the functionalized beads are shown in Figure 3.4. There was a slight increase in the diameter of the sorbent materials after the introduction of ion-exchange groups. The roughness of the functionalized beads reveal a slight change in morphology. The functionalized beads materials containing these ion-exchange groups had the following range of diameters; 188 – 213  $\mu\text{m}$ , showing a slight increase after functionalization.

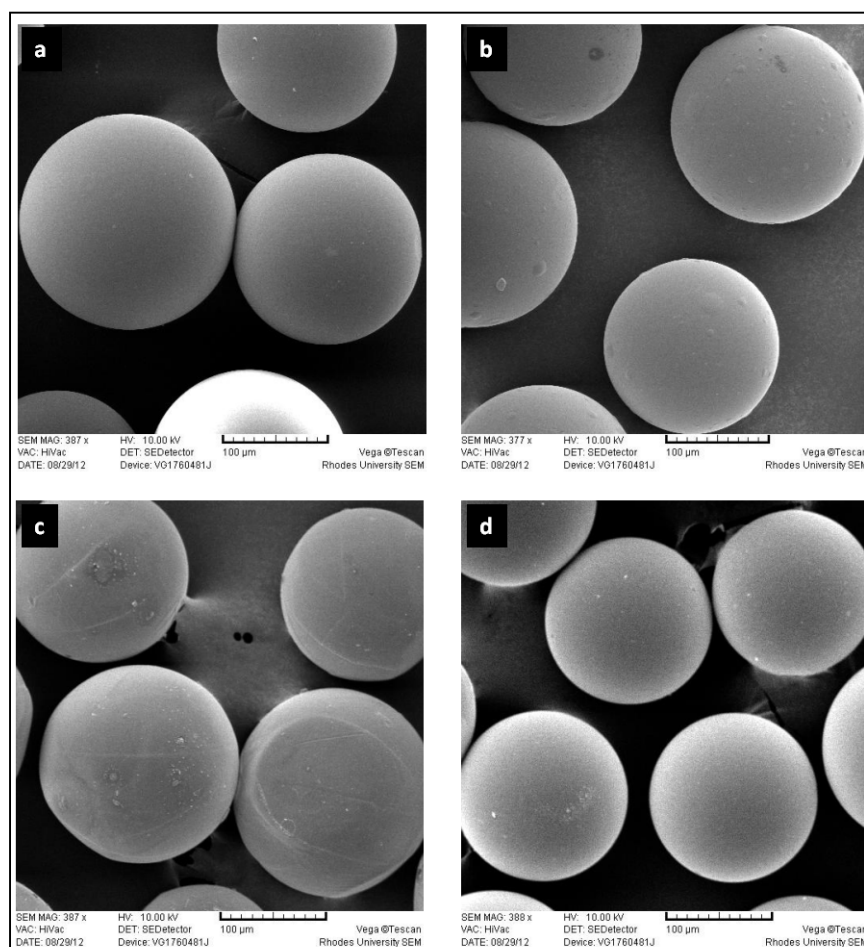


**Figure 3.4** SEM images of beads functionalized with (a) EDA, (b) DETA, (c) TETA and (d) TAEA

**(b) BET surface area**

The surface area of the unfunctionalized and functionalized beads and nanofiber materials were measured using the BET method and the results are presented in Table 3.1.

**Table 3.1** The single point surface area measurements for the unfunctionalized, EDA, DETA, TETA and TAEA-functionalized sorbent materials

Material	Unfunctionalized (m <sup>2</sup> /g)	EDA (m <sup>2</sup> /g)	DETA (m <sup>2</sup> /g)	TETA (m <sup>2</sup> /g)	TAEA (m <sup>2</sup> /g)
Nanofibers	341.9	241.3	68.9	68.8	68.8
Beads	124.0	107.4	72.5	81.2	96.9

From the result in Table 3.1, it can be concluded that the surface area of the sorbent materials was reduced after functionalization with amine groups. The F-EDA sorbent material had the highest surface area compared to the other sorbent materials which had comparable surface areas. The functionalized beads, however, had slightly higher surface areas for other functionalities. The functionalization of the nanofiber with amines seems to fit the bridging pattern (Scheme 3.2) as confirmed by the carbon to nitrogen ratio of (13:2, 31:3, 151:4 and 88:4) for EDA, DETA, TETA and TAEA respectively. The functionalization pattern for the polystyrene-based beads was difficult to prove due to the 1% crosslinking.

### (c) X-ray Photoelectron Spectroscopy (XPS)

The surface chemistry of the functionalized and unfunctionalized polystyrene-based beads and nanofiber sorbents was investigated by XPS. The presence of the Cl 1s and Cl 2s peaks at 200 eV and 270 eV respectively were observed on the unfunctionalized materials representing the chloride group (C-Cl) [134], and the reduction or disappearance of these peaks respectively was noticed upon functionalization (Figures 3.5 and 3.6). The presence of the N 1s peaks observed around 398 eV confirmed the functionalization with amines. The XPS spectra complemented the elemental analyses results in showing the presence of nitrogen on the functionalized sorbent materials. The O 1s peak may be due to water molecules on the surface of the materials.

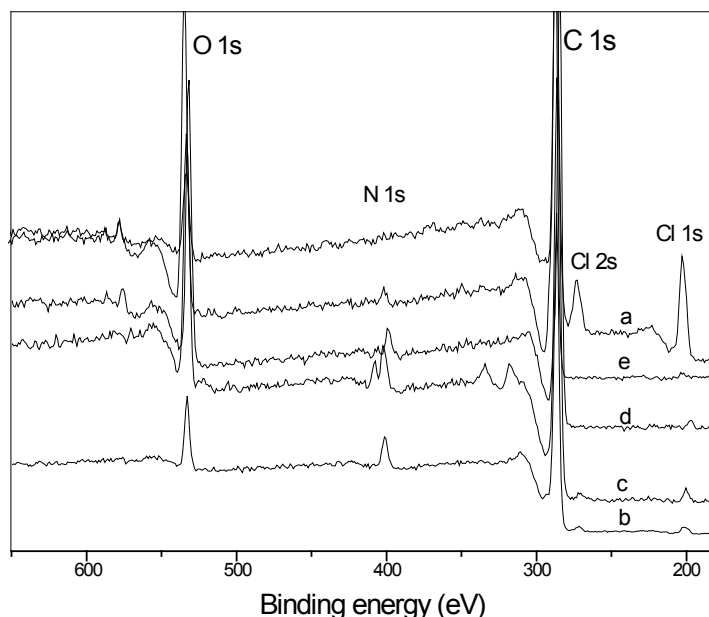


**Figure 3.5** The XPS spectra of the nanofibers; (a) unfunctionalized, (b) EDA, (c) DETA, (d) TETA, and (e) TAEA-functionalized nanofibers

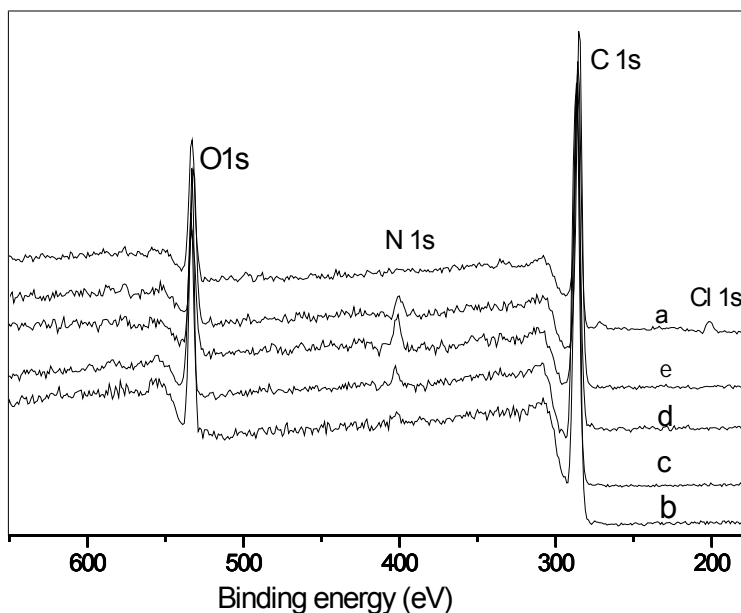


**Figure 3.6** The XPS spectra of Merrifield beads; (a) unfunctionalized and (b) EDA, (C) DETA, (d) TETA, and (e) TAEA-functionalized beads

#### **(d) FTIR Studies**

Figures 3.7 and 3.8 show the infra-red spectra of the functionalized and unfunctionalized polystyrene-based beads and nanofibers, respectively. The unfunctionalized materials showed a strong peak at  $670\text{ cm}^{-1}$  which is characteristic of  $\nu(\text{C-Cl})$ , and another peak at  $1264\text{ cm}^{-1}$  which can be assigned to the non-planar wagging of  $\text{CH}_2$  in  $\text{CH}_2\text{Cl}$  [135]. These peaks disappear after functionalization with the amines and other significant peaks were observed:  $3362\text{ cm}^{-1}$  for  $\nu(\text{N-H})$ ,  $1671\text{ cm}^{-1}$  for  $\delta(\text{N-H})$  and  $1018\text{ cm}^{-1}$  for  $\nu(\text{C-N})$  [135]. These indicated that all the respective sorbent materials were functionalized with amine groups.

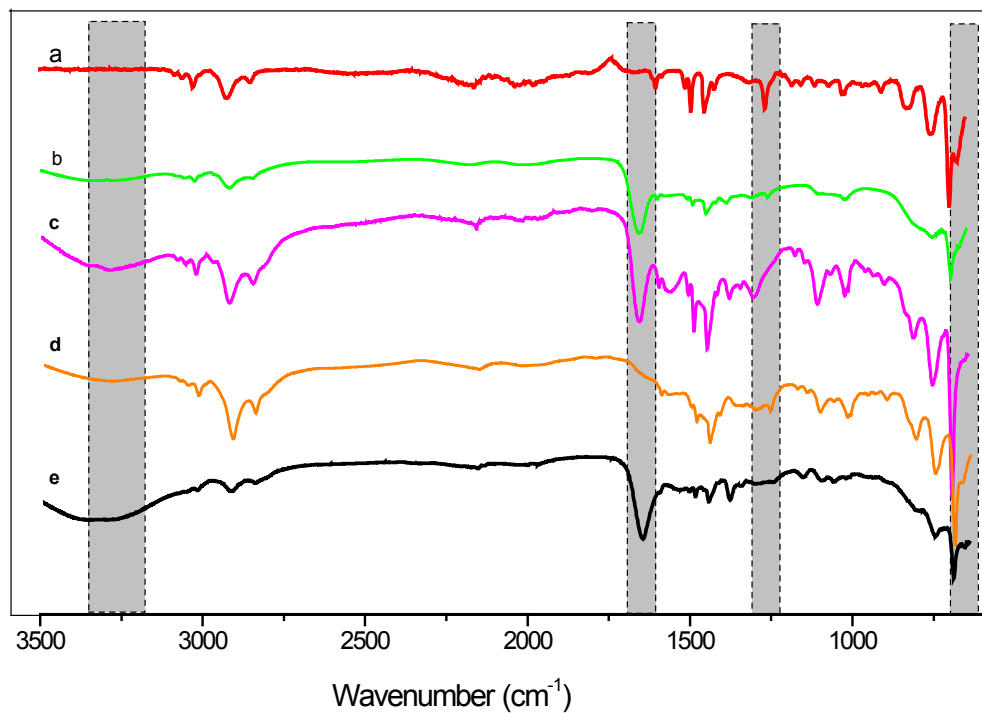


**Figure 3.7** FT-IR spectra of (a) unfunctionalized Merrified beads and functionalized beads (b) M-EDA, (c) M-DETA, (d) M-TETA and (e) M-TAEA

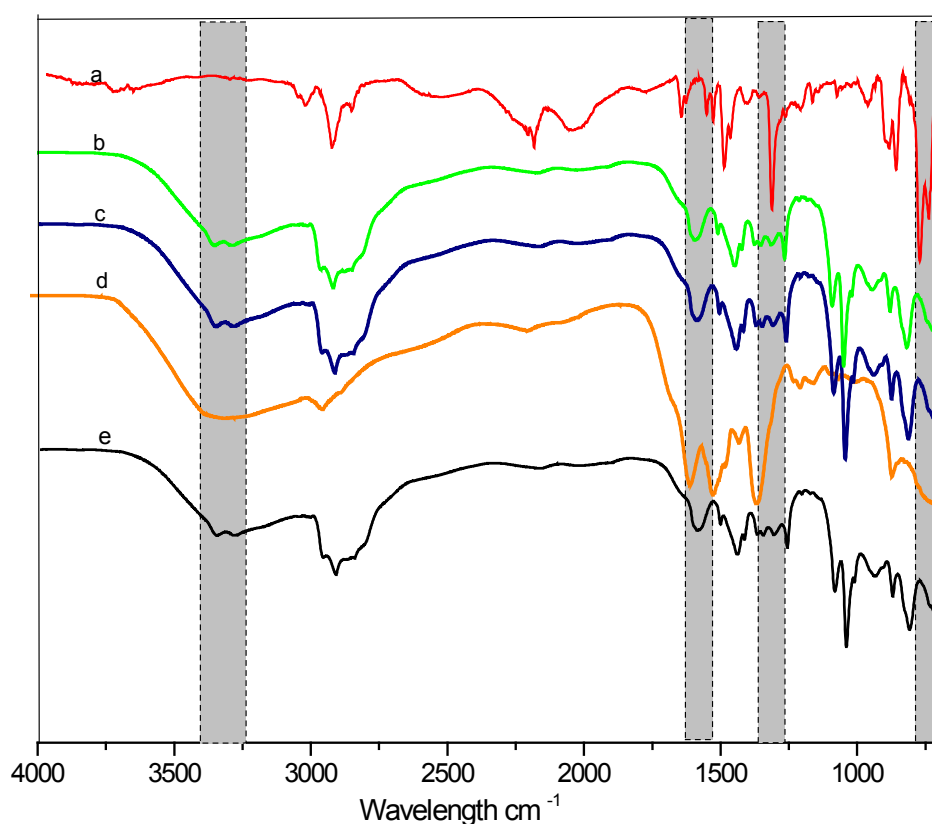


**Figure 3.8** FT-IR spectra of (a) unfunctionalized and functionalized styrene-based nanofibers (b) F-EDA, (c) F-DETA, (d) F-TETA and (e) F-TAEA

### 3.3.2 $^{195}\text{Pt}$ NMR spectra

The possibility of oxidation of  $[\text{PtCl}_4]^{2-}$  was carried out in 1 M HCl solution. The  $^{195}\text{Pt}$  NMR spectra are represented in Figure 3.9. Therefore the corresponding oxidation of 0.01 M  $[\text{PtCl}_4]^{2-}$  in 1 M HCl heated at 50°C for 30 minutes result in the formation of  $[\text{PtCl}_6]^{2-}$  [136].

(a)

(b)

**Figure 3.9**  $^{195}\text{Pt}$  NMR (recorded at 20 °C) spectra of (a) 0.01 M  $\text{PtCl}_4^{2-}$  and (b)  $\text{PtCl}_6^{2-}$  prepared by oxidizing  $\text{PtCl}_4^{2-}$  in 1 M HCl using  $\text{H}_2\text{O}_2$  with heating at 50 °C for 30 minutes.

### 3.3.3 Batch adsorption studies

#### (a) Kinetic experiments

The effect of contact time on the adsorption of  $\text{PtCl}_6^{2-}$  and  $\text{PdCl}_4^{2-}$  on F-EDA is shown in Figure 3.10. The adsorption of platinum and palladium reached maximum in about 5 minutes. Only a slight increase in adsorption of the metals was obtained after 25 minutes, hence 30 minutes was taken as the contact time for subsequent experiments. The same procedure was used for other sorbent materials.

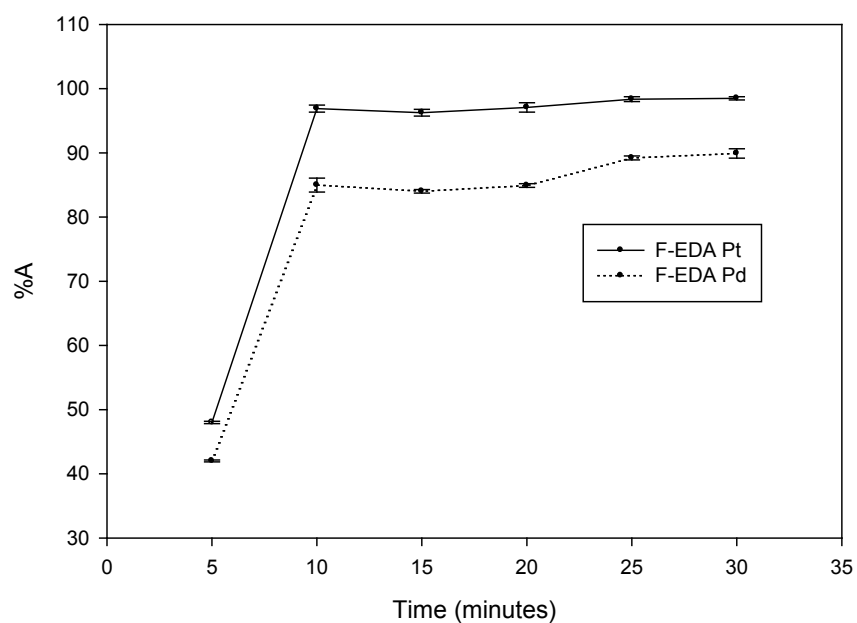
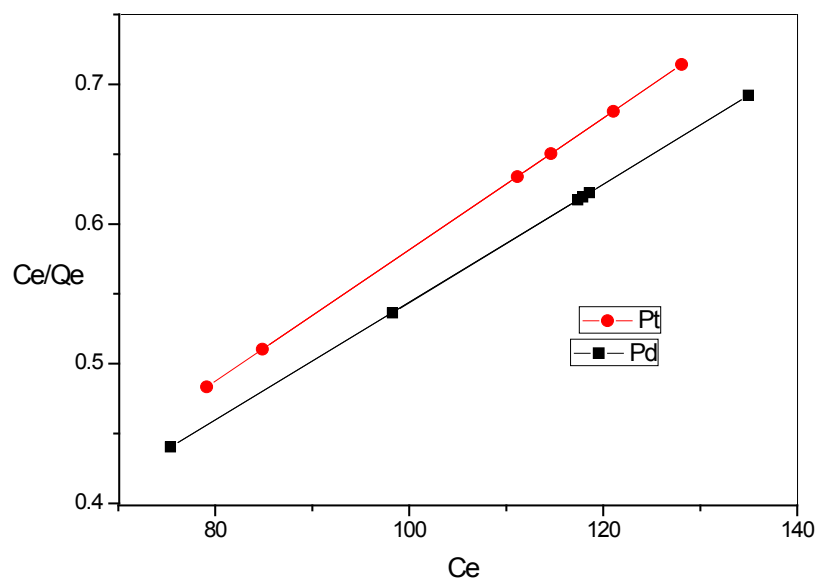


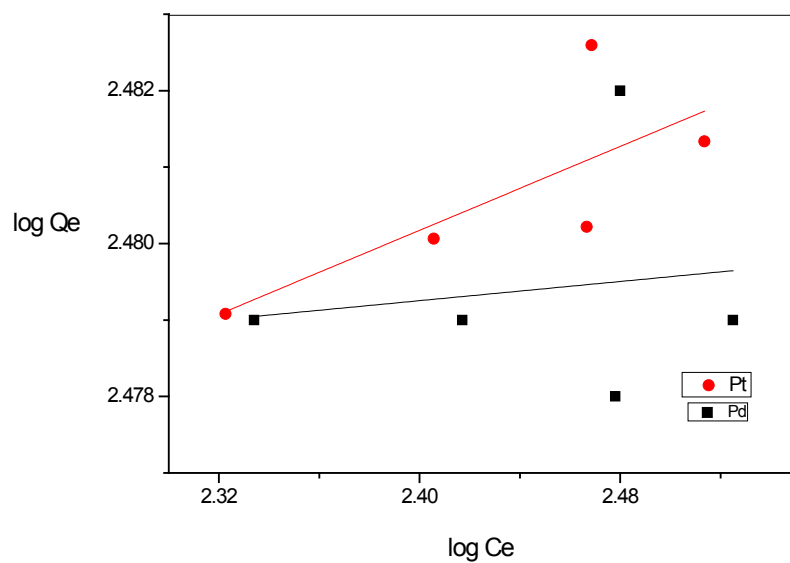
**Figure 3.10** The effect of contact time on the percentage adsorption (A %) using 3 mL of 0.01 M  $\text{PtCl}_6^{2-}$  and  $\text{PdCl}_4^{2-}$  on 0.15 g of F-EDA at room temperature

### **(b) Adsorption isotherms**

In order to investigate the adsorption capacity of  $\text{PtCl}_6^{2-}$  and  $\text{PdCl}_4^{2-}$  on each sorbent, the adsorption studies were carried out using the results from the batch study. The results were fitted on the Langmuir and Freundlich isotherms. The result obtained from the plots of  $C_e/Q_e$  vs  $C_e$  and  $\log Q_e$  vs  $\log C_e$  for the fitting of the experimental data into the Langmuir and Freundlich equations respectively for the F-EDA sorbent (Figure 3.11(a) and (b), and Tables 3.2 and 3.3 for  $R^2$  values) showed that these materials generally obeyed the monolayer adsorption model described by Langmuir. These isotherms are frequently used to describe the adsorption of metal ions during a process of ion exchange [137]. Other sorbent materials also fitted the Langmuir isotherm model.



(a)



(b)

**Figure 3.11** Plots of the (a) Langmuir and (b) Freundlich isotherm at room temperature using 3 mL of 0.01 M  $\text{PtCl}_6^{2-}$  and  $\text{PdCl}_4^{2-}$  adsorption on 0.15 g EDA-functionalized nanofibers

**Table 3.2** Langmuir and Freundlich parameters for adsorption of  $\text{PtCl}_6^{2-}$  and  $\text{PdCl}_4^{2-}$  on functionalized nanofibers

Isotherm	Parameter	<b>F-EDA (Pt)</b>	<b>F-DETA (Pt)</b>	<b>F-TETA (Pt)</b>	<b>F-TAEA (Pt)</b>	<b>F-EDA (Pd)</b>	<b>F-DETA (Pd)</b>	<b>F-TETA (Pd)</b>	<b>F-TAEA (Pd)</b>
Langmuir	$Q_m$ (mg/g)	31.25	52.60	2.32	0.07	50.00	52.60	2.25	0.04
	B	0.53	0.64	1.67	5.88	1.00	0.74	0.65	5.00
	$R^2$	0.999	0.999	0.999	0.991	0.999	0.999	0.999	0.994
Freundlich	$K_f$	1.10	1.05	22.69	1.00	1.22	1.04	11.05	0.15
	N	0.35	0.37	0.33	0.35	0.4	0.36	0.41	0.25
	$R^2$	0.492	0.388	0.998	0.996	0.823	0.157	0.994	0.976

**Table 3.3** Langmuir and Freundlich parameters for adsorption of  $\text{PtCl}_6^{2-}$  and  $\text{PdCl}_4^{2-}$  on functionalized beads

		<b>M-EDA (Pt)</b>	<b>M-DETA (Pt)</b>	<b>M-TETA (Pt)</b>	<b>M-TAEA (Pt)</b>	<b>M-EDA (Pd)</b>	<b>M-DETA (Pd)</b>	<b>M-TETA (Pd)</b>	<b>M-TAEA (Pd)</b>
Langmuir	$Q_m$ (mg/g)	23.26	5.41	10.87	62.50	23.26	1.02	0.09	0.12
	B	0.77	5.00	2.00	0.03	0.61	1.67	0.18	2.27
	$R^2$	0.999	0.996	0.995	0.997	0.999	0.999	0.841	0.981
Freundlich	$K_f$	1.69	1.07	1.03	1.06	1.00	1.01	1.04	1.03
	N	0.35	0.37	0.36	0.36	0.37	0.37	0.37	0.37
	$R^2$	0.998	0.366	0.215	0.166	0.505	0.117	0.349	0.209

The parameters of the Langmuir and Freundlich isotherms for the experimental data are presented in Tables 3.2 and 3.3. The theoretical loading capacity of the sorbent materials for the metal ion complexes is lower than the experimental loading capacity. These results also show high theoretical adsorption capacity for both  $\text{PtCl}_6^{2-}$  and  $\text{PdCl}_4^{2-}$  complexes on the functionalized polystyrene fiber sorbent materials, while the adsorption capacity of  $\text{PtCl}_6^{2-}$  was higher than that of  $\text{PdCl}_4^{2-}$  on styrene-based bead sorbents. The dimensionless equilibrium parameter ( $R_L$ ) represented as  $R_L = 1/1 + b C_0$ , where  $b$  is the Langmuir constant and  $C_0$  is the initial concentration of  $\text{PtCl}_6^{2-}$  and  $\text{PdCl}_4^{2-}$  [138] was used to predict the adsorption efficiency of the adsorption process.  $R_L$  values within the range  $0 < R_L < 1$  indicate favourable adsorption. The sorbents in the present study gave  $R_L$  values for both metal ions ranging from 0.002 to 0.79 which mean that the adsorption of both metal ions on these sorbents was favourable.

### **3.3.4 Column (dynamic) studies**

#### ***(a) Single element studies***

The performance of the sorbents under dynamic flow adsorption conditions was studied. Thiourea was used for the elution step, and it is well known for its affinity for precious metals due to the presence of both amine and sulfur groups. These donor atoms contribute to the binding of the metal ions by complexation, possibly forming a cationic Pd complex such as  $[\text{Pd}(\text{NH}_2)_2\text{CS}_4]^{2-}$  due to the kinetic lability of  $[\text{PdCl}_4]^{2-}$  to ligand substitution reactions [139]. It has been used for desorption of precious metals from loaded sorbents [140]. Pt and Pd were quantitatively desorbed using 3% thiourea in an

acidic medium. The columns were loaded with higher metal quantities so as to allow for the calculation of loading capacities when the un-adsorbed metals have been washed off the column (earlier fractions in Figures 3.12 and 3.13).

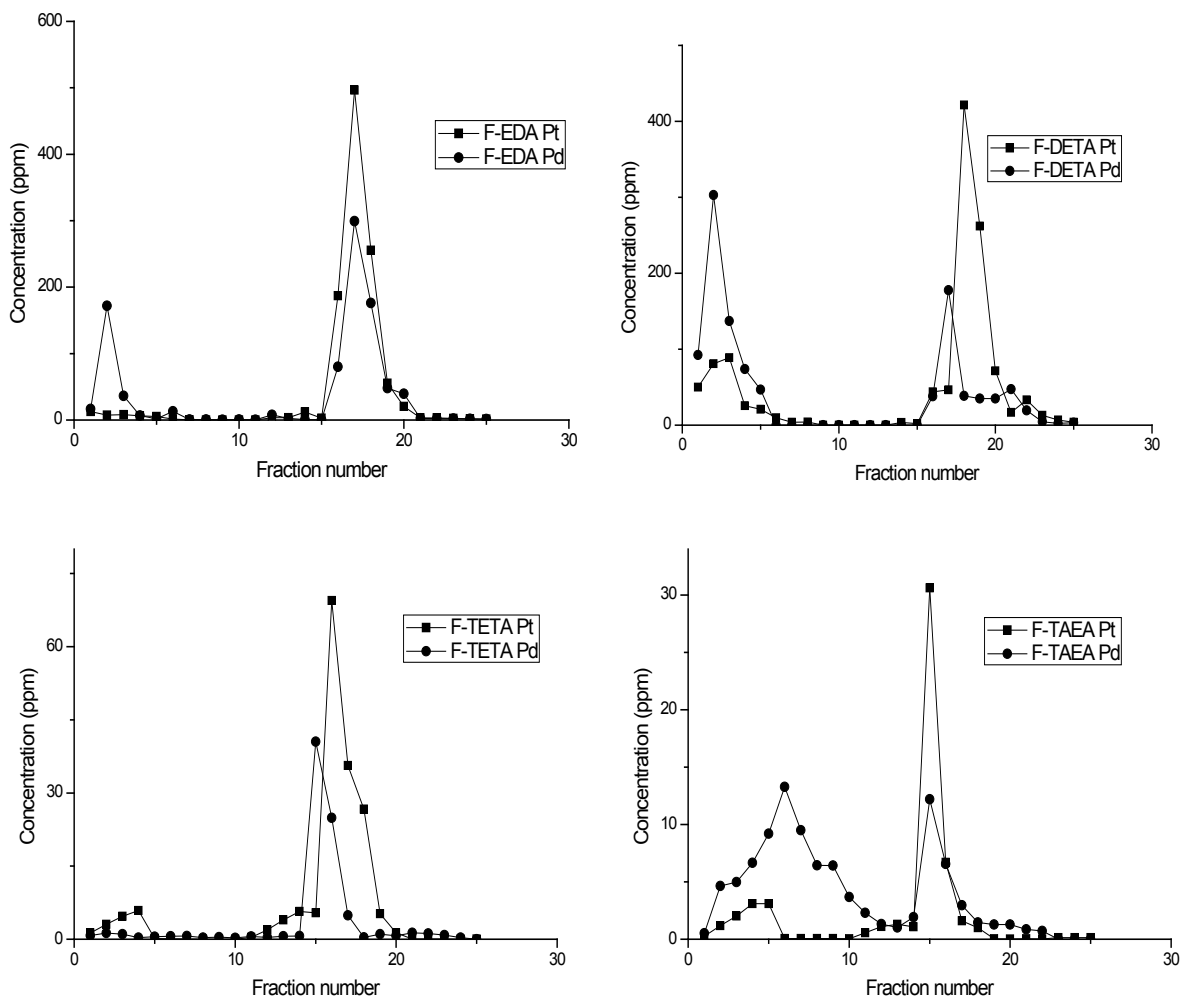


**Figure 3.12** Adsorption/elution profiles using 5 mL of 0.01 M  $\text{PtCl}_6^{2-}$  and  $\text{PdCl}_4^{2-}$  on 0.3 g amine-functionalized beads: F-EDA, F-DETA, F-TETA and F-TAEA were respectively washed with 1 M HCl and eluted with 3% w/v thiourea at room temperature

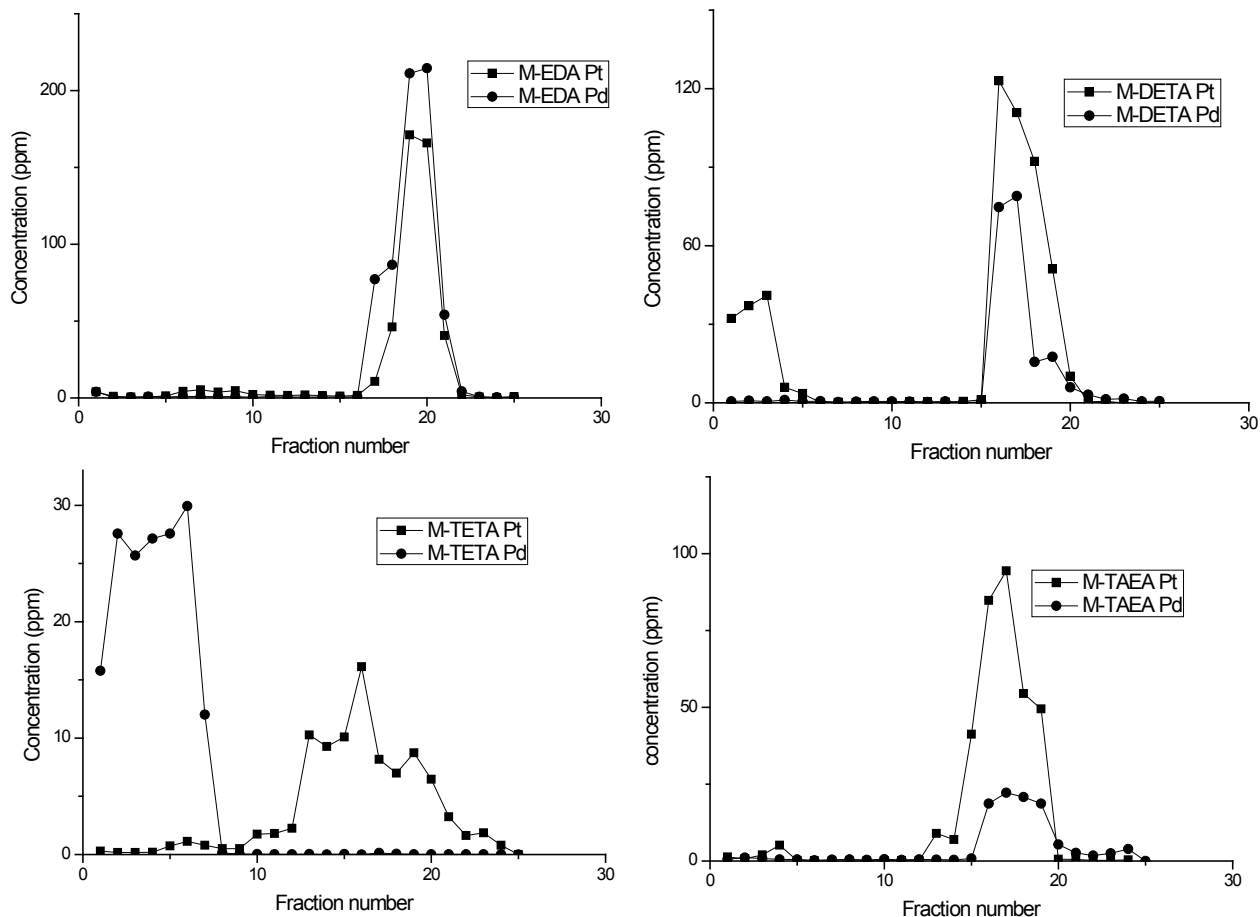


**Figure 3.13** Adsorption/elution profiles using 5 mL of 0.01 M  $\text{PtCl}_6^{2-}$  and  $\text{PdCl}_4^{2-}$  on 0.3 g amine-functionalized beads: M-EDA, M-DETA, M-TETA and M-TAEA were respectively washed with 1 M HCl and eluted with 3% w/v thiourea at room temperature

Figures 3.12 and 3.13 represent the curves for the elution profiles of  $\text{PtCl}_6^{2-}$  and  $\text{PdCl}_4^{2-}$  on functionalized nanofibers and beads, respectively. The curves show that both metal ions were sufficiently loaded on each sorbent (later fractions in Figures 3.12 and 3.13). In general Pt was loaded more than Pd on all the materials and the nanofiber sorbents loaded Pt more than the beads (Table 3.4). Mass balance was generally observed in all

these column studies, the amount of metal loaded onto the column matched the total from all the fractions (within error) indicating that no metals were retained in the sorbent materials after the stripping and elution step. The loading capacity of the sorbents with different amines functionality showed an increase in the order di > tri > tetra (branched) > tetra (straight chain) amines. The trend was also in partial agreement with the elemental analysis that shows the increase in percentage of nitrogen in the sorbents as di > tri > tetra amines. The amine groups function as ammonium sites in the ion exchanger under acidic conditions which induce the adsorption of the chlorido complexes of platinum(IV) and palladium(II) *via* electrostatic interactions. The highest loading for Pt was on F-EDA sorbent which was in agreement with its large surface area and also the elemental analysis revealing the highest percentage of nitrogen. It can be assumed that the increase in percentage nitrogen plays a major role in improving the sorption capacity of the sorbents. The M-TETA was noticeable for its ability to reject Pd, and therefore its selectivity for Pt. However, the only drawback may be its low loading capacity for platinum (0.09 mg/g) which could be compromised considering that selectivity would be the main advantage.

**Table 3.4** The column experimental loading capacities (mg/g) of 0.3 g functionalized sorbent materials for Pt and Pd

Sorbent	Metal ion	EDA (mg/g)	DETA (mg/g)	TETA (mg/g)	TAEA (mg/g)
Fibers	Pt	7.42	2.58	0.47	0.66
	Pd	4.32	1.08	0.39	0.41
Beads	Pt	1.00	0.60	0.09	0.79
	Pd	0.23	0.38	0	0.82

The selectivity of sorbent M-TETA for  $\text{PtCl}_6^{2-}$  was examined by determining the separation factor of  $\text{PtCl}_6^{2-}$  and  $\text{PdCl}_4^{2-}$ . A binary synthetic solution containing equimolar concentration of both metal ions was loaded into the pre-conditioned column, stripped and eluted with 3% w/v of thiourea. The resin was removed from the column after elution and washed for the next determination. The separation factor of  $\text{PtCl}_6^{2-}/\text{PdCl}_4^{2-}$  is 79.

The selectivity of M-TETA for  $\text{PtCl}_6^{2-}$  was further investigated by the breakthrough curves represented in Figure 3.14. From the curve the breakthrough volume for platinum was significantly higher (above 10 mL) while that of palladium was much lower (above 4 mL).

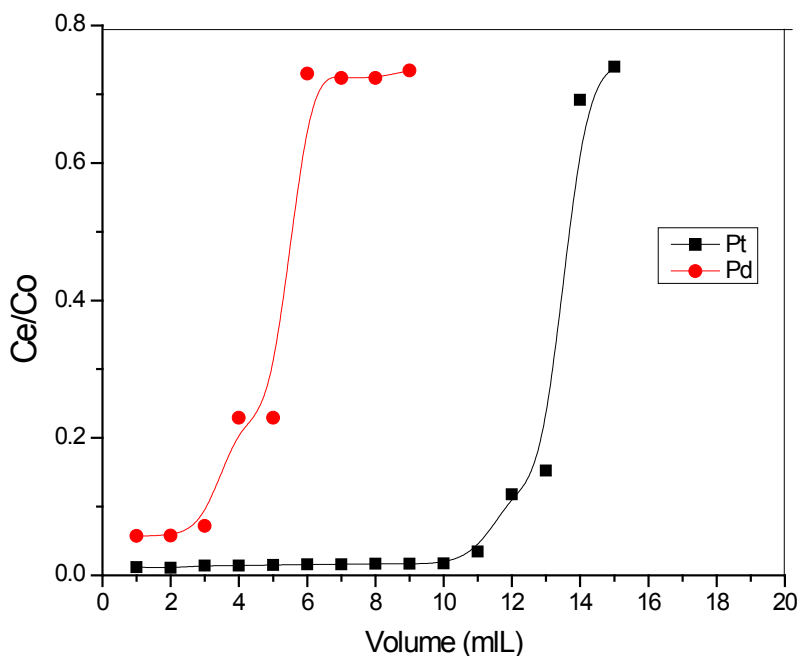


**Figure 3.14** Breakthrough curves using 5 mL of 0.01 M  $\text{PtCl}_6^{2-}$  and  $\text{PdCl}_4^{2-}$  on 0.3 g of M-TETA sorbent at room temperature in 1 M HCl

### **(b) Binary separation of Pt and Pd**

The only sorbent material which displayed selectivity for  $\text{PtCl}_6^{2-}$  over  $\text{PdCl}_4^{2-}$  was M-TETA, however its loading capacity was very low. This therefore necessitated the development of a selective stripping step in order to exploit the recovery of pure metals from other materials which had higher loading capacities (M-EDA, F-EDA, F-TETA and F-TAEA). The results for the separation of Pt and Pd from their mixture are presented in Figure 3.15. The chlorido metal complexes loaded on the sorbent materials were efficiently stripped with 0.5 M  $\text{NaClO}_4$  in 0.05 M HCl for Pt(IV) and 0.5 M thiourea in 1 M HCl for Pd(II). The perchlorate ion displaces the  $\text{PtCl}_6^{2-}$  due to its ion exchange capacity [141], and  $\text{PdCl}_4^{2-}$  is desorbed through formation of a cationic complex with thiourea [142]. The curves of the selective separation of the platinum and palladium revealed that both metal ions can, to some extent, be successfully separated by using a stripping agent that is specific for platinum.

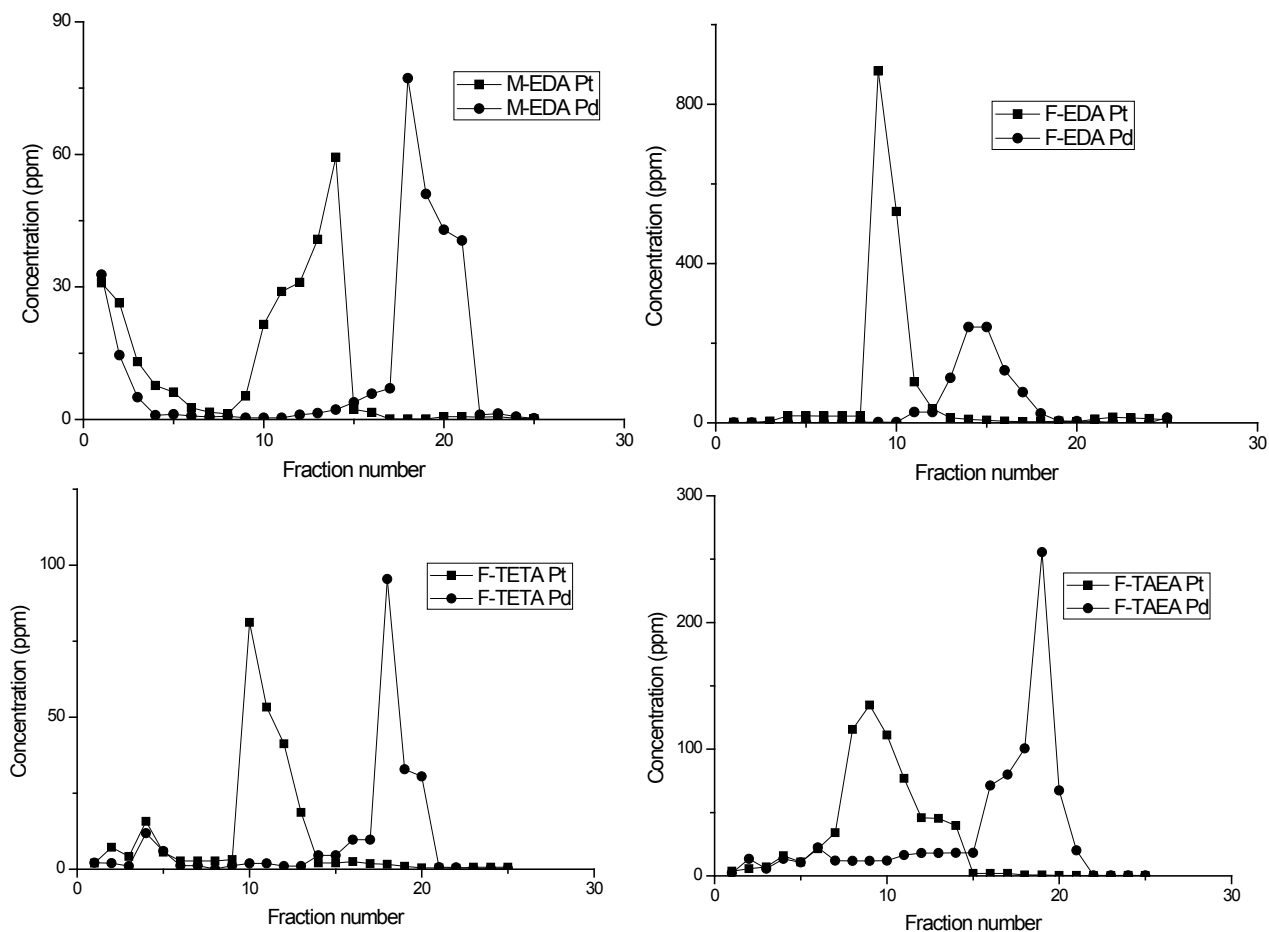


**Figure 3.15** The separation profile using 5 mL of 0.01 M mixture of  $\text{PtCl}_6^{2-}$  and  $\text{PdCl}_4^{2-}$  on 0.3 g M-EDA, F-EDA, F-TETA and F-TAEA by selective stripping of Pt and Pd with  $\text{NaClO}_4$  and thiourea respectively at room temperature

### (c) Separation of Pt from Ir and Rh

The column study of the adsorption and separation of  $\text{PtCl}_6^{2-}$  and  $\text{PdCl}_4^{2-}$  showed M-TETA to be the only  $\text{PtCl}_6^{2-}$  selective material (Figure 3.16). Considering the fact that palladium can be recovered from a mixture of other PGMs by solvent extraction [140], this study was extended to the separation of platinum from a mixture containing Ir(III)

and Rh(III) in order to investigate its selectivity for Pt over other PGMs. Any palladium impurities that remain in the solvent extraction step would pass through this material unadsorbed by this material. The difference in adsorption behavior of these metals in HCl medium depends on the distribution of their chlorido anionic species. Pt(IV) exists as  $\text{PtCl}_6^{2-}$  at 1 M HCl while Ir(III) and Rh(III) form the lower chlorido species under these conditions [143].

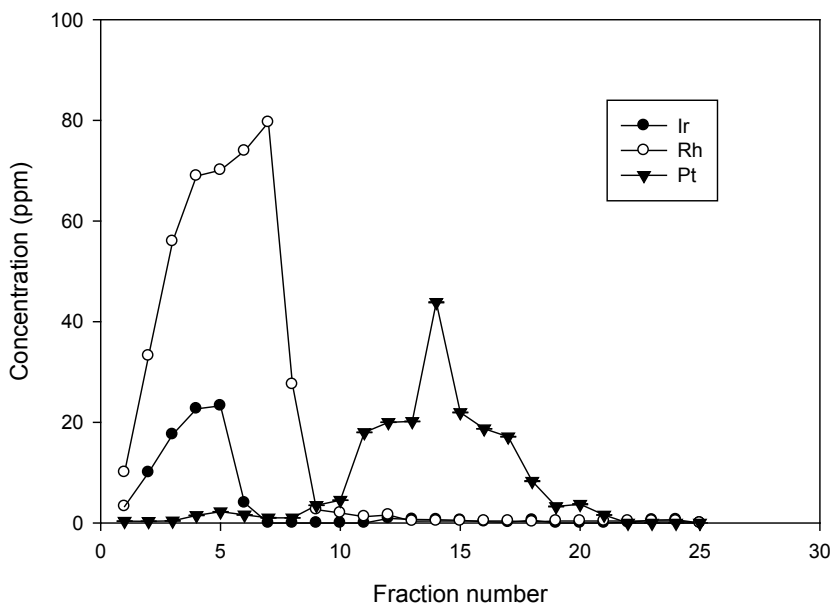


**Figure 3.16** The adsorption/elution profile of Pt from the mixture of Pt, Ir and Rh on 0.3 g M-TETA by washing, stripping and eluting with 1 M HCl, 0.5 M  $\text{HClO}_4$  and 3% w/v thiourea respectively at room temperature

As shown in Figure 3.16, most of the Pt(IV) was loaded onto the M-TETA sorbent while the Ir and Rh were washed out of the column (unloaded) in the earlier fractions. The loading capacity for platinum was 0.1 mg/g under the conditions employed. The

separation of Pt from Rh and Ir was possible at 1 M HCl using M-TETA as an anion exchange sorbent material.

#### **(d) Regeneration of resin**

Regeneration efficiency was studied to determine the level of durability of the resin for more adsorption and elution studies by the method of loading/regeneration/reloading for several usage. The separating efficiency of the resin was fairly retained even after repeated processes and this was determined to be 96% efficiency of the initial capacity according to equation 15. The regeneration efficiency proved that the functionalized polystyrene-based nanofibers and bead resins are reusable, and this suggest they are economically viable alternatives.

### **3.4 Conclusions**

The metal loading capacities of the sorbents were directly proportional to the accessible surface area and also dependent on the percentage of nitrogen in the material. The mechanism of hexachloroplatinate(IV) and tetrachloropalladate(II) complexes binding on the sorbents followed the monolayer adsorption model described by Langmuir. The continuous flow column experiments indicated that the selective separation of hexachloroplatinate(IV) and tetrachloropalladate(II) complexes was only achieved with M-TETA. The separation of these chlorido anions using other non-selective materials was partially achieved by selective stripping of hexachloroplatinate(IV) with 0.5 M NaClO<sub>4</sub> in 0.05 M HCl followed by the elution of tetrachloropalladate(II) with

0.5 M thiourea in 1.0 M HCl. However, the selective stripping process may not be applicable for practical purposes but a platinum-specific material (M-TETA) shows the most potential. The selective separation of Pt from a mixture containing rhodium and iridium was achieved on M-TETA in 1 M HCl.

# CHAPTER 4

## ADSORPTION AND SEPARATION OF PLATINUM GROUP METALS USING POLYAMINE-FUNCTIONALIZED SILICA MATERIAL

### 4.1 Introduction

Recently, ion exchangers with polyamine groups on a silica-based skeleton have been fabricated and applied for the separation of platinum group metals (PGMs). The sorption experiments of Pd, Pt and Rh ions, from the industrial base metal refinery (BMR) effluents and precious metal refinery (PRM), with silica-based (poly)amine ion exchangers exhibited a very high selectivity for platinum group metals (PGMs) [144,145]. There were no detectable amounts of the other transition metals (Ni, Cu and Fe). The fact that the ion exchangers originate from relatively inexpensive starting materials and maximum sorption is obtained at room temperature makes their application in a continuous system commercially feasible [145].

The selectivity of the surface with the immobilized functional groups towards metal ion(s) depends on factors like the size of the modifier [146], and the activity of the loaded group [147,148]. Among the different adsorbents, silica gel functionalized with various organic compounds with metal chelating ability or ion exchange capacity has received great attention and the active silica surface with large specific surface area is of great importance in adsorption and ion exchange [148]. A silica surface interacts with the silane reagent to form a covalent bond with silanol groups [149]. By the introduction of organic functional groups to a silica surface there is a partial conversion of surface

silanol to a new organofunctional surface that acquires organophilic properties. Thus, ligand-functionalized silica gives a set of properties to the surface which differ considerably from the original matrix (Figure 4.1) [150,151].

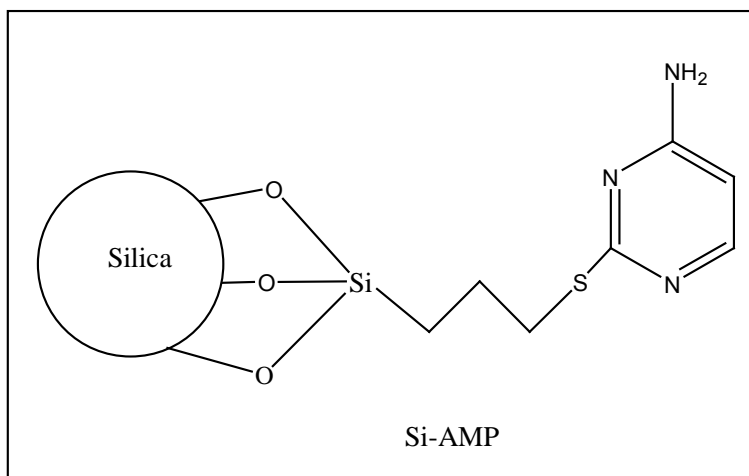


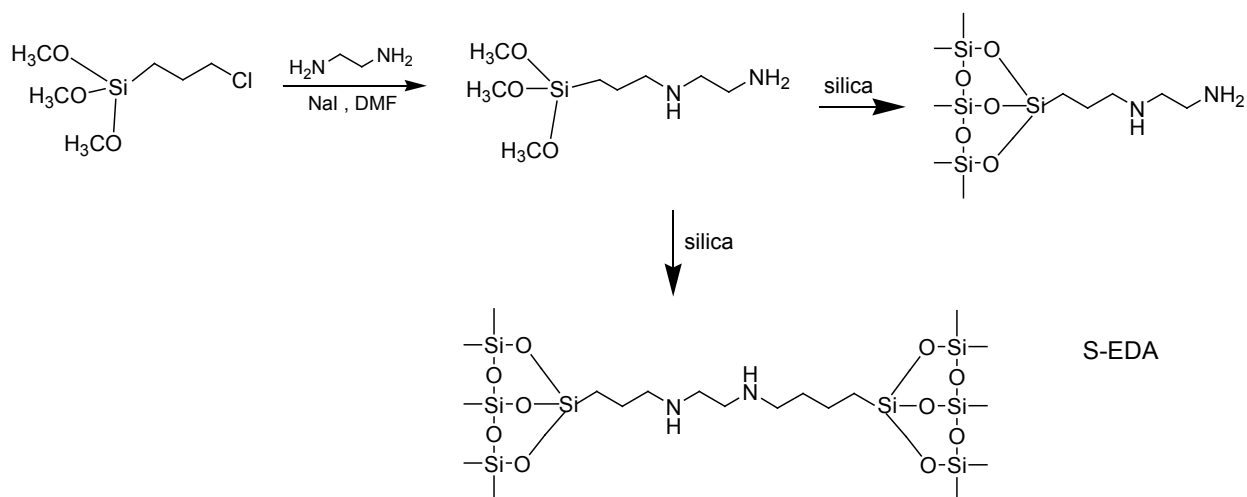
**Figure 4.1** Structure of silica gel functionalized with 4-amino-2-mercaptopyrimidine [151]

The purpose of this work was to functionalize silica microparticles with ammonium centres derived from ethylenediamine (EDA), diethylenetriamine (DETA), triethylenetetramine (TETA) and *tris*-(2-aminoethyl)amine (TAEA) (Figure 4.1). The selective separation of platinum and palladium was investigated as well as the separation of palladium from a mixture containing platinum, rhodium and iridium on a S-TETA showed selectivity for palladium.

## 4.2 Experimental

### 4.2.1 Functionalization of silica-based microparticle

0.22 M ethylenediamine (EDA) was reacted with 0.2 M of 3-chloropropyltrimethoxysilane in 30 mL of DMF. A catalytic amount of sodium iodide was added to the mixture, which was then heated under reflux for 6 days (scheme 4.1). The product was reacted with 4 g of silica gel under reflux without stirring for 8 days. The resin was washed with DMF, Soxhlet extracted in methanol, air dried and sieved (if necessary). The same procedure was used for functionalization with the other amines. FT-IR ( $\text{cm}^{-1}$ ): 1046  $\nu$ (Si-O), 1671  $\delta$ (N-H), 3200-3300  $\nu$ (N-H). Elemental analysis (CHN, %): Anal. found for; **S-EDA** (6.49, 1.78, 1.53), **S-DETA** (12.71, 3.35, 4.28), **S-TETA** (12.04, 3.00, 4.31) and **S-TAEA** (4.60, 1.13, 1.76).



**Scheme 4.1** Functionalization of silica-based sorbent with ethylenediamine (S-EDA)

#### **4.2.2 Batch adsorption studies**

The adsorption studies were carried out in a similar manner as detailed in section 3.3.2 in Chapter 3.

#### **4.2.3 Separation of chlorido complexes of Pt(IV) and Pd(II)**

The quantitative separation of chlorido complexes of Pt(IV) and Pd(II) by each sorbent was studied by a dynamic column method. A 0.3 g of resin was packed into the column of length 10 cm, inner and tip diameters 3.5 and 1.0 mm respectively. A 5 mL solution of both metal ions was passed through the column to examine the competitive adsorption. The column was washed with 1 M HCl and thereafter the adsorbed metal ions were eluted by using 0.5 M of NaClO<sub>4</sub> in 1 M HCl for platinum and 0.5 M thiourea in 1 M HCl for palladium. The concentration of metal ions in each fraction collected at every stage was determined by ICP-OES.

#### **4.2.4 Separation of chlorido complexes of Pd from Pt, Ir and Rh**

The glass column was packed with 0.3 g of sorbent (S-TETA) and plugged with glass wool at the top and bottom. A 5 mL (solution containing a mixture of all four) metal ions solution was passed through the column. The column was washed with 1 M HCl followed by stripping the adsorbed hexachloroplatinate(IV) with 0.5 M of NaClO<sub>4</sub> in 1 M HCl. The 0.5 mL eluate fractions were collected and the concentrations of the metal ions were determined by ICP-OES.

## 4.3 Results and Discussion

### 4.3.1 Characterization of the sorbent materials

#### (a) Scanning Electron Microscopy (SEM)

The morphology of the unfunctionalized and functionalized silica microparticles was observed using a scanning electron microscope (SEM) and the images are shown in Figure 4.2.

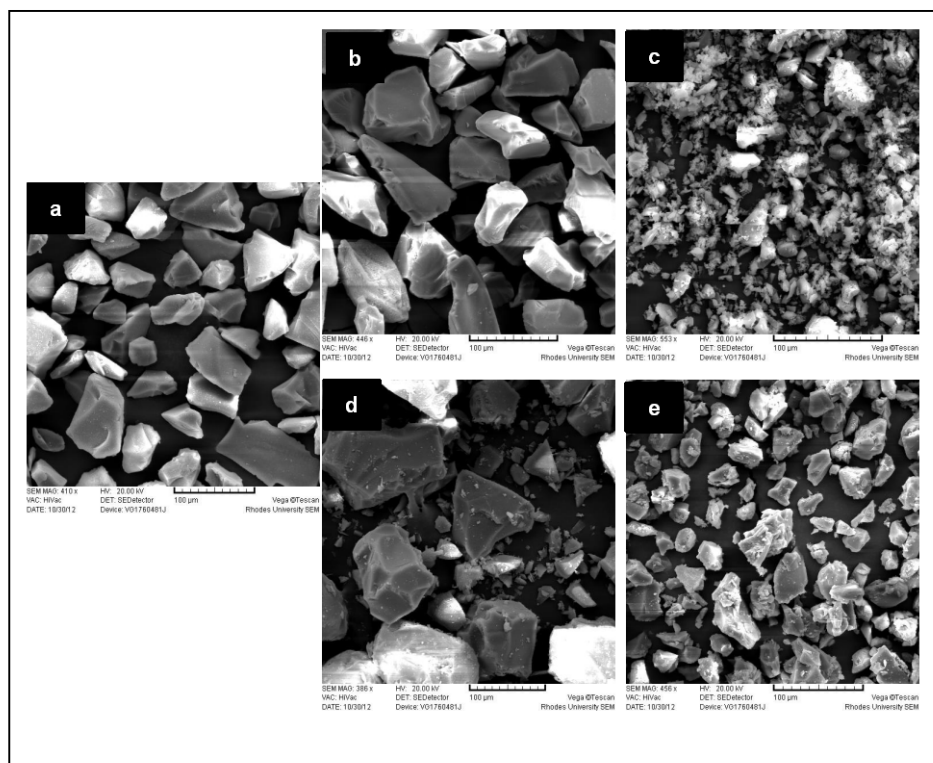


**Figure 4.2** SEM images of silica-based sorbents; (a) unfunctionalized, silica and (b-e) silica functionalized with amines EDA, DETA, TETA and TAEA respectively (before sieving)

There were some changes in sizes of these micro particles after the introduction of different amine groups. The mesh sizes of the unfunctionalized ranges from 42-72  $\mu\text{m}$ , while the size increased on functionalization with EDA and TAEA to the ranges from 39-82 and 80-112  $\mu\text{m}$  respectively. The mesh size of sorbent materials with DETA and TETA functional groups reduced to 16-30 and 17-40  $\mu\text{m}$  respectively.

**(b) Micrographs of the silica microparticles**

The micrographs of the unfunctionalized and functionalized sorbents shown in Figure 4.3 reveal that the unfunctionalized silica changes colour after the introduction of the amine groups. A cream colour was observed with S-EDA and S-TAEA, while S-TAEA gave yellow colour and a very deep yellow colour was observed for the S-TETA sorbent material. These further confirm that the sorbents were functionalized.

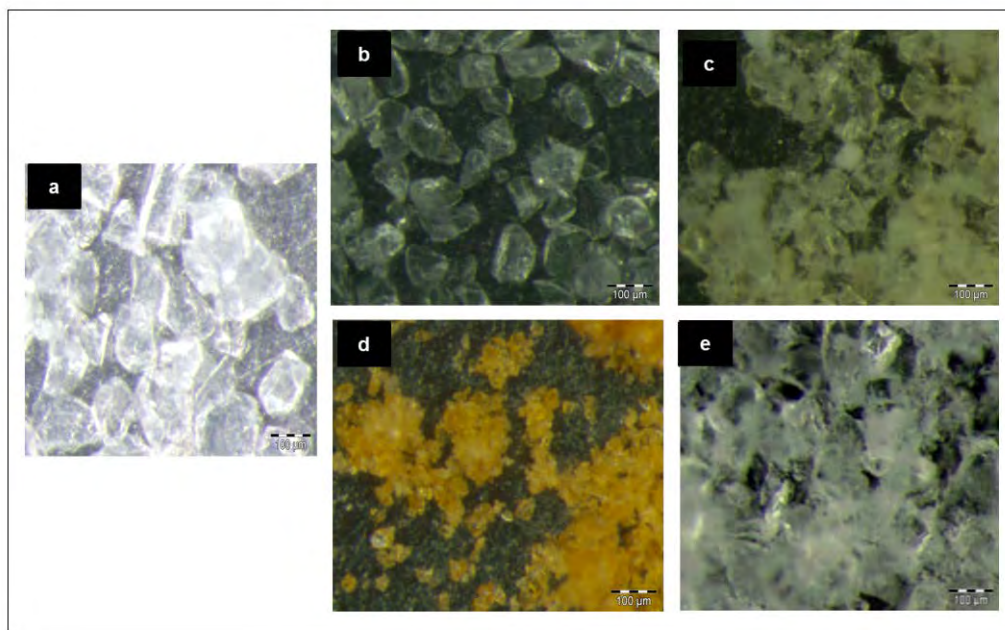


**Figure 4.3** Micrographs of silica-based sorbents; (a) unfunctionalized silica, and (b-e) silica functionalized with amines EDA, DETA, TETA and TAEA respectively

### **(c) BET surface area**

The surface area of the unfunctionalized and functionalized silica materials were measured by using the BET method and the results are presented in Table 4.1.

**Table 4.1** The single point surface area measurements for the unfunctionalized, EDA, DETA, TETA and TAEA-functionalized sorbent materials

Unfunctionalized(m <sup>2</sup> /g)	EDA (m <sup>2</sup> /g)	DETA (m <sup>2</sup> /g)	TETA (m <sup>2</sup> /g)	TAEA (m <sup>2</sup> /g)
155.7	114.8	136.5	141.8	128.9

From the result in Table 4.1, it can be concluded that the surface area of the sorbent materials was reduced after functionalization with amine groups. The S-TETA sorbent material had the highest surface area compared to the other sorbent materials which had comparable surface areas. The functionalization of the silica with amines seems to fit the bridging pattern (scheme 4.2) as confirmed by the carbon to nitrogen ratio of (10:2, 10:3, 13:4 and 12:4) for EDA, DETA, TETA and TAEA respectively.

### **(d) X-ray Photoelectron Spectroscopy (XPS)**

The surface chemistry with respect to expected atoms on the functionalized silica-based sorbents was studied by XPS. The N 1s peaks were observed around 398 eV which confirmed the functionalization with amines [134]. The XPS spectra (Figure 4.4)

complimented the elemental analysis results showing the presence of nitrogen in the functionalized sorbent materials. The small Cl 1s peaks around 199 eV suggest that there is a minor proportion of the silane linker that was not functionalized with amines through substitution of the chloride.

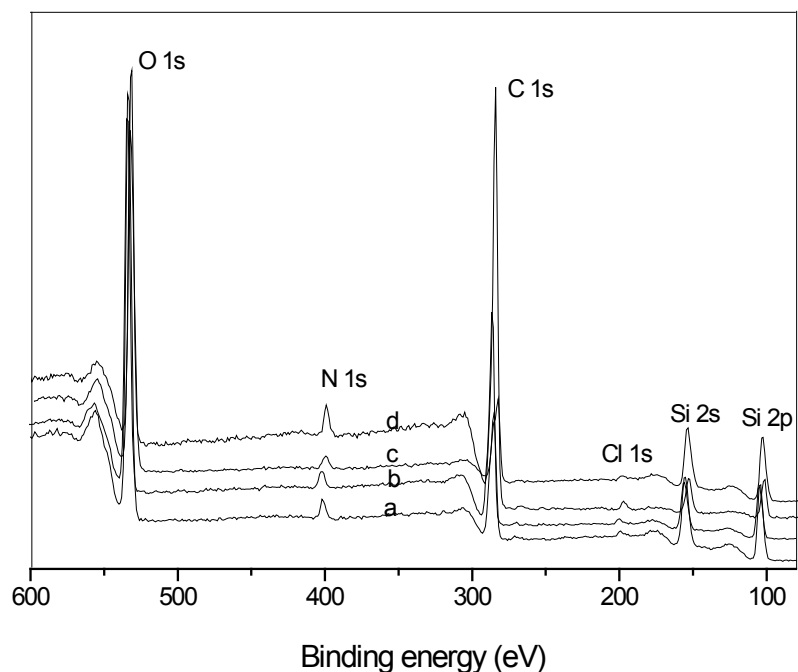


**Figure 4.4** The XPS spectra of (a) EDA, (b) DETA, (c) TETA and (d) TAEA functionalized material

### **(e) FTIR Studies**

The infra-red spectra of the unfunctionalized silica, 3-chloropropyltrimethoxysilane and the functionalized silica are shown in Figure 4.5. The spectrum of the linker for the amines to the silica particles, 3-chloropropyltrimethoxysilane, showed a strong peak at

670  $\text{cm}^{-1}$  which is characteristic of  $\nu(\text{C-Cl})$ . [135] This peak disappears after functionalization of the linker with amines followed by attachment onto the silica surface, and other significant peaks were observed: 1671  $\delta(\text{N-H})$ , and 1046  $\text{cm}^{-1}\nu(\text{Si-O})$ . This indicated that all the sorbent material contained an amine group after functionalization.

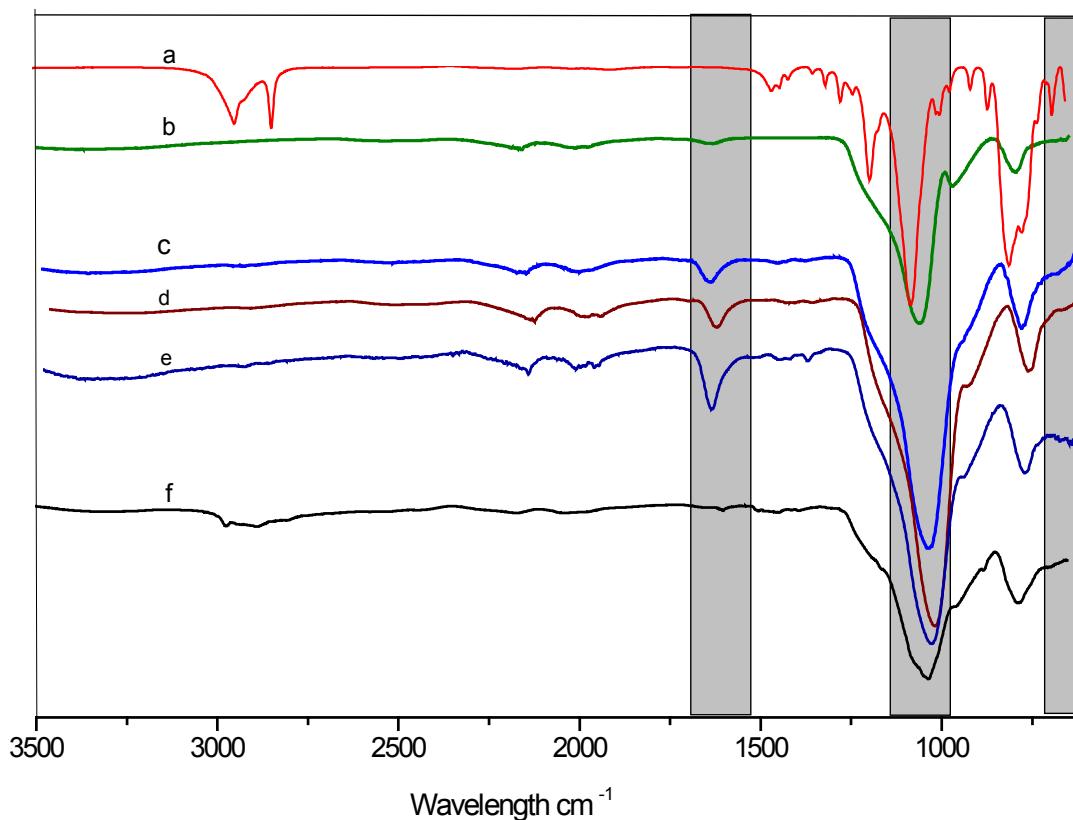


**Figure 4.5** FT-IR spectra of (a) 3-chloropropyltrimethoxysilane (b) S-EDA (c) S-DETA (d) S-TETA (e) S-TAEA and (f) unfunctionalized silica

### 4.3.2 Batch adsorption studies

The effect of contact time on the adsorption of platinum and palladium chlorido species is shown in Figure 4.6. The adsorption of  $\text{PtCl}_6^{2-}$  and  $\text{PdCl}_4^{2-}$  reached maximum in about 5 minutes. Only a slight increase in adsorption of the metals was obtained after 15 minutes, hence 20 minutes was taken as the contact time for subsequent experiments.

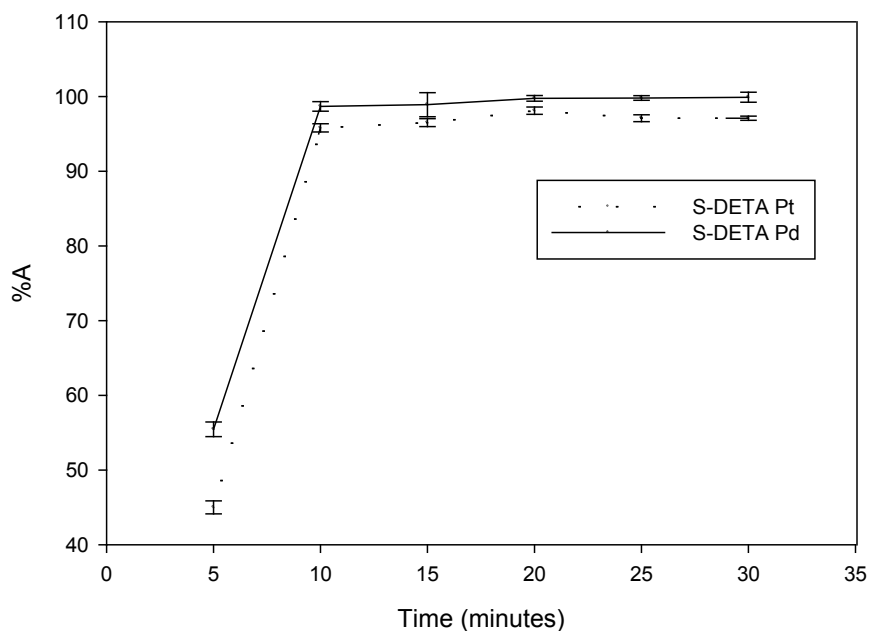


**Figure 4.6** Effect of contact time on adsorption percentage (A %) using 3 mL of 0.01 M platinum and palladium chlorido species on 0.15 g of S-DETA at room temperature

In order to investigate the adsorption capacity of  $\text{PtCl}_6^{2-}$  and  $\text{PdCl}_4^{2-}$  on each sorbent, the adsorption studies were carried out using metal ions concentration range 0.13 – 0.24 M. The results were fitted on the Freundlich and Langmuir isotherms. The adsorption results obtained for both metals ions as the  $\log Q_e$  vs  $\log C_e$  for the Freundlich isotherm on S-DETA sorbent is presented in Figure 4.7. These isotherms are

frequently used to describe the adsorption of metal ions during a process of ion exchange [137] and the results are summarized in Table 4.2.

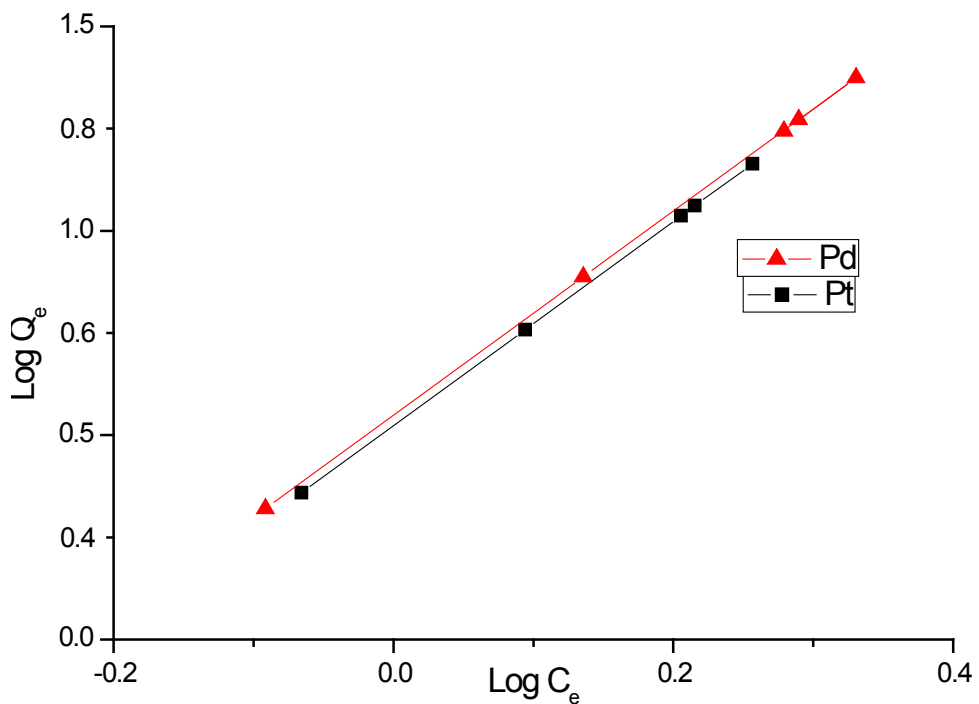


**Figure 4.7** Plots of Freundlich isotherm model using 3 mL of 0.01 M ■Pt and ▲Pd on 0.15 g of S-DETA at room temperature

**Table 4.2** Langmuir and Freundlich parameter for adsorption of  $\text{PtCl}_6^{2-}$  and  $\text{PdCl}_4^{2-}$  on functionalized silica-based microparticles

Isotherm	Parameters	S-EDA	S-DETA	S-TETA	S-TAEA	S-EDA	S-DETA	S-TETA	S-TAEA
		(Pt)	(Pt)	(Pt)	(Pt)	(Pd)	(Pd)	(Pd)	(Pd)
Freundlich	$K_f$	9.98	10.00	10.00	9.98	9.98	9.98	9.98	10.00
	N	1.91	1.92	2.09	1.92	1.92	1.92	1.92	1.92
	$R^2$	0.998	0.999	0.999	0.997	0.998	0.999	0.998	0.999
Langmuir	$Q_m$ (mg/g)	0.34	0.09	0.02	2.8	0.002	0.36	0.13	0.15
	B	4.4	0.2	0.03	2.3	1.0	2.2	3.7	2.2
	$R^2$	0.789	0.842	0.509	0.688	0.567	0.341	0.820	0.506

It was observed, from the higher correlation coefficients ( $R^2$ ) that the Freundlich isotherm model was suitable for representation of the experimental data. This isotherm described the adsorption on heterogeneous surface of the adsorbents. From the results it was clear that the values of  $1/n$  were less than 1 which indicated favourable adsorption.

### **4.3.3 Column (dynamic) studies**

#### ***(a) Single element studies***

The sorbents performance under dynamic flow adsorption conditions was studied. The column was washed with 1 M HCl to remove unabsorbed ions. The Pt and Pd were quantitatively desorbed using 3% w/v of thiourea in 0.5 M HNO<sub>3</sub>. The columns were loaded with higher metal quantities so as to allow for the calculation of loading capacities when the un-adsorbed metals have been washed off the column. Figure 4.8 represents the curves for the elution profiles of PtCl<sub>6</sub><sup>2-</sup> and PdCl<sub>4</sub><sup>2-</sup> on functionalized silica-based sorbent.

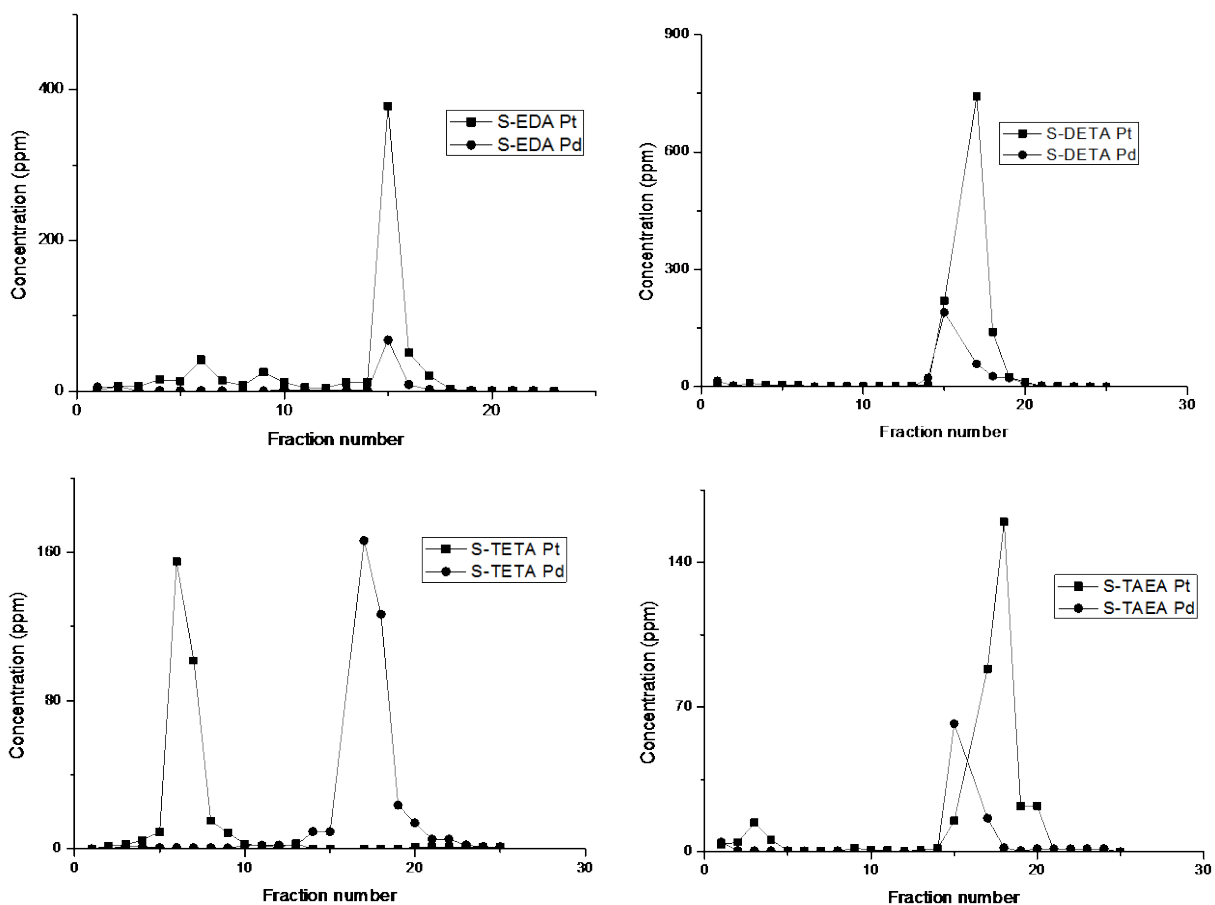


**Figure 4.8** Adsorption/elution profiles using 5 mL of 0.01 M  $\text{PtCl}_6^{2-}$  and  $\text{PdCl}_4^{2-}$  on 0.3 g of amine-functionalized silica-based sorbents: S-EDA, S-DETA, S-TETA and S-TAEA respectively by eluting with 3% w/v thiourea at room temperature

Platinum and palladium were loaded on other sorbents with exception of S-TETA sorbents on which platinum was eluted from the column during the washing step, and the loaded palladium was eluted with thiourea (Figure 4.8). The loading capacity for palladium on the sorbents were in the order S-TETA > S-DETA > S-TAEA > S-EDA and is in agreement with the trend of the BET surface areas and elemental analysis result

with respect to percentage of nitrogen. The mass balance for the column adsorption of both metal ions Pt(IV) and Pd(II) on the functionalized silica materials shows that the recovery efficiency is about 95% of what was loaded into the column.

**Table 4.3** Loading capacities of sorbents for Pt and Pd (mg/g) at room temperature

Metal ions	S-EDA (mg/g)	S-DETA (mg/g)	S-TETA (mg/g)	S-TAEA (mg/g)
Pt	0.24	0.40	0.00	0.29
Pd	0.14	0.16	0.25	0.15

The selectivity of sorbent S-TETA for  $\text{PdCl}_4^{2-}$  was examined by determining the separation factor of Pt(IV) and Pd(II). A binary synthetic solution containing equimolar concentration of both metal ions was loaded into the pre-conditioned column, stripped and eluted with 3% w/v of thiourea. The resin was removed from the column after elution and washed for the next determination. The separation factor of  $\text{PdCl}_4^{2-} / \text{PtCl}_6^{2-}$  was 79. The selectivity of S-TETA was further investigated by the breakthrough curves represented in Figure 4.9. From the curve the breakthrough volume for palladium was significantly higher (above 10 mL).

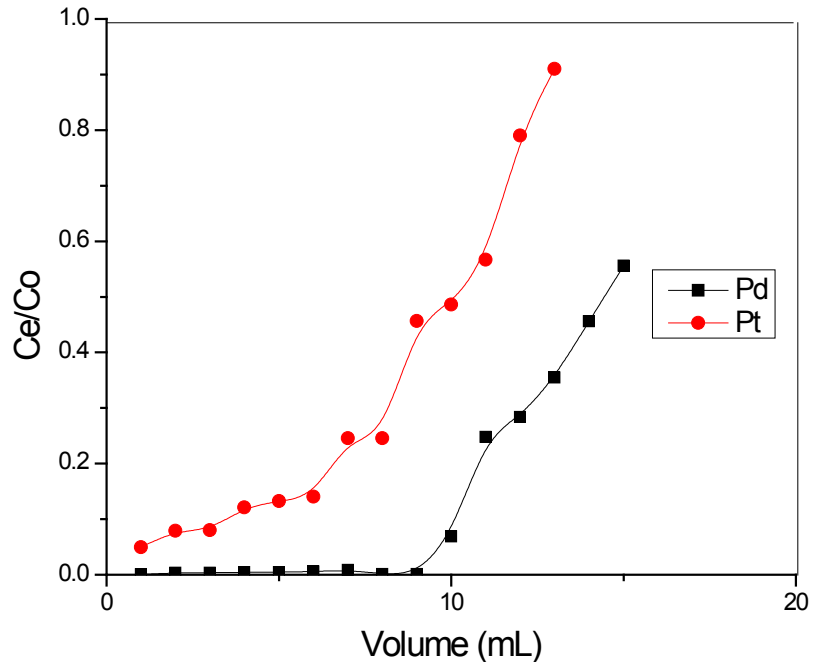


**Figure 4.9** Breakthrough curves using 5 mL of 0.01 M  $\text{PtCl}_6^{2-}$  and  $\text{PdCl}_4^{2-}$  on 0.3 g of S-TETA sorbent at room temperature in 1 M HCl

**(b) Binary separation of Pt and Pd**

The separation of Pt and Pd from their mixture was carried out by taking advantage of their different stripping conditions and the results are presented in Figure 4.10. The metals loaded on the resins were efficiently stripped with 0.5 M  $\text{NaClO}_4$  in 1 M HCl for  $\text{PtCl}_6^{2-}$  and 0.5 M thiourea in 1 M HCl for  $\text{PdCl}_4^{2-}$ .

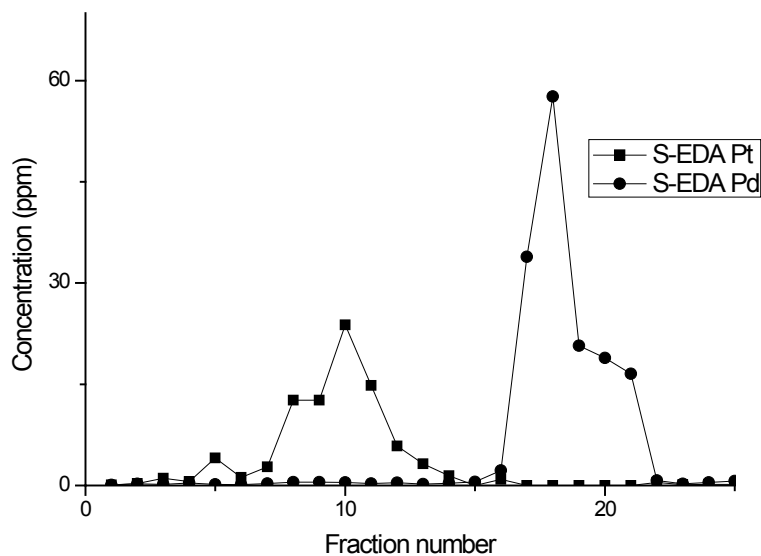


**Figure 4.10** The curves of separation using 5 mL of 0.01 M Pt and Pd by selective stripping of Pt with  $\text{NaClO}_4$  and Pd with thiourea using 0.3 g of S-EDA sorbent at room temperature

The results of the selective separation of the platinum and palladium using the S-EDA sorbent revealed that both metal ions can be successfully separated by using a stripping agent that is specific to one metal chlorido species over the other. In this work  $\text{NaClO}_4$  was used to strip  $\text{PtCl}_6^{2-}$  from the mixture of the metal solution while thiourea in HCl medium was used to elute Pd (II) after the removal of Pt.

### (c) Separation of Pd from Pt, Ir and Rh

A column study of the adsorption of  $\text{PtCl}_6^{2-}$  and  $\text{PdCl}_4^{2-}$  showed the selectivity of S-TETA sorbent for  $\text{PdCl}_4^{2-}$  as shown in the overlaid curves in Figure 4.8. This study was then extended to further investigate the selectivity of the S-TETA sorbent for palladium by separating it from a mixture containing Pt(IV), Ir(IV) and Rh(III). The difference in adsorption behavior of these metals in HCl medium depends on the distribution of their chlorido ionic species. In the case of Ir and Rh; most of these metal ions were eluted from the column at the point of loading while the Pt was eluted during the loading and washing step, the excess unloaded Pd was also eluted during the washing step, and the Pd that was adsorbed in the sorbent was quantitatively stripped and eluted with thiourea solution (Figure 4.11).

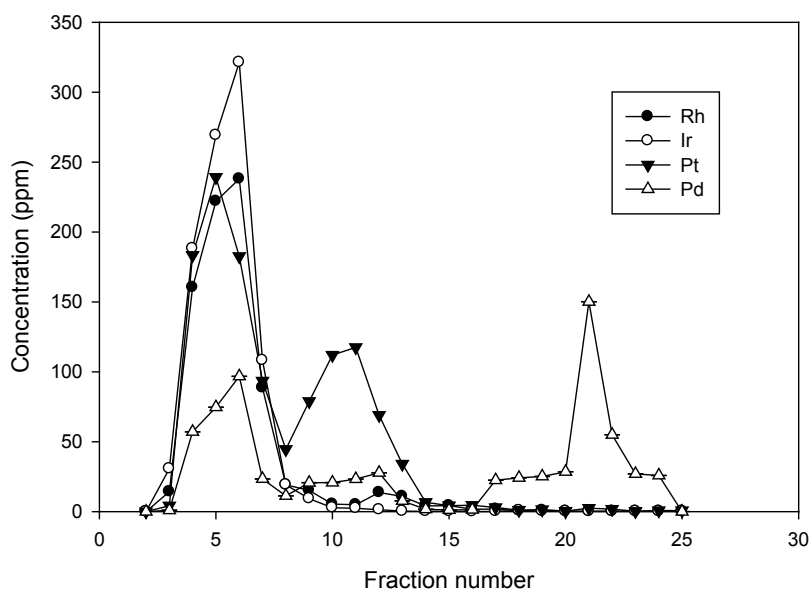


**Figure 4.11** The adsorption/elution profile of Pd from the mixture of Pt, Ir and Rh on 0.3 g S-TETA by eluting with 3% w/v thiourea at room temperature

As shown in Figure 4.11, only Pd loaded onto the S-TETA sorbent was eluted during elution step. The loading capacity of palladium was 0.27 mg/g under the selected conditions. This, therefore, implies that S-TETA is a palladium-specific silica material. It is not clear, however, from the chemical perspective why this kind of behavior was observed but warrants a detailed investigation of the materials from a chemical point of view.

#### **(d) Regeneration of resin**

Regeneration efficiency as described in Chapter 3 also proved that the efficiency of polyamine-functionalized silica materials was retained even after repeated processes and this was determined to be 95% of the initial capacity according to equation 15. The regeneration efficiency further proves that the functionalized silica materials can be used several times for adsorption and separation of platinum group metals.

## **4.4 Conclusions**

The loading capacity of the sorbents was directly proportional to the total exposed surface area and also on the percentage of nitrogen in the materials. The mechanism of hexachloroplatinate(IV) and tetrachloropalladate(II) complexes binding on the sorbents followed the multilayer adsorption on heterogeneous surface of the adsorbents described by the Freundlich isotherm model. The continuous column experiments indicated that separation of hexachloroplatinate(IV) and tetrachloropalladate(II) complexes was achieved on S-EDA sorbent by selective stripping of Pt with 0.5 M

NaClO<sub>4</sub> in 0.5 M HCl and Pd with 0.5 M thiourea in 1 M HCl. The separation of Pd from a mixture containing platinum, iridium and rhodium was achieved on S-TETA rendering it a palladium-specific sorbent material albeit with a low loading capacity (0.27 mg/g). The retention of Pd(II) by S-TETA may be based on the chemistry of the tetrachloropalladate(II) complex which readily forms chelates with amines in mildly acidic chloride-rich solutions ( due to the kinetic lability of [PdCl<sub>4</sub>]<sup>2-</sup> to ligand substitution reactions). However, this warrants a detailed investigation of this chemistry on the solid phase (S-TETA) before the ion-exchange mechanism can be ruled out.

# CHAPTER 5

## CONCLUSIONS AND FUTURE WORK

### 5.1 Conclusions

Polystyrene-based beads and nanofibers as well as silica-based microparticles were functionalized with EDA, DETA, TETA and TAEA. The sorbent materials were characterized by scanning electron microscopy (SEM), microanalysis, infrared (IR), X-ray photoelectron spectroscopy (XPS) and Brunauer-Emmet-Teller (BET) method for surface area measurements. The functionalization of nanofibers (Scheme 3.2) and silica-based sorbents materials (Figure 5.1) seemed to fit the bridging pattern as confirmed by their carbon to nitrogen ratio. Moreover it was difficult to confirm the reaction of the amines with the chloromethylated polystyrene beads due to the 1% crosslinked involved on the beads sorbent material (Figure 5.2).

Nanofibers proved to be efficient in uptake of the PGMs due to the surface functionalization but specificity was not observed. The comparative studies of the sorbent materials revealed that EDA functionalized polystyrene-based nanofiber (F-EDA) gave the highest loading capacity for column adsorption of platinum and palladium. This was attributed to the large surface area and high nitrogen content of F-EDA. In the continuous column experiments, the separation of  $\text{PtCl}_6^{2-}$  and  $\text{PdCl}_4^{2-}$  on F-EDA was achieved by selective stripping of  $\text{PtCl}_6^{2-}$  with 0.5 M  $\text{NaClO}_4$  in 0.5 M HCl and  $\text{PdCl}_4^{2-}$  with 0.5 M thiourea in 1 M HCl. This process, however is not considered the best for practical applications, and metal-complex specific materials are more preferred.

S-TETA and M-TETA gave better selectivity for  $\text{PtCl}_6^{2-}$  and  $\text{PdCl}_4^{2-}$  respectively in the presence of other PGMs such as iridium(IV) and rhodium(III) chlorido species at 1 M HCl. The palladium process can further be optimized and applied in the industry in order to eliminate the solvent extraction step currently employed by some PGM industries for the separation of palladium, however, the loading capacity of the material will need to be improved. There have been no studies done to try and elucidate the behavior of these materials due to the difficulty of studying this chemistry on solid phases.

## **5.2 Future work**

The sorbents S-TETA and M-TETA used in this study showed selectivity for palladium and platinum respectively. These two materials show promise from an engineering chemistry research point of view, but need to be investigated from a fundamental chemistry approach with regards their selectivity. This, however, was deemed outside the scope of this investigation. It is also desirable to investigate the effect of methylene spacers between a diamine functional group by extending ethylenediamine to tetramethylenediamine, hexamethylenediamine, and so forth, so as to investigate the effect of the charge density of the diammonium centres for the anions  $\text{PtCl}_6^{2-}$  and  $\text{PdCl}_4^{2-}$ .

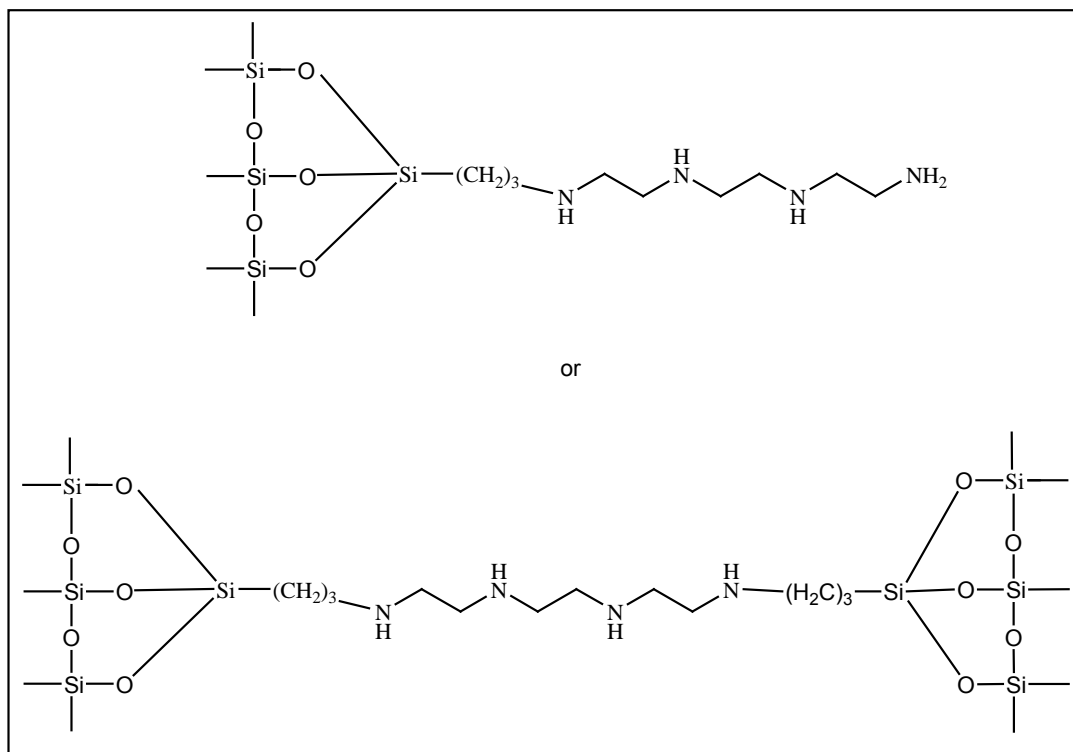


**Figure 5.1** The possible chemical structures of the proposed S-TETA resin

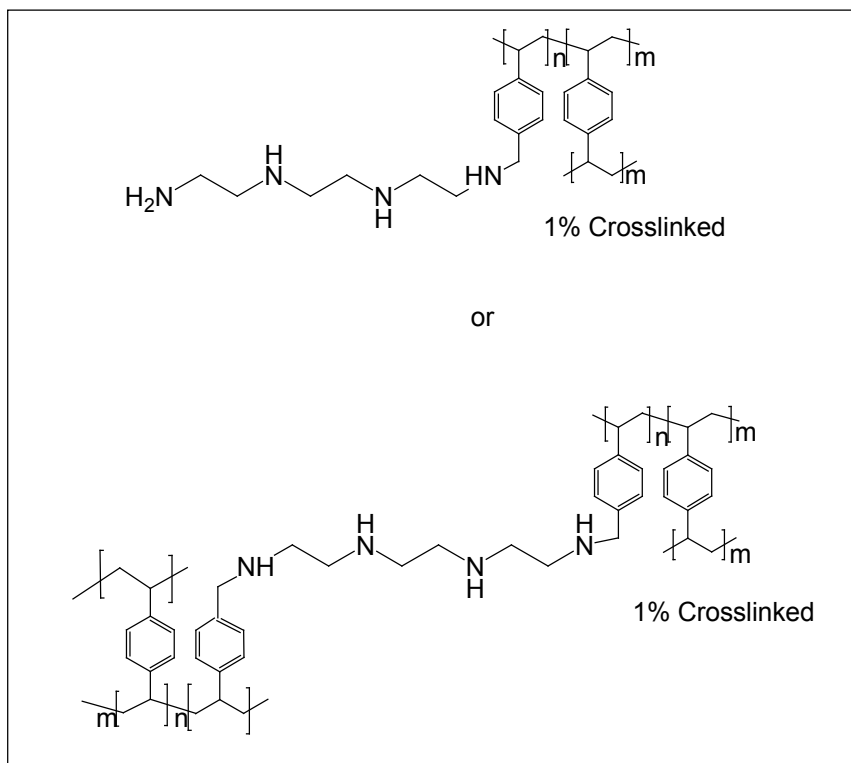


**Figure 5.2** The possible chemical structures of the proposed M-TETA resins

# References

- 1 F.A. Cotton, G. Wilkinson, *Advanced inorganic chemistry*, John Wiley & sons, New York (1980).
- 2 W. Lewis, *Phil. Trans*, 18 (1755) 638-689.
- 3 D. Ms Donald, L.B. Hunt, *A history of Pt and its allied metals*, Johnson Matthey and Co. Ltd. Hatton Garden, London, (1982).
- 4 J.T. Kummer, *Prog. Energy Combust. Sci.*, 6 (1980) 177–199.
- 5 J.M. Wei, E. Iglesia, *J. Catal.*, 22 (2004) 116–127.
- 6 *Platinum series*, Johnson Matthey, London, UK, Published annually since, (1985).
- 7 K. Ravindra, L. Bencs, R. Van Grieken. *Sci. Total Environ.* 318 (2004) 1-43.
- 8 J.D. Whiteley, F. Murray. Anthropogenic platinum group element (Pt, Pd, and Rh) concentrations in road dusts and roadside soils from Perth, Western Australia. *Sci. Total Environ.* 317 (2003) 121-135.
- 9 R.J. Seymore, J.I. O'Farrelly, L.C. Potter, M. Howe-Grant, Edit. *Kirk–Othmer Encyclopedia of Chemical Technology* (fourth ed.), Wiley, New York. 19 (1997) 347-374.
- 10 B.D. Craig, D.S. Anderson, International, A.S.M. "Platinum". *Handbook of corrosion data*, (1995) 8-9.

- 11 L.J. Cabri, *Platinum-Group Elements: Mineralogy, Geology and Recovery*, Canadian Institute of Mining and Metallurgy, Montreal, 23 (1981).
- 12 World Academy of Science, *Engineering and Technology*, 69 (2010) 1-795.
- 13 D.W. Bullet, *Platinum Metals Rev.*, 23 (1979) 109-111.
- 14 J. Fu, S. Nakamura, K. Akiba, *J. Min. Sci.*, 107 (1995) 283-288.
- 15 L. Pan, Z.-de Zhang, *Miner. Eng.*, 22 (15) (2009) 1271-1276.
- 16 F.R. Hartley (ed), *Chemistry of the platinum group metals, recent development*, Elsevier Science Publisher., (1991) 9-30.
- 17 S.D. Alexandratos, *Ind. Eng. Chem. Res.*, 48 (2009) 388–398.
- 18 A. Parodi, T. Vincent, M. Pilsniak, A.W. Trochimczuk, E. Guibal, *Hydrometallurgy*, 92(1–2) (2008) 1-10.
- 19 Grant, in: L. Manzeik (Ed), *Proceedings of IPMI seminar on precious metals recovery and refining*, Scottsdale, Az, USA, 1989, International Precious Metals Institute, Allentown, P.A. (1990).
- 20 G.B. Harris, in *Precious Metals*, R.K. Mishra, Ed., IPMI, Allentown, USA. (1993) 351-373.
- 21 A. Warshwsky, in *Ion Exchange and Separation Processes in Hydrometallurgy*, M. Sreat and D.Naden, Eds., John Wiley and Sons, New York. (1987) 127.

- 22 R.A. Grant, in *Precious Metals Recovery and Refining*, L. Manziak, Ed., IPIM, Allentown, USA (1990) 7-11.
- 23 P. Kovacheva, R. Djingova, *Anal. Chim. Acta.*, 464(1) (2002) 7-13.
- 24 S.C. Dhara, in *Precious Metals: Mining, Extraction and Processing*, AIME, V. Kuddryk, D.A. Corrigan and W.L. Liang. Eds, New York, (1984) 199.
- 25 *Precious Metals Science and technology*, L.S. Benner, T.Suzuki, K. Maguro and S. Tanaka, Eds., IPMI, Allentown, USA, (1991) 401
- 26 T. Louw, *The separation of platinum and gold from an industrial feed solution*, PhD Thesis, Nelson Mandela Metropolitan University, (2008).
- 27 R.M. Smith, A.E. Martell, *Inorganic Complexes*, 4 (1976) 106-122.
- 28 D.E. Ryan, *Can. J. Chem.*, 39 (1961) 2389-2393.
- 29 H. Jonck, *Development of platinum metal specific separation agents*, M.Sc Thesis, Nelson Mandela Metropolitan University, (2008).
- 30 M. Jayakumar, K.A. Venkatesan, T.G. Srinivasan, P.R. Vasudeva Rao, *Electrochim. Acta*, 54 (3) (2009) 1083-1088.
- 31 A. Wolowicz, Z. Hubicki, *Chem. Eng. J.*, 152 (1) (2009) 72-79.
- 32 W.J. Gerber, *Rhodium(III) Speciation-A Chromatographic Study With ICP-MS*, PhD Thesis, Nelson Mandela Metropolitan University, (2006).

- 33 E. Benguerel, Solvent Extraction of Rhodium from Chloride Solutions in the Presence of SnCl<sub>2</sub> with Kelex 100, PhD. Thesis, McGill University, Montreal, (1996).
- 34 L.G. Sillen, Stability Constants of Metal-Ion Complexes, The Chemical Society, London, UK, 2nd<sup>Ed.</sup>, (1964).
- 35 W. Robb, G.M. Harris, J. Am. Chem. Soc., 87 (1965) 4472-4476
- 36 W. Robb, M.M. de V. Steyn, Inorg. Chem., 6(3) (1967) 616-619.
- 37 L.G. Sillen, Stability Constants of Metal-Ion Complexes. Supplement No. 1. Part 1. Inorganic Ligands, The Chemical Society, London, (1971).
- 38 Butterworth-Heinemann, N.N. Greenwood, A. Earnshaw, Chemistry of the elements, (1984).
- 39 G.G. Tertipis, F.E Beamish, Talanta, 10 (1963) 1139-1151.
- 40 J.G.H. du Preez, C. Viviers, T. Louw, E. Hosten, H. Jonck, Solvent Extr. Ion Exch., 22 (2) (2004) 175-188.
- 41 V.Camel, Spectrochim. Acta, Part B: At. Spectrosc., 58 (2003) 362-373.
- 42 V.A. Lemos, L.S.G. Teixeira, M.D. Bazerra, A.C.S. Costa, J.T. Castro, L.A.M. Cardoso, D.S. de Jesus, E.S. Santos, P.X. Baliza, L.N. Santosi, Appl. Spectrosc. Rev., 43 (2008) 303-334.
- 43 S. Meesri, N. Praphairaksit, A. Imyim, Microchem J, 87 (2007) 47-55.

- 44 K. Pyrzynska, T. Wierzbiński, *Microchim Acta*, 147 (2004) 59-64.
- 45 A. Stafiej, K. Pyrzynska, *Microchem J*, 89 (2008) 29-33.
- 46 M. Elisaveta, K. Irina, L.T. Dimiter, *J. Sep. Sci.*, 35 (2012) 1249-1265.
- 47 D. Jermakowicz-bartkowiak, B.N. Kolarz, A. Sewin, *React. Funct. Polym.*, 65 (2005) 135-142.
- 48 I. Matsubara, Y. Takada, K. Ishida, *Anal. Sci.*, 19 (2003) 1427-1429.
- 49 I. Jarvis, M.M. Totland, K.E. Jarvis, *Analyst*, 122 (1997) 19-26.
- 50 Z. Hubicki, A. Wolowicz. *J. Hazard Mater.* 164 (2-3) (2009) 1414 -1419.
- 51 Z. Hubicki, A. Wolowicz. *J. Hazard Mater.* 28 (2010) 124-159.
- 52 D.G. Pearson, S.J. Woodland, *Chem. Geol.*, 165 (2000) 87-107.
- 53 M. Brzezicka, I. Baranowska, *Spectrochim. Acta, Part B.* 56 (2001) 2513-2520.
- 54 S. Hann, G. Koellensperger, K. Kanitsar, G. Stingeder, *J. Anal. At. Spectrom.*, 16 (2001) 1057-1063.
- 55 K. Kanitar, G. Koellensperger, *J. Anal. At. Spectrom.*, 18 (2003) 239-246.
- 56 M. Muller, K.G. Heumann, *Fresenius, J. Anal. Chem.*, 368 (2000) 109-115.
- 57 J.E.G. Mdoe, D.J. Macquarrie, J.H. Clark, *J. Mol. Catal. A: Chem.*, 198 (2003) 241-247.

- 58 G. Sartori, F. Bigia, R. Sartorio, D.J. Macquarrie, M. Lanarda. L. Storaro, S. Coluccia, G. Martra, *J. Catal.*, 22 (2004) 410-418.
- 59 R.V.S. Alfaya, S.T. Fujiwara, Y. Gushikem, Y.V. Kholin, *J. Colloid Interf. Sci.*, 269 (2004) 32-36.
- 60 F. Xi, J. Wu, *J. Chromatogr., A* 1057 (2004) 41-47.
- 61 W. Wasiak, I. Rykowska, A. Voelkel, *J. Chromatogr., A* 969 (2002) 133-141.
- 62 M.M. Osman, A.S. Kholeif, A.N.A. Al-Maaty, E.M. Mahmoud, *Microchim. Acta*, 143 (2003) 25-31.
- 63 W. Ngeontae. W. Aeungmaitrepirom, T. Tuntulani, *Talanta*, 71 (2007) 1075-1082.
- 64 J. Venugopal, S. Ramakrishna, *Appl. Biochem. Biotechnol.*, 125 (2007) 147-157.
- 65 S. Ramakrishna, R. Jose, P.S. Archana, A.S. Nair, R. Balamurugan, J. Venugopal, W.E. Teo, *J. Mater. Sci.*, 45 (2010) 6283–6312.
- 66 S. Chigome, G. Darko, U. Buttner, N. Torto, *Anal. Methods.*, 2 (2010) 623-626.
- 67 S. Chigome, G. Darko, N. Torto, *Analyst*, 136 (2011) 2879-2889.
- 68 R.S. Walmsley, A.S. Ogunlaja, M.J. Coombes, W. Chidawanyika, C. Litwinski, N. Torto, T. Nyokong, Z.R. Tshentu, *J. Mater. Chem.*, 22(12) (2012) 5792-5800.
- 69 C.J. Thompson, G.G. Chase, A.L. Yarin, D.H. Reneker, *Polymer* 48 (2007) 6913-6922.
- 70 A. Greiner, J.H. Wendoff, *Angew. Chem. Int. Ed.*, 46 (2007) 5670-5703.

- 71 D.H. Reneker, A.L. Yarin, *Polymer*, 49 (2008) 2837-2435.
- 72 G. Bhat, Y. Lee, *Proceedings of the twelfth international symposium of processing and fabrication of advanced materials*, Ed TS Srivatsan and RA Vain, TMS, (2003) 1-317.
- 73 S. Agarwal, H. Joachim, A. Wendorff, A. Greiner, *Polymer*, 49 (2008) 5603–5621.
- 74 M. Bognitzki, W. Czado, T. Frese, A. Schaper, M. Hellwig, M. Steinhart, A. Greiner, J.H. Wendorff, *Adv. Mater.*, 13 (2001) 70-72.
- 75 J. Dosh, D.H. Reneker, *J. Electrostat.*, 35 (1995) 151-160.
- 76 D.H. Reneker, I. Chun, *Nanotechnology*, 7 (1996) 216-223.
- 77 Y. Zhang, C.T. Lim, S. Ramakrishna, Z. M. Huang, *J. Mater. Sci. – Mater. Med.*, 16 (2005) 933-946.
- 78 Z.M. Huang, Y.Z. Zhang, M. Kotaki, S. Ramakrishna, *Compos. Sci. Technol.*, 63 (2003) 2223-2253.
- 79 Z. Ma, M. Kotaki, R. Inai, S. Ramakrishna, *Tissue Eng.*, 11 (2005) 101-109.
- 80 J.I. Kroschwitz, *Encyclopedia of polymer science and engineering*, 2<sup>nd</sup> Edn. John Wiley & Sons, New York, 6 (1986) 812-815.
- 81 T. Ondarcuhu, C. Joachim, *Europhys. Lett.*, 42 (1998) 215-220.
- 82 P.X. Ma, R. Zhang, *J. Biomed. Mater. Res.*, 46 (1999) 60-72.

- 83 A. Ndreu, Electrospun nanofibrous scaffolds for tissue engineering, MSc Thesis, Middle East Technical University, (2007).
- 84 R.Jaeger, M. Bergshoef, C. Martin-Batille, H. Schoenherr, and G.J. Vamsco. Macromol. Symp., 127 (1998) 141-150.
- 85 T. Grafe, K. Graham, Polymeric nanofibers and nanofiber webs: A new class of nonwoven, presented at international technical conference Atlanta, Georgia, (2002) 24-26.
- 86 R.S. Barhate, C.K. Loong, S. Ramakrishna, J. Membr. Sci., 283 (2006) 209-218.
- 87 A.L. Yarin, S. Koombhongse, D.H. Reneker, J. Appl. Phys., 89 (2001) 3018-3026.
- 88 M.Y. Shin, MM.Hohman, M. Brenner, G.C .Ruteldge, Polymer, 42 (2001) 9955-9967.
- 89 K.H. Lee, H.Y. Kim, Y.M. La, D.R. Lee, N.H. Sung, J. Polym. Sci.: Part B: Polym. Phys., 40 (2002) 2259-2268.
- 90 D.S. Katti, K.W. Robinson, F.K. Ko, and C.T. Laurencin, J. Biomed. Mater. Res. 70B, (2004)286-96.
- 91 T. Subbiah, G.S. Bhat, R.W. Tock, S. Parameswaran, S.S. Ramkumar, J. Appl. Polym. Sci., 96 (2005) 557-569.
- 92 C.L. Casper, J.S. Stephens, N.G. Tassi, B.D. Chase, J.F. Rabolt, , Macromol., 37 (2004) 573-578.
- 93 M.G. McKee, M.T. Hunley, J.M. Layman, T.E. Long, Macromol., 39 (2006) 575-583.

- 94 M.M. Hohman, M. Shin, G. Rutledge, M.P. Brenner, *Phys. Fluids.*, 13 (2001) 2201-2220.
- 95 J.M. Deitzel, J. Kleinmeyer, D. Harris, N.C.B. Tan, *Polymer*, 42 (2001) 261-272.
- 96 C.J. Buchko, L.C. Chen, Y. Shen, D.C., *Polymer*, 40 (1999) 7397-7407.
- 97 G.I. Taylor, *Proc. Roy. Soc. London*, A313 (1969) 453-475.
- 98 J. Doshi, M.H. Mainz, G.S. Bhat, *Proceedings of the tenth TANDEC Nonwoven Conference*, Knoxville, TN, (2000).
- 99 J.M. Deitzel, W. Kosik, S.H. Mcknight, N.C.B. Tan, J.M. Desimone, S. Crette, *Polymer*, 43 (2002) 1025-1029.
- 100 M. Bognitzki, H. Hou, M. Ishaque, T. Frese, M. Hellwig, C. Schwarte, A. Shaper, J. H. Wendorff, A. Greiner, *Adv. Matter*, 12 (2000) 637-640.
- 101 B. Venkatesachar, L. Sibaiya, *Nature*, 136 (1935) 65-66.
- 102 M.A. Ivanov, E.F. Shender, 69 (1975) 350-363.
- 103 J. Kramer, K.R. Koch, *Inorg. Chem.*, 46 (2007) 7466-7476.
- 104 Elementar Analysensysteme GmbH, CHNOS Elemental Analyzer Vario Microoperating instruction, (2005).
- 105 Elementar.de, *Technologia Aplicada Internacionan*, San Jose, Costa Rica, America Central, (2000).
- 106 U. S. Environmental protection agency, method 200. 7 Trace elements in water, solids, and biosolids by ICP-OES, Revision, (2001).

- 107 H.J. Van de Wiel, *Horizontal*, 19 (2004) 1-46.
- 108 SII Nanotechnology Inc, *Product Brochure*,(2012).
- 109 Balzers Union Ltd, *Sputtering device operating instruction, Accessories for Electron Microscopy*, (1988) 1-9.
- 110 R. Cross, *The preparation of material for scanning electron microscopy (SEM)* Electron Microscopy Unit, Rhodes University, South Africa, (2001) 55-56.
- 111 R. Hermann, P. Walther, M. Muller, *J. Struct. Biol.*, 107 (1991) 38-47.
- 112 G.M. Hodges, *Arch. Histol. Cytol.*, 55 (1992) 27-38.
- 113 T. Osawa, M. Abe, A. Morigami, Y. Nozaka, *J. Electron Microsc.*, 47 (1998) 273-276.
- 114 E. Suzuki, *J. Microsc.*, 208 (2002) 153-157.
- 115 S.K. Edvarson, K.M. Siegbahn, *Nuc. Phys.*, 1 (1956) 160-169.
- 116 K.M. Siegbahn, *Physics Nobel Lecture.*, (1981-1990) 61-63.
- 117 F.J. Watts, J. Wolstenholme, *An introduction to surface analysis by XPS and AES*, John Wiley, New York. 2<sup>nd</sup> Ed., (2003).
- 118 M.E. Mahmoud, M.M. Al-Essawi. S.A. Kholeif, E.M.I. Fathalla, *Anal. Chim. Acta* 525 (2004) 123-132.
- 119 S. Brunauer, P. H. Emmett, E. Teller, *J. Am. Chem. Soc.* 60 (1938) 309-326.
- 120 I. Langmuir, *J. Am. Chem. Soc.* 38 (1916) 2221-1195.

- 121 H.M.F. Freundlich, *J. Phys. Chem.*, 57 (1906) 385-470.
- 122 A. Wolwicz, Z. Hubicki, *Solvent Extr. Ion Exch.*, 28 (2010) 124-159.
- 123 JR. J. Thomas, F.B. Bohor, *Clay Clay Miner.*, 17 (1969) 205-209.
- 124 J.M. Deitzel, W. Kosik, S.H. McKnight, N.C. Beck Tan, J.M. Desimone, S. Crette, *Polymer*, 43 (2002) 1025-1029.
- 125 B. Godlewska-Zylkiewicz, *Microchim. Acta.*, 147(4) (2004) 189-210.
- 126 K. Pyrzynska, M. Trojanowicz, *Crit. Rev. Anal. Chem.*, 29 (1999) 313-321.
- 127 A. Uheida, M. Iglesias, C. Fontas, M. Hidalgo, M. Salvado, Y. Zhang, M. Muhammed, *J. Colloid Interface Sci.*, 301 (2006) 402-408.
- 128 R. Galta, S.J. AL-Bazi, *Talanta*, 42 (2) (1995) 249-255.
- 129 Z. Hubicki, A. Wolowicz, M. Leszczynska, *J. Hazard. Mater.*, 159(2-3) (2008) 280-286.
- 130 A.M. Donia, A.A. Atia, K.Z. Elwakeel, *J. Sep. Purif. Tech.*, 42(2) (2005) 111-116.
- 131 N.S. Jayasinghe, F.P. Lucien, T. Tran, *Indust. Engin. Chem. Res.*, 44 (19) (2005) 7496-7504.
- 132 Lu. Jinni, H.T. Patrick, *Chem. Rev.*, 109 (2009) 815–838.
- 133 E. M. Soliman , E. Mohamed, S. Mahmoud , A. Ahmed, *Talanta* 54 (2001) 243–253.
- 134 A. Proctor, P.M.A. Sherwood, *Anal. Chem.*, 54 (1982) 13–19.

- 135 K. Nakamoto, *Infrared and raman spectra of inorganic and coordination compounds*, 4th Ed.; John Wiley & Sons, Inc., New York, (1986).
- 136 J. Kramer, K.R. Koch. *Inorg. Chem.*, 45 (2006) 7843-7855.
- 137 Z. Zainol, M.J. Nicol, *Hydrometallurgy*, 96(4) (2009) 283-287.
- 138 G. McKay, H.S. Blair, J.R. Gardner, *J. Appl. Polym. Sci.*, 27(8) (1982) 3043-3057.
- 139 G. Zuo, M. Muhammed, *React. Polym.*, 24(3) (1995) 165-181.
- 140 K. Fujiwara, A. Ramesh, T. Maki, *J. Hazard. Mater.*, 146 (1-2) (2007) 39-50.
- 141 M. Iglesias, E. Antico, V. Salvado. *Anal. Chim. Acta*, 61 (1999) 381
- 142 D.P. Shillington, B.K. Tait. *Solvent Extr. Ion Exch.*, (1991) 749
- 143 T. Kakoi, M. Goto, F. Nakashio, *J. Membr. Sci.*, 120 (1996) 77-88.
- 144 E. Benguerel, G.B. Demopoulos, *Hydrometallurgy*, 40 (1994) 135-152.
- 145 Z. Hubickia, G. Wójcika, *Desalin.*, 197 (2006) 82–93.
- 146 J. Kramer, W.L. Driessen, K.R. Koch, J. Reedijk, *Hydrometallurgy*, 64 (2002) 59-68.
- 147 M.E. Mahmoud, *Anal. Lett.*, 29 (1996) 1791-1804.
- 148 M.E. Mahmoud, E.M. Soliman, *Talanta*, 44 (1997) 15-22.
- 149 R.K. Iler, *The chemistry of silica: Solubility, polymerization, colloid and surface properties, and biochemistry*, Wiley, New York, (1979).

150 P. Pasucci, Y. Senddon, Pittsburgh conference presents, New Orleans, abstracts of reports, 1992, p. 1177.

151 U. Pyell, G. Stork, J. Anal. Chem., 343 (1992) 576-581.